Order Number 9409268

Null steering in phased and adaptive arrays by controlling the element positions

Ismail, Taisir Hasan, Ph.D.

King Fahd University of Petroleum and Minerals (Saudi Arabia), 1991

U·M·I
300 N. Zeeb Rd.
Ann Arbor, MI 48106

KING FAHD UNIVERSITY OF PETROLEUM AND MINERALS
ELECTRICAL ENGINEERING DEPARTMENT

PhD DISSERTATION

NULL STEERING IN PHASED AND ADAPTIVE ARRAYS BY CONTROLLING THE ELEMENT POSITIONS

by

TAISIR HASAN ISMAIL

August 1991

KING FAHD UNIVERSITY OF PETROLEUM AND MINERALS

DHAHRAN 31261, SAUDI ARABIA

COLLEGE OF GRADUATE STUDIES

This thesis, written by ***TAISIR HASAN ISMAIL*** under the direction of his Dissertation Advisor and approved by his Dissertation Committee, has been presented to and accepted by the Dean of the College of Graduate Studies, in partial fulfillment of the requirements for the degree of DOCTOR OF PHILOSOPHY in ELECTRICAL ENGINEERING.

DISSERTATION COMMITTEE

Mahmoud M. Dawoud

Dr. M. M. Dawoud (Advisor)

Dr. M. Bettayeb (Member)

Dr. S. Abdul-Jauwad (Member)

H. A. Ragheb

Dr. H. Ragheb (Member)

Muhammad Aslam

Dr. M. Chaudhry (Member)

Al-Shehri

Department Chairman

Dean, College of Graduate Studies

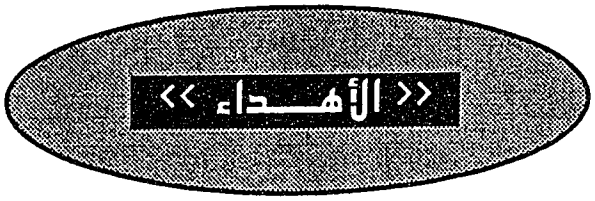

الى والدى الكريم -رحمه الله- الذى غرس فيّ حب العلم والمعرفة .

الى أمى الحنون التى غمرتنى بعطفها وحبها .

الى زوجتى الكريمة التى وقفت بجانبى صابرة .

الى أخوتى الأعزاء الذين آزرونى فى رحلتى العلمية .

الى ابنائى ... فلذات كبدى .

الى كل هؤلاء اهدى هذا البحث .

تيسير

ACKNOWLEDGEMENT

Acknowledgement is due to ***King Fahd University of Petroleum and Minerals*** for support of this research.

I wish to express my appreciation to my dissertation advisor, ***Dr. Mohmoud Dawoud***, for his supervision, valuable discussion, and his kind co-operation. I also wish to thank my committee members, ***Dr. Maamar Bettayeb***, ***Dr. Samir Abdul-Jauwad***, ***Dr. Hassan Ragheb***, and ***Dr. Mohammad Chaudhry***, for their valuable suggestions, remarks and their kind co-operation.

CONTENTS

LIST OF TABLES

TABLE

LIST OF FIGURES

FIGURE

LIST OF SYMBOLS

a_n : The current excitation of the n'th element

BW : Half power main beam width of the array pattern

C : The sidelobe peak cancellation ratio

c_m : The beam coefficient of the m'th cancellation beam

d_0 : The unperturbed interelement spacing in wavelength

d_n : The unperturbed position of the n'th element

Δ_n : The n'th element position perturbation

$\hat{\Delta}_n$: Truncated element position perturbation of the n'th element

EF : Element pattern

Δf : Interference signal bandwidth

Dir : Array directivity

F : Ideal perturbed array pattern

F_0 : Unperturbed array pattern

F_c : Cancellation pattern

F_1 : The spurious pattern caused by the truncation error

f_0 : Operating frequency of the array

k : Wave number ($\frac{2\pi}{\lambda}$)

λ : Operating wavelength of the array

φ : Angle in the elevation plane

LMS : Least mean square algorithm

MSD : Mean square difference between the perturbed and the unperturbed patterns

R : Antenna separation distance

SLL : Side lobe level of the array pattern

SNR : Signal-to-noise ratio

SNIR : Signal-to-noise and interference ratio

θ : Angle in the azimuth plane from broad side

θ_m : Angular location of the m'th jammer

$\overline{\theta}_m$: Angular null location accompanied by the m'th jammer

θ_s : Main beam steering angle

x_n : The n'th element perturbed position

w_{0n} : The n'th element unperturbed coefficient

w_n : The n'th element perturbed coefficient

y_n : An arbitrary real coefficient

Z_{ij} : Mutual impedance between the i'th and j'th elements

Zd_i : Driving point impedance of the i'th element

خلاصة الرسالة

اسم الطالب : تيسير حسن محمد اسماعيل
عنوان الرسالة : توجيه انعدامية الإشعاع للمصفوفات الهوائية الطورية والمتكيفة بتغيير مواضع وحداتها
التخصص : هندسة كهربائية - اتصالات
تاريخ الشهادة : صفر ١٤١١هـ

لقد طورت طريقة جديدة لتوجيه انعدامية الإشعاع للمصفوفات الهوائية الطورية والمتكيفة بتغيير مواضع وحداتها مع المحافظة على خصائص فص الإشعاع الرئيس لنمط إشعاع المصفوفة الهوائية . إن هذه الطريقة قد درست نظريا وأجريت التجارب المعملية لتوجيه انعدامية إشعاع المصفوفات الهوائية من أجل إلغاء إشارات التشويش والإشارات المتداخلة المعروفة الاتجاه ، وفى نفس الوقت الإبقاء على الإشارة المطلوبة . وقد برهنت النتائج النظرية والتجريبية على فعالية هذه الطريقة بتوجيه انعدامية الإشعاع لأى اتجاه ، وفى نفس الوقت أمكن تجاوز بعض السلبيات للطرق الأخرى . إن استعمال هذه الطريقة لتوجيه انعدامية الإشعاع يحقق كثيرا من الفوائد . فهذه الطريقة تتم آلياً وبدون الحاجة الى تغييرات جوهرية فى دوائر التشغيل . وتسمح الطريقة الجديدة بتوجيه فص الإشعاع الرئيس لنمط إشعاع المصفوفة الهوائية وانعدامية الإشعاع لاتجاهات غير مرتبطة بعضها ببعض . كذلك يمكن توجيه انعدامية الإشعاع لاتجاهات متماثلة تماما حول الفص الرئيس لنمط الإشعاع . وبما أن إزاحات مواضع وحدات المصفوفة متماثلة حول مركزها ، فأن كمية الحسابات تنقص الى النصف . ان هذه الطريقة فى حساب إزاحات وحدات المصفوفة الهوائية لتوجيه انعدامية الإشعاع يعتمد على افتراض أن هذه الإزاحات صغيرة مقارنة بالمسافة بين هذه الوحدات . وتعمل هذه الطريقة بصورة ممتازة مادام عدد الإشارات المتداخلة وغير المرغوب فيها صغيراً بالنسبة لعدد وحدات المصفوفة ، وكذلك ما دامت هذه الإشارات باتجاه فصوص الإشعاع الجانبية لنمط إشعاع المصفوفة . وتملك هذه الطريقة القدرة على إلغاء الإشارات ذات عرض نطاق الموجات الكبيرة .

درجة الدكتوراه فى الفلسفة
جامعة الملك فهد للبترول والمعادن
الظهران - المملكة العربية السعودية
صفر ١٤١٢هـ

ABSTRACT

A new method for null steering in phased arrays by controlling the element positions is presented. This technique is studied both theoretically and experimentally for placing nulls in the radiation pattern to suppress interference and unwanted signals. The study shows the effectiveness of null steering to arbitrary directions while overcoming some of the limitations associated with other known techniques. The experimental results demonstrate the capability of this technique in forming nulls in the required directions. Many advantages can be achieved using this method. The phase shifters can be used solely for steering the main lobe towards the direction of the desired signal. This new technique allows the independent steering of the main beam and the nulls to arbitrary independent directions. It also possesses an even symmetry pattern cancellation which allows nulls to be imposed at symmetrical positions around the main beam. The position perturbations are symmetrical about the center of the array which results in reducing the amount of computation. In addition, if the number of jammers increases, then the formed pattern will be less sensitive to variation in element positions. This technique of null steering, based on the small element position perturbations, works satisfactorily as long as the nulls are imposed in the sidelobe region and the number of nulls is small compared to the number of elements. This technique is also capable of obtaining sidelobe cancellation and wide band signal rejection.

CHAPTER 1

INTRODUCTION

Adaptive antenna arrays for radar and communication applications have been the subject of considerable interest during the last few decades. The main reason for this interest is that the interference signals can be suppressed by steering the nulls and hence reducing the sidelobe levels in the directions of interference and unwanted signals, while keeping the main beam pointing towards the desired signal. This interference suppression capability is a principal advantage of adaptive arrays compared to conventional waveform processing techniques. Most work concerned with adaptive nulling has been directed towards maximizing a performance index such as signal-to-noise and interference ratio (SNIR) or antenna gain indices.

On the other hand, synthesis techniques which provide control of the nulls of the antenna pattern are of great interest. They represent generalizations of classical pattern synthesis techniques, which deal with the main beam shape and the side lobe envelope, but neglect the detailed sidelobe structure and the placement of the nulls in real space. They also provide insight into the performance of adaptive antenna systems. In general these methods involve the

search for appropriate set of complex weights (full amplitude/phase), phase only or amplitudes of the current in the array elements only, so that the main beam remains pointing towards the desired signal, while nulls are formed in the directions of strong undesired signals. The most efficient method is based on full amplitude/phase control at each array element, which is a very costly choice. The null synthesis method based on small phase perturbations was distinguished from large phase perturbations, and results in an analytic solution .

In this dissertation, a new synthesis technique is proposed, and studied both theoretically and experimentally for placing nulls in arbitrary directions in the radiation pattern of antenna systems in order to suppress interference signals. Since it is possible to form very deep pattern nulls over a narrow bandwidth region by controlling the antenna element positions, very strong interferences can be suppressed.

1.1 Historical background

Unequal spacing of array elements has been used in the past to design arrays for a given gain, beamwidth and sidelobe level while minimizing the number of elements [1,2]. The current key capability for adaptive interference nulling was not available until 1966, when S. Applebaum's classic report [3], "Adaptive arrays" appeared and presented the control law theory, an algorithm that maximizes a generalized SNR. Also, in the same year a second contribution towards the capability of adaptive interference nulling was available. B. Widrow reported the familiar LMS (least mean square) algorithm

for controlling the weights of the adaptive RF antenna systems, achieving the first open literature publication in this area [4]. Although, these first two adaptive algorithms arrived independently and with complete different backgrounds, they are in fact very similar. Both derive their adaptive weight adjustment control by sensing the correlation between element signals, on the bases of covariance matrix of the set of system inputs, and both converge toward the optimum Weiner solution on the bases of the eigenvalues involved.

The LMS algorithm was developed further by Griffiths [5], and Frost [6], with the result that one can maintain a chosen frequency characteristics for the array in a desired direction, while discriminating against noise coming from other directions. Compton noted a power equalization phenomena [36], which was also addressed by Zahm [8], and shown to permit acquisition of weak signals in the presence of strong interferences.

The null steering arrays that use full amplitude and phase weighting have been designed and tested by using analog correlation between the sum channel and each element channel [3, 35]. Further work had been done by many authors , where they studied the solution to the problem with different cancellation beam shape [9, 24]. Thus, the number of adaptively controlled elements is kept small, because of the cost per control loop. However, it is desirable to control as many elements as possible, in order to maximize the number of steerable nulls as well as maximize the null depth as a function of signal bandwidth and minimize the loss in gain and sidelobe deterioration. Also, it cannot always steer the main

beam and one null toward two prespecified directions simultaneously with a single set of weights [39].

A second technique for null steering is obtained through perturbation of element phase only, which is attractive since in a phased array the required controls are available at no extra cost. Thus, in order to minimize complexity and cost Baird and Rassweiler used the phase-only method to control the null-steering arrays [10]. This method is aimed at adaptively controlling every element of a moderately large array. In their work, the following simplifications were made,

a) Only phase-shifters weights are used (rather than amplitude and phase)

b) Digitally-controlled search optimization of the phase shifters is used, rather than analog correlation control.

c) Beam-space weight decomposition is used to minimize the dimension searched for optimization.

The first two simplifications degrade the array performance, and search optimization creates hunting noise in the output. Nevertheless, this approach offers simple adaptive array hardware, particularly in the case of large arrays where rapid searching is not required.

In the following Sections, some of the adaptive null steering methods are surveyed. The two classic algorithms , Widrow-Hopf LMS algorithm and Howells-Applebaum algorithm, are introduced briefly as they are known to represent the class of problems which converge toward the optimum Weiner

solution. A specific adaptive nulling technique recently appeared in the literature, using multimode feed horn antenna. The adaptive null steering synthesis techniques which can be found in the existing literature are introduced in Section 1.5.

1.2 LMS adaptive nulling

Consider the adaptive array structure with a known desired signal shown in Fig.1.1.The input signal vector X_j^T of the adaptive linear combiner is defined as,

$$X_j^T = [\, x_{1j}, x_{2j}, \ldots\ldots\ldots, x_{Nj}]^T \tag{1.1}$$

The input signal components are assumed to appear simultaneously on all input lines at discrete times indicated by the subscript j. The weight vector W is

$$W^T = [\, w_1, w_2, \ldots\ldots\ldots, w_N]^T \tag{1.2}$$

Then the array output signal is given by,

$$y_j = X_j^T W = W^T X_j \tag{1.3}$$

The error ε_j is defined as the difference between the desired response d_j (an externally supplied input sometimes called the "training signal") and the actual response y_j :

$$\varepsilon_j \equiv d_j - W^T X_j = d_j - X_j^T W \tag{1.4}$$

In adaptive systems the desired response may be derived by various methods, one of which is to inject a "pilot signal" whose characteristics determine the "look" direction and frequency response of the main beam [4,22].

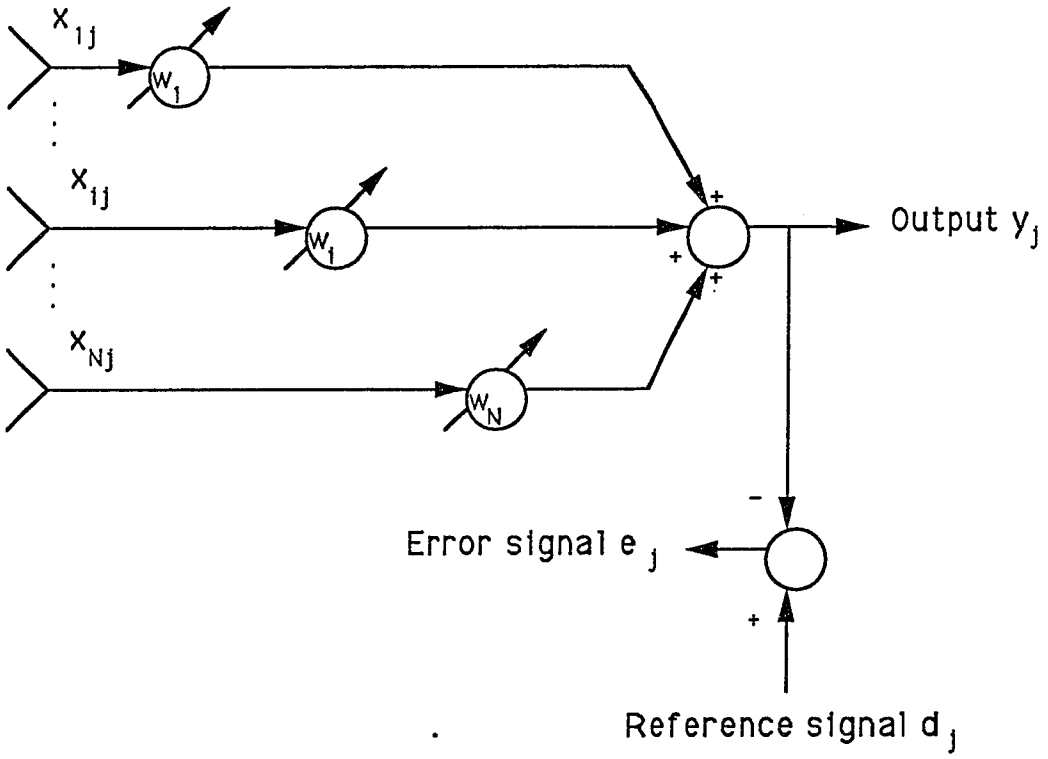

Figure 1.1 : Basic adaptive array structure with a known desired signal

It is the purpose of the adaptive process to adjust the weight of the adaptive linear combiner to minimize the mean square of the error ε_j (MSE). Let the input signals X_j and the desired signal d_j be statistically stationary. During adaptation the weight vector varies, so that even with stationary inputs the output y_j and the error ε_j will generally be nonstationary. Care must thus be taken in defining the MSE for an adaptive system. The only possibility is an ensemble average, which can be established in the following manner.

At the kth iteration let the weight vector be W_k. Squaring and expanding (1.4) and letting $W = W_k$ yields

$$\varepsilon_j^2 = d_j^2 - 2d_jX_j^TW_k + W_k^TX_jX_j^TW_k \tag{1.5}$$

The MSE is just the expected value of

$$E[\varepsilon_j^2]_{W=W_k} = E[d_j^2] - 2\,E[d_jX_j^T]W_k + W_k^T\,E[X_jX_j^T]W_k$$

or

$$E[\varepsilon_j^2]_{W=W_k} = E[d_j^2] - 2\,r^TW_k + W_k^T\,RW_k \tag{1.6}$$

where the cross correlation r is given by

$$r = E[\,d_j\,X_j^T]$$

and the autocorrelation R is given by

$$R = E[\,X_j\,X_j^T]$$

Note that the MSE is a quadratic function of the weights that can be depicted as a concave hyperparapoloidal surface. The method of steepest decent can be exploited to find the bottom of quadratic performance bowl. The

gradient is obtained by differentiating the MSE with respect to the weight vector to yield

$$\nabla (E[\varepsilon_j^2]_{W=W_k}) = -2r + 2RW_k \tag{1.7}$$

The optimal weight vector W^*, generally called the Weiner weight vector, is obtained by setting the gradient to zero:

$$W^* = R^{-1} r \tag{1.8}$$

This equation is a matrix form of the Weiner-Hopf equation [22,35 pp.157]. Solving (1.8) directly certainly provides a straightforward way to obtain the desired solution, but such an approach has several drawbacks. One of these is that serious computational problems could arise from the necessity of computing and inverting an $N \times N$ matrix when the number of weights N is large and when input data rates are high. However, the method of steepest descent can be used if the statistics describing the signal environment are perfectly known. So the gradient at any point on the performance surface can be determined exactly. The method of steepest descent can be expressed in discrete mathematical form by the following iterative relation [35, PP.158]

$$W_{k+1} = W_k - \mu \nabla (E[\varepsilon_j^2]_{W=W_k}) \tag{1.9}$$

where μ is a scalar constant determining step size and controlling the convergence and stability.

When the signal statistics describing the operational environment are stationary but unknown, then one is no longer be able to compute exactly the gradient of the performance surface at any point since the signal statistics must

now be estimated. Under these conditions the LMS algorithm introduced by Widrow has proven particularly useful [4]. The LMS algorithm is an implementation of the method of the steepest descent that employs a gradient estimation technique more efficient than derivative measurement. The error ε_j of the adaptive linear combiner of Fig.1.1 is given by (1.4). A gradient estimate may be obtained by squaring the signal value of and differentiating it as if it were the MSE:

$$\hat{\nabla}\ (E[\varepsilon_j^2]_{W=W_k}) = -2\varepsilon_j X_j \tag{1.10}$$

substituting (10) into (9) yields the LMS algorithm:

$$W_{j+1} = W_j + 2\mu\varepsilon_j X_j \tag{1.11}$$

Since a new gradient estimate is obtained with each data sample, an adaptive iteration is effected with the arrival of each sample. The index k is thus replaced with the index j. A block diagram representation of the weight adjustment rule represented by (1.11) is illustrated in Fig.1.2.

1.3 The Howells-Applebaum adaptive processor

The Applebaum algorithm maximizes a generalized SNR with the assumptions that the desired signal is absent most of the time (as in a pulsed radar or sonar system) and the direction of arrival of the desired signal is known. Because the Howells-Applebaum processor is practical to implement, it has been applied extensively in radar system to suppress jammers and clutter.

The simplest adaptive array configuration consists of a two-element array

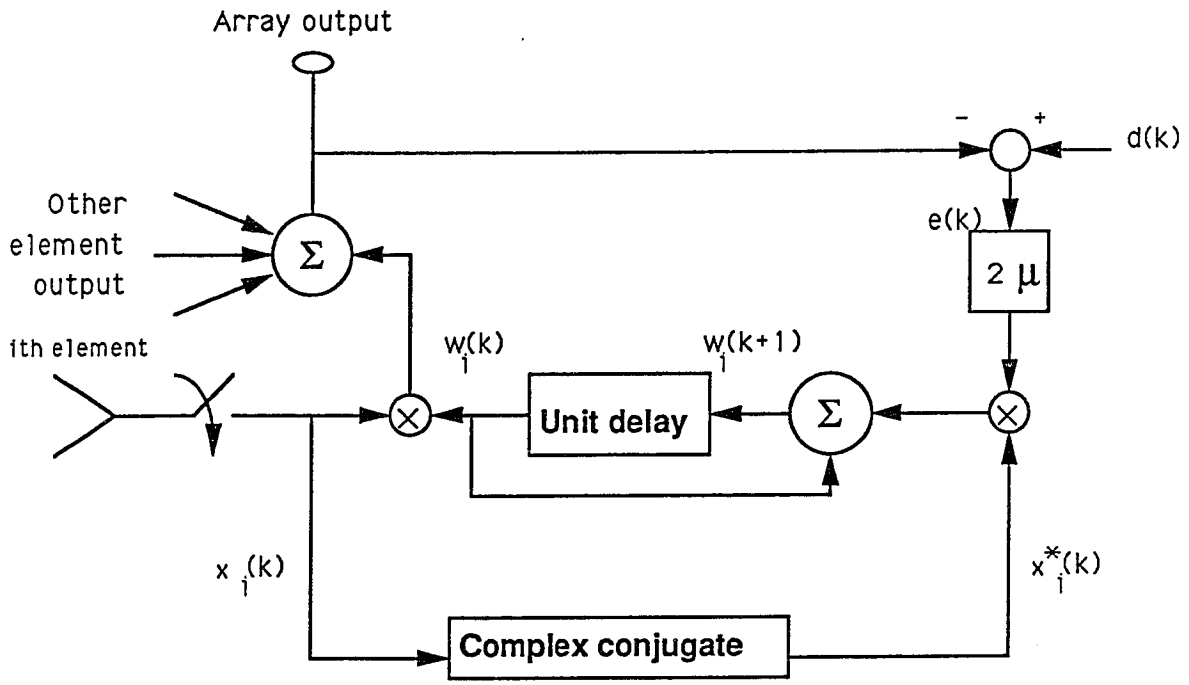

Figure 1.2 : Digital realization of the LMS weight adjustment algorithm.

with a single Howells-Applebaum adaptive loop as shown in Fig.1.3, [60]. The analysis of the loop of Fig.1.3 is carried out under the assumed condition of desired signal absence which is different from the LMS algorithm and with the notation followed by Monzingo [35, PP.217-290]. The purpose of the beam-steering b_1^* and b_2^* is to steer the received beam in a desired azimuth direction. The quiescent (initial) pattern F_0 can be written as

$$F_0(u) = \frac{1}{2}\left[w_1 e^{-j u} + w_0 e^{-j u_0}\right] = \cos(u-u_0) \tag{1.12}$$

where $u = \dfrac{\pi d}{\lambda} \sin(\theta)$

$$u_0 = \frac{\pi d}{\lambda} \sin(\theta_0)$$

$$w_1 = e^{j u_0}$$

$$w_0 = w_1^* = e^{-j u_0}$$

Now b_1^* is simply set equal to w_1, but b_2^* is related to w_0 through a gain constant c_2 (to be evaluated later), so that

$$b_2^* = c_2 w_0 = c_2 e^{-j u_0} \tag{1.13}$$

Let the sensor element signals x_1 and x_2 consist of receiver channel noise voltages n_1 and n_2 plus a statistically independent narrowband noisy signal j_i caused by a single interference source located at the angle θ_i. Furthermore assume the interference signal is abruptly turned on at time $t=0$ in a step function manner. The element signals may be described by

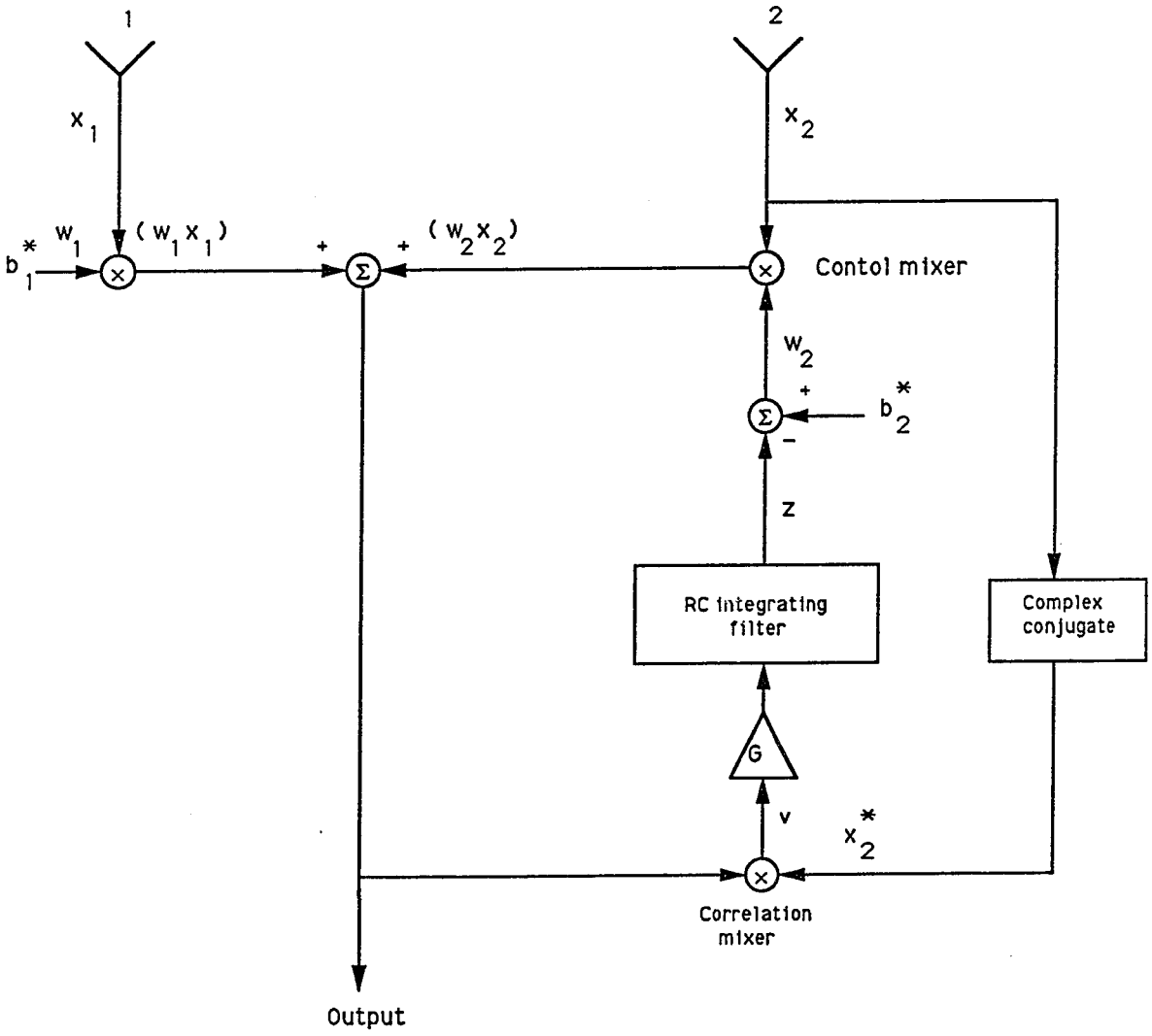

Figure 1.3 Two-element array with a single Howells-Applebaum adaptive loop. From Gabriel,[60].

$$x_1 = n_1 \qquad \text{for } t<0 \qquad (1.14)$$
$$x_2 = n_2$$

and

$$x_1 = n_1 + j_i\, e^{-ju_i} \qquad \text{for } t>0 \qquad (1.15)$$
$$x_2 = n_2 + j_i\, e^{ju_i}$$

where $u_i = \frac{\pi d}{\lambda} \sin(0_i)$

The adaptive weight w_2 is given by

$$w_2 = b_2^* - z \qquad (1.16)$$

The cross-correlator consists of the correlation mixer, amplifier, and integrator (or smoothing filter). The transient behavior of the cross-correlator may be given as, [35, PP.227],

$$\tau_0 \frac{dz}{dt} + z = Gv \qquad (1.17)$$

where G is the amplifier gain and v is the output signal from the correlation mixer. The correlation mixer output signal is given by

$$v = k^2(w_1x_1 + w_2x_2)x_2^* \qquad (1.18)$$

in which k is a mixer conversion constant.

Substituting (1.18) and (1.16) into (1.17), we then can write the filter output voltage as,

$$\tau_0 \frac{dz}{dt} + z[1 + k^2G|\bar{x}_2|^2] = k^2G|\bar{x}_2|^2.[b_2^* + \frac{w_1\overline{(x_1x_2^*)}}{|\bar{x}_2|^2}] \qquad (1.19)$$

where the overbar denotes expected value. The solution of the differential

equation represented by (1.19) is give by

$$z(t) = [z(0+) - z(\infty)]\, e^{-\alpha t} + z(\infty) \tag{1.20}$$

where,

$$z(\infty) = \frac{k^2 G|\bar{x}_2|^2 . \{b_2^* + [w_1 \overline{(x_1 x_2^*)}/|\bar{x}_2|^2]\}}{1 + k^2 G|\bar{x}_2|^2} \tag{1.21}$$

and

$$\alpha = \frac{1 + k^2 G|\bar{x}_2|^2}{\tau_0} \tag{1.22}$$

This solution of z may be substituted into (1.16) to obtain the solution of the adaptive weight $w_2(t)$.

Define the quantity w_{opt} as the optimum value of the weight w_2 which minimizes the array output noise power. If y_n is the output noise voltage, then the mean square of y_n is given by

$$\overline{|y_n|^2} = \overline{|(w_1 x_1) + (w_2 x_2)|^2} \tag{1.23}$$

Setting the partial derivative of (1.23) with respect to the weight w_2 equals to zero, then the optimum value required to minimize (1.23) is given by

$$w_{2_{opt}} = -\frac{\overline{(w_1 x_1) x_2^*}}{\overline{|x_2|^2}} = -\frac{w_1 \overline{(x_1 x_2^*)}}{\overline{|x_2|^2}} \tag{1.24}$$

The above value of $w_{2_{opt}}$ is the normalized retrodirective weight that results in placing an adapted spatial pattern null in the direction of the external interference source.

Ueno introduced a new systolic array architecture for the Howells-Applebaum array [27,28]. The proposed architecture employed the preprocessor technique. The Gram-Schmidt processor was used as the preprocessor. It has been shown that the orthogonality in the Gram-Schmidt processor output signals can eliminate the global signal feedback loop for the Howells-Applebaum array and that the systolic array architecture can be used to implement the Howells-Applebaum processor.

As conclusion, the Howells-Applebaum adaptive processor that maximize the output SNR is very closely related to the LMS algorithm. The Howells-Applebaum processor is generally employed in situation where the desired signal is usually absent and makes use of the beam-steering vector instead of a reference signal. In contrast to LMS algorithm which require that the desired signal be present.

1.4 Adaptive nulling using multimode feed horn antenna

The concept of adaptive nulling by means of multimode feed horn antenna is considered to be new. Most of the multimode designs in the past have concentrated on the reduction of sidelobe levels. T. V. Ho and J. Litva developed a technique for implementing adaptive nulling of interfering signal which is based solely on a single feed horn antenna [30]. The model uses a multimode feed antenna in which various modes are generated or extracted by means of slot coupling. Adaptive nulling is then carried out by treating each mode as an element of a phased array antenna.

With the proper choice of modes and design parameters for the feed horn antenna, the authors showed that wide bandwidth, low sidelobe levels, and high signal to noise and interference ratio (SNIR) can be achieved with the new beamforming method. This technique demonstrated that in adaptive antennas, a single feed horn antenna can substitute for an array of antenna elements.

1.5 Synthesis techniques

Synthesis techniques which provide control of the nulls of the antenna pattern are of interest for two reasons. First, they represent generalizations of classical pattern synthesis techniques, which deal with the main beam shape and the side lobe envelope, but neglect the detailed sidelobe structure. The second reason is that they provide insight into adaptive antenna systems. Several methods for synthesis of array antenna patterns with prescribed nulls exist in the literature.

1- Full amplitude/phase control method

The most efficient method is based on full amplitude and phase control at each array element, which is a very costly choice. A typical adaptive amplitude and/or phase control configuration is shown in Fig.1.4-a. The method for pattern null synthesis starts from a given original pattern $F_0(u)$, with desired main beam and sidelobe envelope, corresponding to a given element coefficients $\{a_n\}$ and an initial interelement equal spacing d. These element coefficients are then perturbed such that the perturbed pattern has nulls at the desired

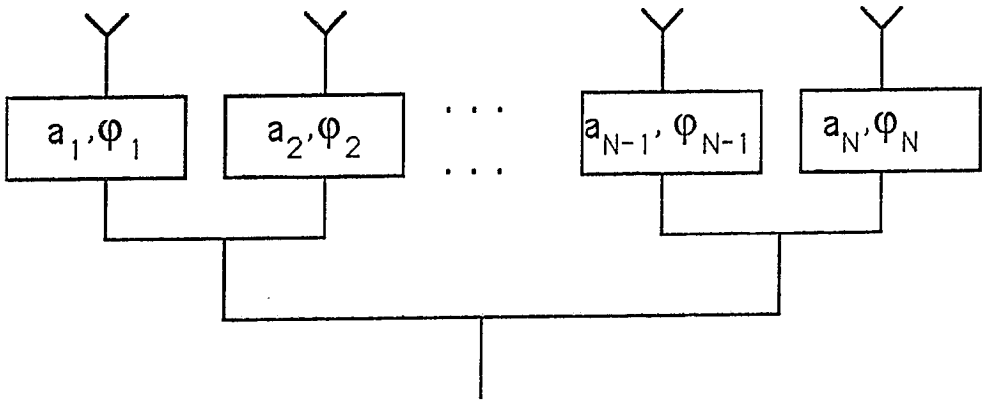

(a)

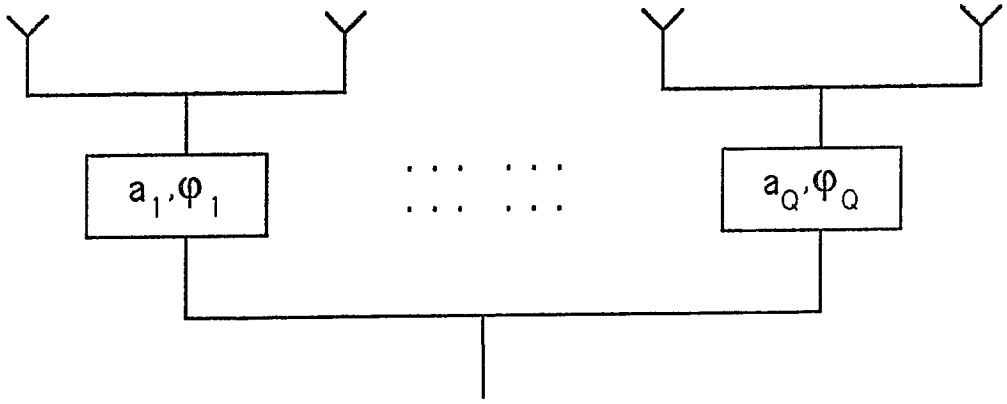

(b)

Figure 1.4 : a) Typical adaptive amplitude and/or phase control configuration.

b) Typical adaptive subarray control configuration.

directions, where their locations are assumed to be known. A detailed discussion of this technique is given in chapter two.

2- Phase-only control method

A second alternative for synthesis of array patterns with prescribed nulls is through perturbation of the element phases only. This subject is of great practical interest, and several publications have appeared in the literature [12-13, 24, 25]. Further work had been done by many authors to study and develop this method [32].

The case with small phase perturbations are distinguished from that of arbitrary large phase values. The case with small phase perturbations are achieved by placing a relatively small number of nulls in the region of low sidelobes constitutes a relatively modest pattern perturbation. A more detailed discussion of small phase only nulling technique is given in chapter two. This method which is based on the small phase perturbations approximation is satisfactory for most situations. However, a general limitation of this approach is that it is incapable of realizing two nulls which are imposed perfectly symmetrically about the main beam.

Generally, large phase perturbations are required when a null is imposed in the main beam vicinity, when two nulls are imposed symmetrically about the main beam, when multiple nulls are imposed within a relatively narrow angular sector, or when the number of nulls become large relative to the array element

number. Large phase perturbations null synthesis problem seems amenable only to numerical solution. With the nonlinear programming algorithm VMCON [9]. The solution of null synthesis for this case can be obtained. The symmetry of the original pattern will be lost in the perturbed pattern. This approach solves the problem at the cost of main beam gain and substantial increase in sidelobe level over the rest of the pattern.

3- Nulling with limited number of degrees of freedom

Large arrays require expensive hardware or a lot of time to form the nulls. In contrast, the nulls can be formed quickly if there are receivers or correlators at every element,which is not part of the antenna and must be added at considerable cost.

Frequently the number of required nulls is much smaller than the number of the array element. In this case, null synthesis method with a reduced number of degrees of freedom become more suitable. Two approaches to implement complex amplitude control are known, at either selected elements in the array or at the subarray level.

a) Nulling at the subarray level

This approach reduces either the amount of extra hardware or time to form the null. Often a large array is divided into subarrays in order to place delay units at the subarray outputs [15], as shown in Fig.1.4-b. Time delay units are very expensive and bulky so they are usually not placed at every element in the

array. Thus only the subarray outputs receivers have a time delay. The problem of pattern distortion due to the subarray nulls limits this method However, the criterion for pattern null synthesis with subarray case can be given as [9],

$$f(u_m) = f_0(u_m) + \sum_q^Q \delta_q \sum_p^P a_{0pq}\, e^{j k d_{pq} u_m} = 0, \qquad m = 1, \ldots, M$$

$$\sum_q |\delta_q|^2 = \min. \tag{1.25}$$

Where the array is partitioned into Q subarrays with P elements per subarray. The subscript pq denotes the pth element in the qth subarray and δ_q is the weight perturbation of each subarray.

The amount of distortion to the far-field antenna pattern is inversely proportional to the subarray far-field pattern. Thus, Subarray nulls near the main beam produces little distortion. However, the distortion increases dramatically when the null is placed far from the main-beam.

b) Partially adaptive array method

The second approach is to implement full amplitude/phase control at a number of selected elements in the array [16-18]. The criterion for pattern null synthesis with Q selected elements is given as [9],

$$f(u_m) = f_0(u_m) + \sum_q a_{0q}\, \delta_q\, e^{j k d_q u_m} = 0, \qquad m = 1, \ldots\ldots, M$$

$$\sum |\delta_q|^2 = \min. \tag{1.26}$$

where the controlled elements denoted by q, have complex relative amplitude perturbation δ_q, such that their total amplitude $a_q = a_{0q}(1 + \delta_q)$, and it is

assumed that M < Q. Partial adapting array method is preferred when nulls are required in the sidelobe region. On the other hand, subarray nulling is more effective for main beam nulling.

4- Amplitude-only control method

Null steering method can be achieved by controlling the current amplitudes only which overcome some of the limitations of the phase only method while simplifying the adaptive system. So, the phase shifters are used solely for steering the main beam towards the desired signal.

Vu [19-21], achieved the null steering without using phase shifters by forcing the zeros of the array factor to occur in conjugate pairs on the unit circle in the complex plane. A brief discussion of the amplitude nulling technique is given in chapter two.

1.6 Experimental realization

The LMS algorithm applies the method of steepest descent to the MSE performance measure to obtain a simple implementation that is particularly well suited to continuous signal communication system. The LMS algorithm requires the generation of a reference signal that is compared with the array output to form an error signal. The heart of the LMS loop is the correlator (multiplier), which forms the product $e(t)\,x_i(t)$ that is required to obtain the estimated gradient. Therefore, N correlators are required to implement the LMS algorithm

to control N element array. The detailed discussion of the results may be found in Monzingo [35, PP.207-211].

Because the Howells-Applebaum processor is practical to implement, it has been applied extensively to the problem of clutter and interference rejection in radar system. The Howells-Applebaum processor is studied in detail in many references [11,35, PP.217-290]. Each element of an N element linear array has an associated adaptive loop for weight adjustment purposes similar to that shown in Fig.1.3.

The basic operation of phase only nulling was proved experimentally by Braid and Rassweiler, [10]. A breadboard, null steering, linear array consists of 16 C band elements, at 4.4-4.6 GHz. The phase sifters were 4-bit, PIN diodes plus a vernier varactor phase shifters with effectively five more bits. A general computer was controlling the array phase shifters. Both beam space and other general algorithms had been tested with uniformly current distribution. The experimental results demonstrated that the phase only nulling is an interesting theoretical concept and also of practical value.

On the other hand, the experimental work for synthesis technique is rarely found in the literature. However, R. Haupt implemented a fully adaptive phase-only gradient search algorithm that simultaneously places nulls in the sum and difference patterns of a low sidelobe monopulse antenna [54]. The algorithm was experimentally verified using 80 element low sidelobe linear array with 8 bit phase shifters.

The same authors Haupt and Shore accomplished an experiment on the partially adaptive nulling in a low sidelobe phased array, [55]. A linear array antenna of 80 H-sectoral horn radiators was used. Adaptive cancellation was performed by minimizing the total array output power using the gradient search algorithm. A single CW noise signal had been considered for all cases. The experimental results showed the effectiveness of the method in placing a pattern null at the prescribed location.

Also, Vu with Thai, and Lau implemented an experiment to prove the amplitude only null steering, [56]. The array consists of 8 microstrip antennas which are connected to a back of 3-bit digital phase shifters and a bank of digitally controlled attenuators. The phase shifters were used solely for steering the main beam of the radiation pattern, whereas null steering was independently achieved by using the digitally controlled attenuators.

1.7 Proposed method for null steering

In this work we develop a different technique, where the process of null steering is carried out by controlling the element positions. In this way the amplitudes and phases of the array elements can be solely used for controlling the pattern structure and directing the main beam for maximum signal reception. The suggested method starts from a given original pattern $F_0(u)$, with desired main beam and sidelobe envelope, corresponding to a given element coefficients $\{a_n\}$ and an initial interelement equal spacing d_0. These element

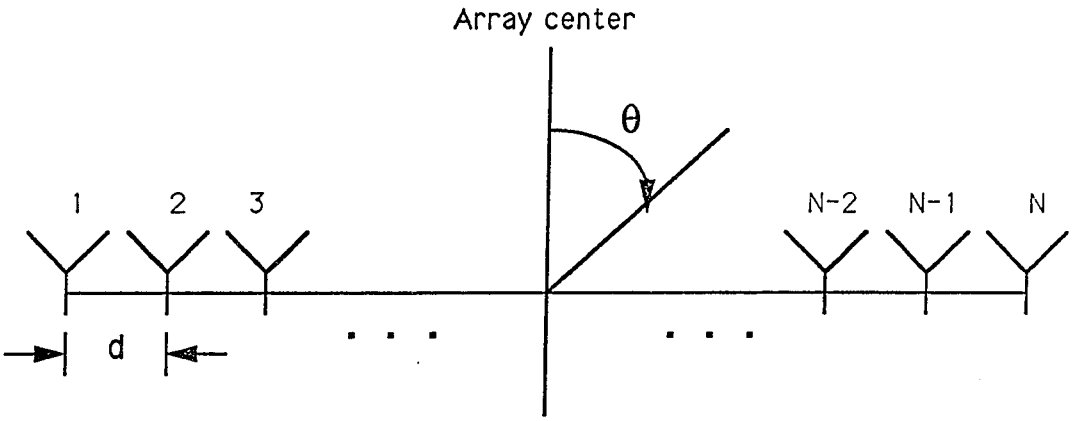

Figure 1.5: Geometry of an isotropic equipanel linear array.

positions are then perturbed such that the perturbed pattern has nulls at the desired directions, where their locations are assumed to be known. Fig.1.5 shows a typical geometry of a linear array of N equally spaced elements. Then the array factor F takes the well known expression as given below,

$$F = \sum_{n=1}^{N} a_n e^{j d_n u} \tag{1.27}$$

where, a_n is the current excitation

$$d_n = d_0 (n - \frac{N}{2} - .5)$$

d_0 : the interelement spacing in wave lengths

u : $k \sin(0)$, 0: angle from broadside

k : wavenumber $(\frac{2\pi}{\lambda})$

Assume a position change of Δ_n will produce the required nulls in the far field pattern. The new element positions are represented by

$$x_n = d_n + \Delta_n \tag{1.28}$$

Substituting (1.28) into (1.27) gives,

$$F(u) = \sum_{n=1}^{N} a_n e^{j x_n u}$$

$$= \sum_{n=1}^{N} a_n e^{j d_n u} e^{j \Delta_n u} \tag{1.29}$$

Eq.(1.29) represent a nonlinear problem which does not have a closed form solution in general. The case with small element position perturbations are distinguished from that of arbitrary large perturbation values. The case with

small element position perturbations are achieved by placing a relatively small number of nulls in the region of low sidelobes constitutes a relatively modest pattern perturbation.

This new technique allows the independent steering of the main beam and the nulls to arbitrary independent directions and greatly simplifies the feed network for the adaptive array. It also possesses an even symmetry pattern cancellation which allows nulls to be imposed at symmetrical positions around the main beam. The fact that the position perturbations are symmetrical about the center of the array means that the amount of computation is reduced. In addition, the sensitive of the perturbed pattern to variation in the element position perturbations is less as the number of forming nulls increases. This technique is also capable of obtaining sidelobe cancellation and wide band signal rejection.

1.8 Line of research

The outlines of the research work presented in this thesis are as follows

1) Formulation of the new technique of null steering by controlling the element positions only.

2) Solving for the element position perturbations to steer the nulls in the prescribed directions using this technique.

3) Testing the validity of the developed method.

4) Studying the basic capabilities of this new method as far as,

   a) Effects of varying the number of nulls on the array performance.

b) Effects of varying the pattern type on the array performance.

c) Testing the pattern sensitivity with respect to the values of the perturbed element positions.

d) Effects of main beam steering angle on the array performance. Also, the array parameters such as the half-power beam width (HPBW), array directivity, range of steering angle to avoid formation of grating lobes for different interelement spacing.

e) The capability of this method to generate two nulls, one very close to the main beam and the other very far.

5) Investigation of the capability to suppress wide band interfering signals, and sidelobe cancellation by element position perturbations.

6) A small array will be tested experimentally to verify the concept of null formation due to position perturbations. The initial pattern will be experimentally verified. Also, arbitrary nulls will be imposed in arbitrary directions and the experimental patterns will be compared to the predicted ones.

CHAPTER 2

SYNTHESIS TECHNIQUES FOR NULL STEERING

The problem of forming nulls in the radiation pattern of an antenna, in order to suppress interference from certain directions, has recently received much attention. Most of this work is in the area of adaptive nulling systems, as discussed by Applebaum [3], where the (SNR) is maximized as the performance index. In the case where the jammers are the dominant noise source this process automatically places pattern nulls in the directions of jammers. Drane and McLlvenna [40] used a different approach where the antenna gain index is maximized, subject to a set of null constraints on the pattern. In both methods the performance index is the quantity of prime interest, rather than the antenna pattern shape.

On the other hand, synthesis techniques which provide control of the null of the antenna pattern represent generalizations of classical pattern synthesis techniques, which deal with the main beam shape and the sidelobe envelope, but neglect the detailed sidelobe structure. Also they provide insight into adaptive antenna system [9,19-26].

As mentioned in chapter one, pattern control in an array antenna can be achieved in various ways. In this chapter the features of the full amplitude and phase, phase-only and amplitude only methods will be discussed. In the following discussion we consider a linear array of N equispaced isotropic elements as shown in Fig.1.5. The spacing between the elements is d_0 and the phase reference center is taken to be the center of the array. Letting w_{0n}, be the initial complex weight of the n'th array element, the array field pattern,

$$F_0(u) = \sum_{n=1}^{N} w_{0n}\, e^{j d_n u} \tag{2.1}$$

where, $d_n = d_0 (n - \frac{N}{2} - 0.5)$

and $u = k \sin(0)$, 0 : angle from broadside

with k : wave number $= \frac{2\pi}{\lambda}$

Assuming the element excitations are adjusted according to a gain amplitude taper a_n, n = 1, 2, ..., N, and a direction u_s for the array pattern maximum (look direction), then the initial array coefficients are

$$w_{0n} = a_n\, e^{-j d_n u_s} \tag{2.2}$$

2.1 Full amplitude and phase method

In the following analysis an array of N elements is used to locate M nulls in the directions of interfering signals (jammers) by means of full amplitude and phase perturbations. It is assumed that M < N. Assume the array pattern

maximum is in the broadside direction, $u_s = 0$. In this case where both the amplitude and the phase of the element weights can be perturbed from their original values, the perturbed coefficients can be represented as,

$$w_n = a_n + \Delta w_n \tag{2.3}$$

where, $\Delta w_n = a_n (\delta_n + j \varphi_n)$.

The first term on the right hand side of Eq.(2.3) is the initial value of the n'th element weight a_n, and the second term is the perturbation of the weight. The perturbed array field pattern is then,

$$\begin{aligned} F(u) &= \sum_{n=1}^{N} w_n e^{j d_n u} \\ &= \sum_{n=1}^{N} a_n e^{j d_n u} + \sum_{n=1}^{N} \Delta w_n e^{j d_n u} \\ &= F_0(u) + F_c(u) \end{aligned} \tag{2.4}$$

where $F_0(u)$ is the original or unperturbed array pattern as given in Eq.(2.1) and $F_c(u)$ is the cancellation pattern which is given by,

$$\begin{aligned} F_c(u) &= \sum_{n=1}^{N} \Delta w_n e^{j d_n u} \\ &= \sum_{n=1}^{N} a_n (\delta_n + j \varphi_n) e^{j d_n u} \end{aligned} \tag{2.5}$$

However, M nulls are required in the pattern to cancel M jammers at angular location u_m, $1 \le m \le M$. Therefore, the resultant field equals zero when $u = u_m$,

$$F(u_m) = F_0(u_m) + F_c(u_m) = 0 \quad , m = 1,2,....M$$

or

$$F_c(u_m) = - F_0(u_m) \tag{2.6}$$

The above system of equations has 2N unknowns and 2M equations [considering the real and imaginary parts of Eq.(2.6) separately]. In practice, because the number M of prescribed nulls is less than N (the number of array elements), the equation system as it stands does not have a uniquely determined solution. A further requirement (or requirements) must be imposed on the solution to yield a unique solution.

Because we desire to keep the weight perturbations as small as possible, two types of approximation criteria are considered in the literature [9,24]. The first is to find the solution to Eq.(2.6) which minimizes the sum of squares of the absolute values of the weight perturbations relative to the original weights.

Thus for the case with full amplitude and phase control the final system of equations can be written as,

$$F_c(u_m) = - F_0(u_m) \tag{2.7-a}$$

$$\sum_{n=1}^{N} |\delta_n + j\,\varphi_n|^2 = \min. \tag{2.7-b}$$

Eq.(2.7-a) ensures that the the synthesized pattern has nulls at the desired direction u_m, and 2.7-b ensures that the array excitation is only minimally perturbed.

The solution for the perturbed elements coefficients [9]

$$\Delta w_n = a_n^2 \sum_{m=1}^{M} \gamma_m\, e^{-j\, d_n\, u_m} \tag{2.8}$$

where the beam coefficients γ_m are determined from an M'th order system of

linear equations 2.7-a. Substituting (2.8) in (2.5) we get,

$$F_c(u) = \sum_{m=1}^{M} \gamma_m \sum_{n=1}^{N} a_n^2 \, e^{j d_n (u - u_m)} \tag{2.9}$$

Accordingly the perturbed pattern equals the original pattern plus the sum of M cancellation beams each corresponding to a taper of the amplitude of the element excitations proportional to the square of the original amplitude taper and with a pattern peak in the direction of one of the desired null locations.

The second condition is to find the solution to Eq.(2.6) which minimizes the sum of squares of the absolute values of the total weight perturbations. For this case the system of equations can be written as,

$$F_c(u_m) = - F_0(u_m) \tag{2.10-a}$$

$$\sum_{n=1}^{N} |a_n^2 (\delta_n + j \varphi_n)|^2 = \min. \tag{2.10-b}$$

The solution for the perturbed elements coefficients [9],

$$\Delta w_n = \sum_{m=1}^{M} \gamma_m \, e^{-j d_n u_m} \tag{2.11}$$

where the beam coefficients γ_m are determined from the system of linear equations 2.10-a . And the cancellation pattern is obtained by substituting Eq.(2.10) in (2.5),

$$F_c(u) = \sum_{m=1}^{M} \gamma_m \sum_{n=1}^{N} e^{j d_n (u - u_m)} \tag{2.12-a}$$

$$= \sum_{m=1}^{M} \gamma_m \frac{\sin[N \, d_n (u - u_m)/2]}{\sin[d_n (u - u_m)/2]} \tag{2.12-b}$$

Thus , the perturbed pattern is equal to the sum of the original pattern and M cancellation beams each corresponding to a uniform amplitude distribution of the element excitations and with a peak in the direction of the null locations.

The above solution is also the solution that minimizes the mean square difference between the original field pattern and the perturbed field pattern [26].

2.2 Small phase perturbations

In the case where only phase perturbations of the original excitation are allowed, the perturbed coefficients are represented by,

$$w_n = a_n e^{j\varphi_n} \tag{2.13}$$

placing a relatively small number of nulls ($M << N$) in a region of low sidelobes constitutes a relatively modest pattern perturbation and therefore it is reasonable to expect that the associated phase perturbations are small, $|\varphi_n| << 1$. Thus, a two term Taylor expansion of the phase term in 2.13 leads to

$$w_n \approx a_n (1 + j\varphi_n) \tag{2.14}$$

when Eq.(2.14) is substituted in (2.4), then the perturbed array pattern is given by,

$$\begin{aligned} F(u) &= F_0(u) + j \sum_{n=1}^{N} a_n \varphi_n e^{j d_n u} \\ &= F_0(u) + F_c(u) \end{aligned} \tag{2.15}$$

where $F_0(u)$ the initial pattern given by Eq.(2.1) and $F_c(u)$ the cancellation pattern given as,

$$F_c(u) = j \sum_{n=1}^{N} a_n \varphi_n e^{j d_n u} \tag{2.16}$$

For M nulls in the pattern, the equation system has 2M equations with N unknowns (considering the real and imaginary parts) and hence, as in the case of perturbations of both amplitude and phase, a unique solution to the system of equations can be obtained only if a further requirement is imposed on the solution. As above we have two cases which are most common in the literature. The first corresponding to the requirement that the solution minimizes the sum of the squares of the phase perturbations. Then , for this case the system of equations is given by,

$$F(u_m) \approx F_0(u_m) + j \sum_{n=1}^{N} a_n \varphi_n e^{j d_n u_m} = 0 \tag{2.17-a}$$

$$\sum_{n=1}^{N} |\varphi_n|^2 = \min. \tag{2.17-b}$$

which constitutes a linear problem with an analytic solution.

The solution for the perturbed element phases can be written in the form [12],

$$\varphi_n = a_n \sum_{m=1}^{M} \alpha_m \sin[d_n u_m] \tag{2.18}$$

where the coefficient α_m are determined from the M linear equations 2.17-a . The corresponding cancellation pattern can be written as,

$$F_c(u) = \sum_{m=1}^{M} \alpha_m \sum_{n=1}^{N} \frac{a_n^2}{2} [e^{j d_n (u+u_m)} - e^{j d_n (u-u_m)}] \tag{2.19}$$

The perturbed pattern is thus approximately equal to the sum of the original

pattern and the sum of differences of M pairs of cancellation beams. Each of these pairs of beams corresponds to an element amplitude taper proportional to the square of the original amplitude taper, with one member of the pair having a peak in the direction of a null location and the other member of the beam pair having a peak in the symmetric direction on the other side of the original main lobe direction. Thus the placing of nulls in the prescribed location is accompanied by doubling of the pattern at symmetric locations of the other side of the main lobe direction.

The second case, for small phase only perturbations, corresponding to the requirement that the solution minimizes the sum of the squares of the absolute values of the total weight perturbations which leads to

$$F(u_m) \approx F_0(u_m) + j \sum_{n=1}^{N} a_n \varphi_n e^{j d_n u_m} = 0 \qquad (2.20\text{-a})$$

$$\sum_{n=1}^{N} |a_n \varphi_n|^2 = \min. \qquad (2.20\text{-b})$$

The solution to the above system of equation is given as [24],

$$\varphi_n = \frac{1}{a_n} \sum_{m=1}^{M} \alpha_m \sin[d_n u_m] \qquad (2.21)$$

where the coefficients α_m are determined from the M linear Eqs.(2.20-a). Eq.(2.21) shows that the phase perturbations are inversely proportional to the amplitudes of the weights, in contrast to the minimum phase perturbations solution, Eq.(2.18), where the phase perturbations are directly proportional to the weight amplitudes.

Substituting Eq.(2.21) in (2.16), we obtain the cancellation pattern as,

$$F_c(u) = \sum_{m=1}^{M} \frac{\alpha_m}{2} \sum_{n=1}^{N} [e^{j d_n (u+u_m)} - e^{j d_n (u-u_m)}] \qquad (2.22)$$

The perturbed pattern leads to a result similar to that for minimizing the squares of the phase perturbations. It is approximately equal to the sum of the original pattern and the sum of differences of M pairs of cancellation beams as given by Eq.(2.22). Each of these pairs of beams corresponds to a uniform amplitude distribution of the element weights. As before, one member of the pair having a peak in the direction of a null location and the other member having a peak in the symmetrical direction on the other side of the original main lobe direction. Therefore, placing nulls in the prescribed location is accompanied by doubling of the pattern nulls at symmetric locations of the other side of the main lobe direction. It is also shown in [24,26], that for half-wavelength element spacing the pattern given by the sum of Eqs.(2.22) and (2.15), is also the pattern that differs least from the original pattern in a mean square sense, while having nulls at the desired locations obtained with small phase only perturbations.

2.3- Basic features of full weight and phase-only methods

In this section we discuss some of the basic features of the solutions obtained in the previous sections for both amplitude and/or phase methods. The computations were done for an array comprising 20 isotropic elements with half-wavelength element spacing. The initial pattern corresponds to a 30 dB Chebyshev taper of the element excitations. The initial array excitations are

given in Appendix D.

Figs.2.1 and 2.2 show the perturbed patterns with one null imposed at 20°. when the relative and the total weight perturbations are allowed to vary, respectively. For each of these two cases we show three graphs. Figs.2.1a and 2.2a show the perturbed pattern and Figs.2.1b and 2.2b show the corresponding cancellation pattern in the range $\theta = -90°$ to $\theta = 90°$. Figs.2.1c and 2.2c show both the perturbed and the initial patterns in the range from 0° to 50°. We see that Fig.2.1b for minimized relative weight perturbations, which corresponds to a taper of the element amplitude excitations equal to the square of the original amplitude taper, has a much broader mainlobe and much lower sidelobes than the cancellation beam in Fig.2.2b which corresponds to a uniform distribution of the element excitations. Because the cancellation pattern of Fig.2.1b is much broader than the cancellation pattern of Fig.2.2b, the initial pattern is distorted more strongly in the vicinity of the null for minimized relative weight perturbations than it is for minimized total weight perturbations, as shown in Figs.2.1c and 2.2c. And conversely that the initial pattern is distorted less strongly far a way from the null for minimized relative weight perturbations than it is for minimized total weight perturbations. However, in the mean square sense, minimizing the total weight perturbations corresponding to minimizing the MSE [24].

Figs.2.3a and 2.4a show the perturbed patterns for a single null at 20° corresponding to the perturbations of the total and the relative phases only of

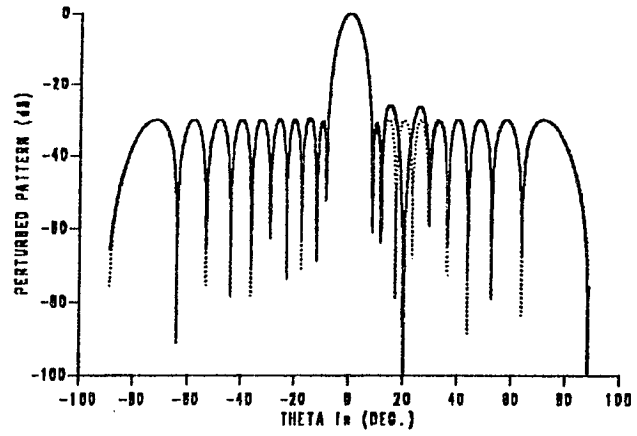

(a)

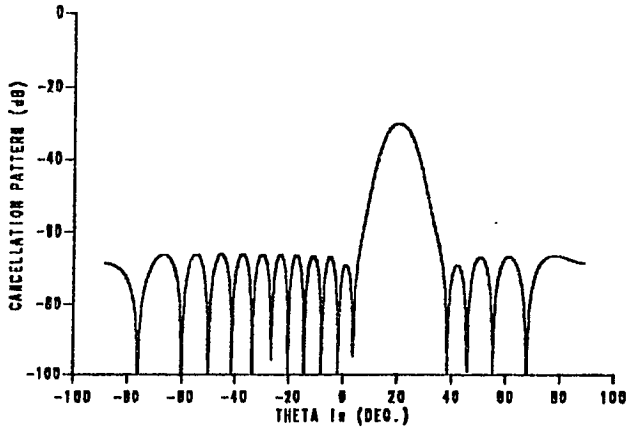

(b)

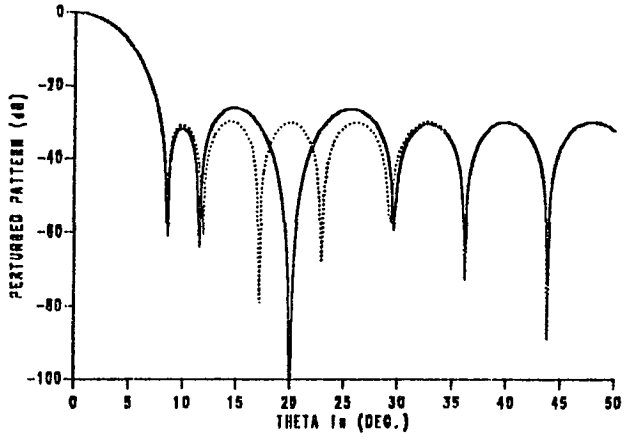

(c)

Fig.2.1 : Relative full amplitude and phase perturbations. $\sum|\frac{\Delta w_n}{a_n}|^2 = Min.$

a) Perturbed pattern (solid) with one null imposed at 20°.
b) Cancellation pattern. c) Perturbed pattern, $\theta = 0°$ *to* 50°.
Initial 30-dB Chebyshev pattern (dotted), $N = 20$, $d_0 = \frac{\lambda}{2}$.

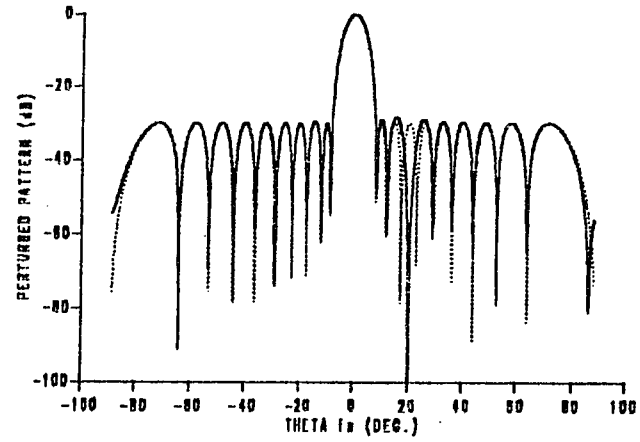

(a)

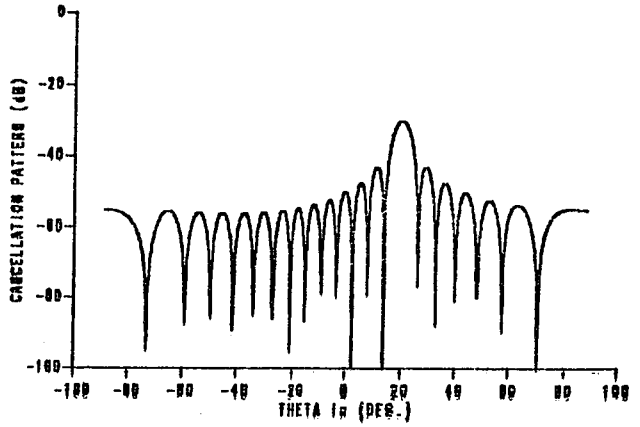

(b)

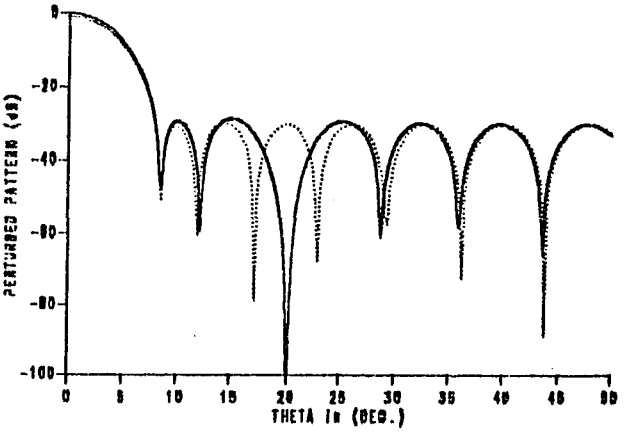

(c)

Fig.2.2 : Total full amplitude and phase perturbations, $\sum|\Delta w_n|^2 = Min$.
a) Perturbed pattern (solid) with one null imposed at 20°.
b) Cancellation pattern. c) Perturbed pattern, $\theta = 0°$ *to* 50°.
Initial 30-dB Chebyshev pattern (dotted), $N = 20$, $d_0 = \frac{\lambda}{2}$.

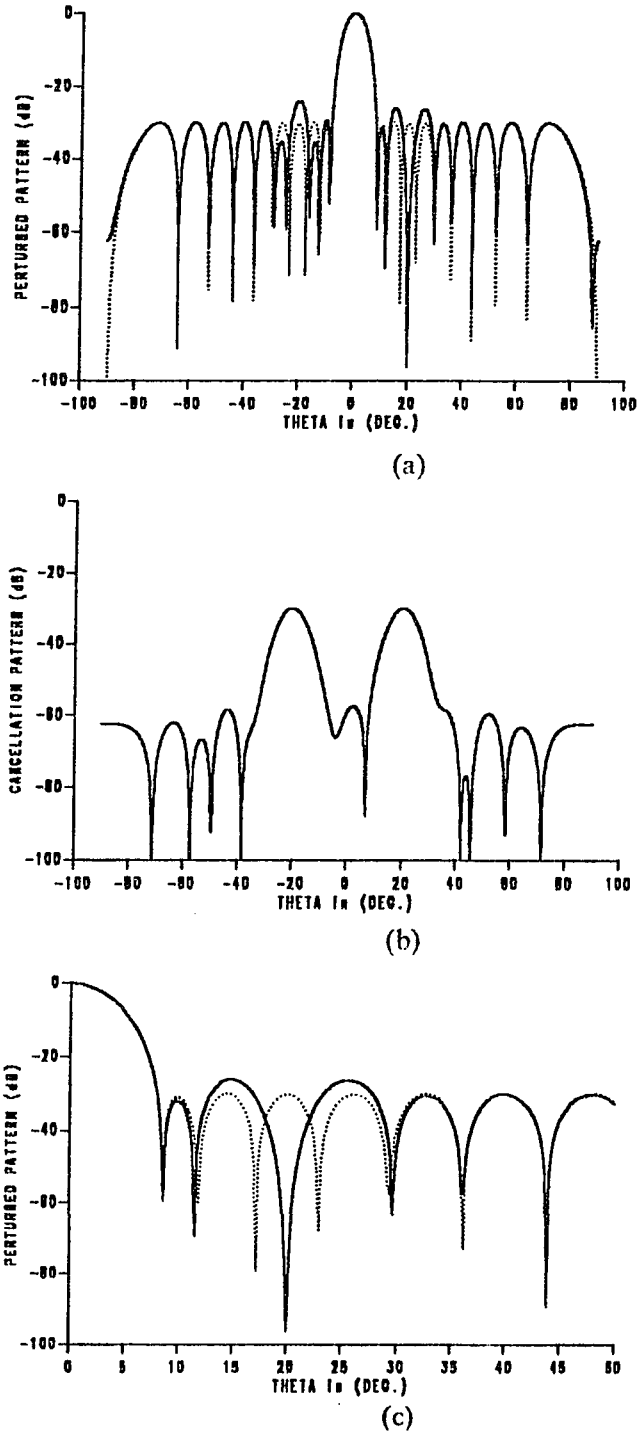

Fig.2.3 : Total phase-only perturbations. $\sum|\varphi_n|^2 = Min.$
a) Perturbed pattern (solid) with one null imposed at 20°.
b) Cancellation pattern. c) Perturbed pattern, $0 = 0°$ *to* 50°.
Initial 30-dB Chebyshev pattern (dotted), $N = 20$, $d_0 = \frac{\lambda}{2}$.

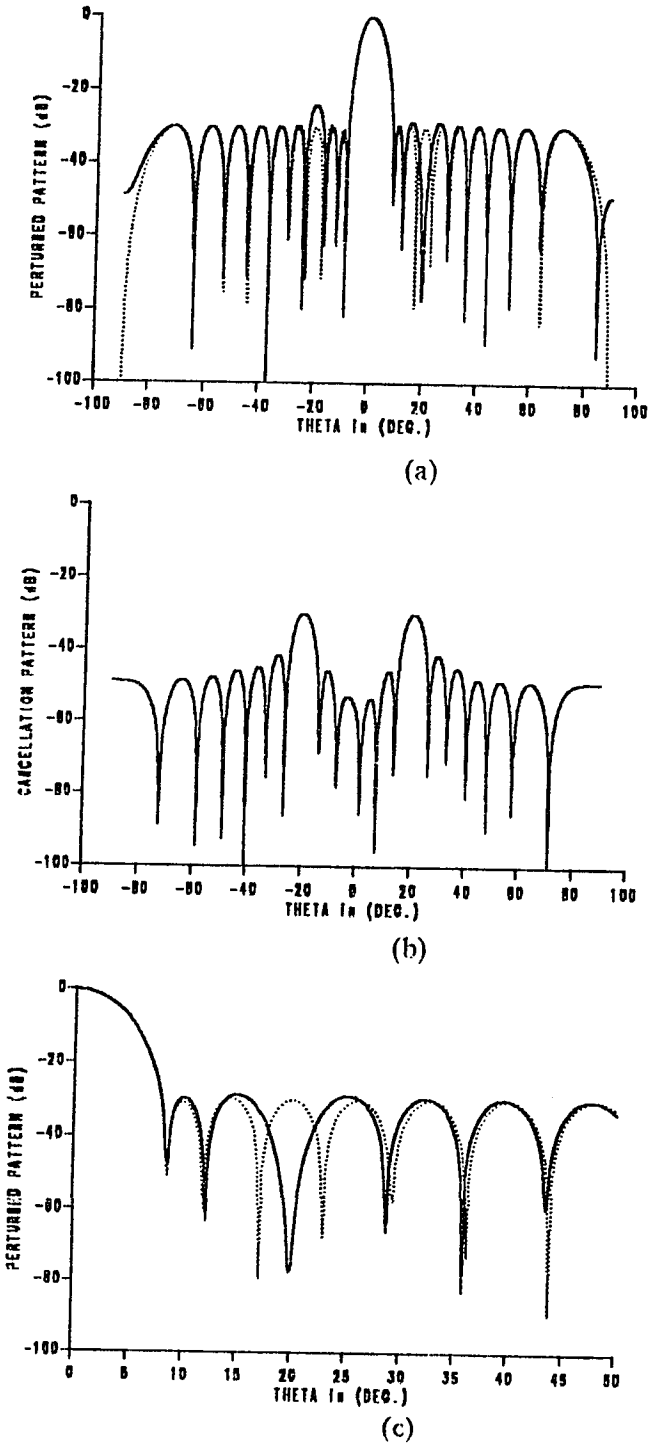

Fig.2.4 : Relative phase-only perturbations. $\sum|a_n \varphi_n|^2 = Min.$
a) Perturbed pattern (solid) with one null imposed at 20°.
b) Cancellation pattern. c) Perturbed pattern, $0 = 0°$ *to* 50°.
Initial 30-dB Chebyshev pattern (dotted), $N = 20$, $d_0 = \frac{\lambda}{2}$.

the element coefficients, respectively. The corresponding cancellation patterns for both approximation criteria for the phase only method are shown in Figs.2.3b and 2.4b. The main difference in these patterns from those in Figs.2.1b and 2.2b corresponding to full weight perturbations is that now the cancellation patterns are the superposition of two beams, one with a peak in the direction of the imposed null, and the other with a peak of opposite phase in the symmetric direction on the other side of the main beam. Hence any change in the pattern on the null side of the main beam is accomplished by an equal and opposite change on the other side of the main beam. The cancellation pattern of Fig.2.3b consists of two beams corresponding to an amplitude taper equal to the square of the original current excitations, while the cancellation pattern of Fig.2.4b consists of two beams corresponding to a uniform element current excitations. Hence the basic features of the phase only patterns for the right side of the main beam as shown in Figs.2.3c and 2.4c, are the same as those noted above for combined amplitude and phase perturbations as shown in Figs.2.1c and 2.2c.

2.4- Amplitude-only control method

Null steering can be achieved by controlling the current amplitudes only which overcome some of the limitations of the phase only method while simplifying the adaptive system. So, the phase shifters are used solely for steering the main beam towards the desired signal.

Vu [19-21], achieved the null steering without using phase shifters by forcing the zeros of the array factor to occur in conjugate pairs on the unit circle in the complex plane. Fig.1.5 shows a typical geometry of a linear array of N equally spaced elements. If the current amplitudes of the array elements are all equal, and if the phases are such that there is a constant progressive phase shift α, then the array factor F, takes the well known form which is given by,

$$F = \sum_{n=0}^{N-1} e^{jn\psi} \tag{2.23}$$

where, $\psi = k\, d_0 \sin(\theta) + \alpha$

Hence, if we let $z = e^{j\psi}$, Eq.(2.23) becomes,

$$F = 1 + z + z^2 + \ldots\ldots + z^{N-1} = \frac{(1-z^N)}{(1-z)} \tag{2.24}$$

This means all zeros of the array factor are equally spaced on the circumference of the unit circle in the complex plane. Fig.2.5 shows the distribution of the zeros of the array factor when N=8. Thus the direction of θ_i of the i'th null will satisfy the following equation:

$$\theta_i = \cos^{-1}\left[\frac{(\psi_i - \alpha)}{k\, d_0}\right]$$

where ψ_i is the angle of the i'th zero on the unit circle.

Null steering can be achieved without having to change the phase by choosing the zeros so that they occur in conjugate pairs. Thus, two cases have to be considered,

a) N= even= 2k : In this case, the expression of the array factor becomes

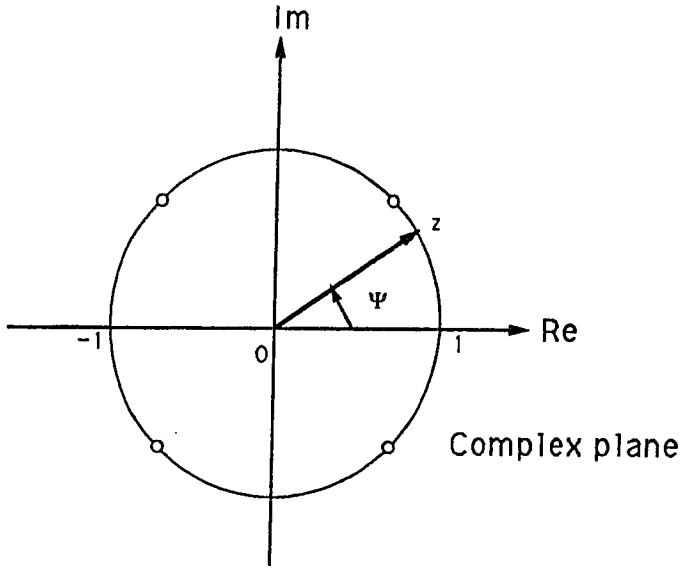

Fig. 2.5: Distributions of zeroes of array factor of eight-element uniform array.

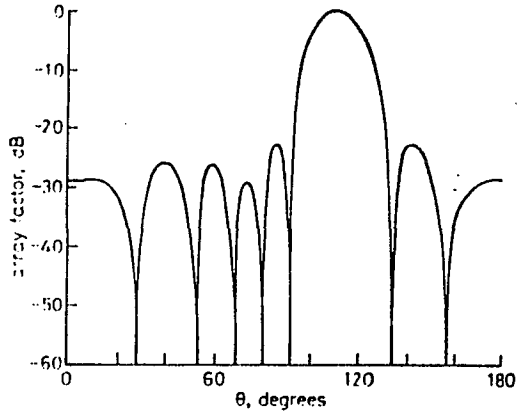

Fig. 2.6 : Perturbed pattern with three nulls imposed at 28°, 80°, and 92°. From Vu, [19]. Initial uniform current distribution, N = 8, θ_s = 112°, d_n = .5λ

$$F = (z+1)(z-z_1)(z-z_1^*).....(z-z_{k-1})(z-z_{k-1}^*) \quad (2.25)$$

b) n = odd = 2k+1 : In this case we have,

$$F = (z-z_1)(z-z_1^*).....(z-z_k)(z-z_k^*) \quad (2.26)$$

Each product $(z-z_i)(z-z_i^*)$, has real coefficients. It is clear that the array factor also has real coefficients A_i of z_i, which are the current amplitude of the $(i+1)$'th element of the array. However, this is achieved at a price, namely the total number of arbitrary nulls that can be created is effectively halved.

For an example consider the case of an eight element linear array with element spacing $d_0 = \frac{\lambda}{2}$. The array pattern as given by Eq.(2.25) can be written as

$$F(z) = 1 + A_1 z + A_2 z^2 + ... + A_1 z^6 + z^7 \quad (2.27)$$

The coefficients A_i's, can be obtained from Eq.(2.25) directly or by using the iterative method derived by Vu [19]. Fig.2.6 shows the perturbed pattern with three nulls imposed at 28°, 80°, 92° respectively, where the desired signal direction is 112° as given in the above reference. It can be seen that the main beam is pointing directly towards the desired signal, while the nulls are steered to the exact direction of the interferences. Thus the main advantage is that the phase shifters can be used solely for steering the main beam to the direction of the desired signal.

CHAPTER 3

NULL STEERING IN PHASED ARRAYS BY CONTROLLING THE ELEMENT POSITIONS

In this work, we solve the problem of null steering in phased and adaptive arrays, using a new method. Both amplitudes and phases of the original array are kept unchanged from their original values obtained from synthesizing the unperturbed array pattern. The nulls are formed in the desired directions by means of perturbations to the element positions. This approach is based on direct synthesis of array pattern with the array nulls in the desired directions, in contrast to the usual iteration solution resulting from used adaptive algorithms. A set of element positions $\{x_n\}$ is determined which, subject to the null constraints, best approximates a given set of element positions $\{d_n\}$. The problem associated with this method is generally nonlinear but can be linearized by assuming that the required element position perturbations are small. The small perturbations assumption is valid in certain applications involving null placement in low sidelobe regions. First, exact solutions are obtained for the perturbed element positions based on small perturbations assumption and with a generalized approximation criteria, where the sum of the squares of the

weighted element position perturbations is minimized; that is,

$$\sum_{n=1}^{N} \frac{[a_n (x_n - d_n)]^2}{y_n^2}$$

where y_n is an arbitrary non-zero coefficient. Then, particular solutions are obtained for two types of approximation criteria

a) minimizing the sum of the squares of the total element position perturbations; that is, $\sum(x_n - d_n)^2 = \text{Min.}$

b) minimizing the sum of the squares of the relative element position perturbations; that is, $\sum[a_n (x_n - d_n)]^2 = \text{Min.}$

The solution for all cases are interpreted as pairs of cancellation beams superimposed on the initial pattern. Mean while the theoretical results of this method will be compared with the corresponding full amplitude and phase and phase-only methods. In this work, we are not concerned with the various methods of locating the undesired sources.

3.1. Pattern nulling by element position perturbations

A linear array of N isotropic equispaced elements is considered, which has the pattern,

$$F_0(u) = \sum_{n=1}^{N} a_n e^{j d_n (u - u_s)} \tag{3.1}$$

where, a_n is the n'th element excitation

$$d_n = d_0 \left(n - \frac{N}{2} - 0.5\right)$$

d_0 : the interelement spacing in wave lengths

$u = k \sin(\theta)$, θ: angle from broadside

k : wave number $(\frac{2\pi}{\lambda})$

$u_s = k \sin(\theta_s)$, θ_s : steering angle from broadside direction.

The corresponding geometry is shown by Fig.1.5. Because the element positions reference center is taken to be the center of the array, the element positions, d_n, have odd symmetry with respect to the array position reference center that is,

$$d_n = -d_{N-n+1} \quad , n = 1,2....,N$$

The suggested method starts from a given original pattern $F_0(u)$, with desired main beam and sidelobe envelope, corresponding to a given element coefficients $\{a_n\}$ and an initial interelement equal spacing d_0. These element positions are then perturbed such that the perturbed pattern has nulls at the desired directions, where their locations are assumed to be known.

Assume a position change of Δ_n will produce the required nulls in the far field pattern. The new element positions are represented by

$$x_n = d_n + \Delta_n \tag{3.2}$$

when there is no position change, $\Delta_n = 0$, then $x_n = d_n$. The perturbed pattern corresponding to the perturbed element positions, x_n, can be written as,

$$F(u) = \sum_{n=1}^{N} a_n e^{j x_n (u-u_s)}$$

$$= \sum_{n=1}^{N} a_n e^{j\Delta_n (u-u_s)} e^{j d_n (u-u_s)} \tag{3.3}$$

The above result can be written as,

$$F(u) = \sum_{n=1}^{N} w_n e^{j d_n (u-u_s)} \tag{3.4}$$

where,

$$w_n = a_n e^{j \Delta_n (u-u_s)}$$

Eq.(3.4) shows that the perturbed pattern can be expressed as if the original current coefficients $\{a_n\}$, are perturbed to have the values $\{w_n\}$, which places nulls in the prescribed directions.

In general, M nulls are required in the pattern to cancel M jammers at angular location u_m, $1 \le m \le M$. We now wish to determine the perturbations Δ_n to place nulls at the M locations u_m, or equivalently to find the solution to the equation system,

$$F(u_m) = \sum_{n=1}^{N} a_n e^{j\Delta_n (u_m-u_s)} e^{j d_n (u_m-u_s)} = 0 \tag{3.5}$$

Equation (3.5) represents a nonlinear problem which does not necessarily have a solution. The problem can be simplified if the number of required nulls is small compared to the number of elements, where they are imposed in the sidelobe region.

3.2. Small element position perturbations

Placing a relatively small number of nulls ($M << N$) in a region of low sidelobes constitutes a relatively modest pattern perturbation and therefore it is reasonable to expect that the associated element position perturbations, $|\Delta_n|$ is

small compared to the interelement spacing. In this case, if the phase which is achieved from the element position perturbations are also small,

$$|\Delta_n (u-u_s)| << 1,$$

then using two term Taylor expansion, the result of Eq.(3.3) can be approximated as,

$$F(u) \approx \sum_{n=1}^{N} \{a_n e^{jd_n (u-u_s)} [\, 1 + j\, \Delta_n (u-u_s)\,]\}$$

$$= F_0(u) + F_c(u) \tag{3.6}$$

where, F_c is the cancellation pattern given as,

$$F_c(u) = j(u-u_s) \sum_{n=1}^{N} \Delta_n a_n e^{jd_n (u-u_s)} \tag{3.7}$$

For the case of small element position perturbations the perturbed coefficients $\{w_n\}$ can be written as,

$$w_n \approx a_n [\, 1 + j\, \Delta_n (u-u_s)\,] \tag{3.8}$$

So that the coefficient perturbations are given as,

$$\Delta w_n = a_n - w_n \approx j\, a_n \Delta_n (u-u_s)$$

Because we are interested in the case of real symmetric coefficient and hence to real symmetric pattern $F_0(u)$ which can be written as,

$$F_0(u) = \sum_{n=1}^{N} a_n \cos[d_n (u-u_s)] \tag{3.9}$$

As mentioned before, M nulls are required in the pattern to cancel M jammers at angular location u_m, $1 \le m \le M$. Therefore, the resultant field pattern equals zero when $u = u_m$. Substituting this result in Eq.(3.6) to get,

$$F(u_m) = F_0(u_m) + j\,(u_m - u_s) \sum_{n=1}^{N} \Delta_n\, a_n\, e^{j\, d_n (u_m - u_s)} = 0$$

or

$$F_0(u_m) = -j(u_m - u_s)\,\{\sum_{n=1}^{N} \Delta_n\, a_n \cos[\, d_n\,(u_m - u_s)\,] + j \sum_{n=1}^{N} \Delta_n\, a_n \sin[\, d_n\,(u_m - u_s)\,]\,\} \qquad (3.10)$$

Equating the real and imaginary parts of both sides in Eq.(3.10), we get,

$$\sum_{n=1}^{N} \Delta_n\, a_n \sin[\, d_n\,(u_m - u_s)\,] = \frac{F_0(u_m)}{(u_m - u_s)} \qquad (3.11\text{-a})$$

$$\sum_{n=1}^{N} \Delta_n\, a_n \cos[\, d_n\,(u_m - u_s)\,] = 0 \qquad (3.11\text{-b})$$

This equation system has 2M equations for N unknowns and hence a unique solution to the system of equations can be obtained only if a further requirement is imposed on the solution, where the number of unknown element position perturbations is assumed greater than twice the number of null locations. At this point we treat the generalized case specified in the introduction of this chapter. The treatment of this case is based on the following theorem which can be found in [44, PP.46],

Theorem:

Let A be an $M \times N$ complex matrix of rank M, $M \leq N$, Y an $N \times N$ real matrix of full rank N, and B is any $M \times 1$ vector, then the solution, X, of the problem:

$$\min.\ X^{\dagger}YX$$

$$\text{such that } AX = B$$

is

$$X = Y^{-1}A^{\dagger}(AY^{-1}A^{\dagger})^{-1}B \tag{3.12}$$

where † represents the Hermitian transpose operator.

Proof: (see Theorem 3.1.3, PP.46, [44])

We shall need in the sequel the following immediate remark.

Remark:

It is easy to observe that the components of the X solution of the above minimization problem are a linear combination of the columns of $Y^{-1}A^{\dagger}$, with coefficients from C,

$$C = (AY^{-1}A^{\dagger})^{-1}B \tag{3.13}$$

3.3 General minimum weighted norm solution

As mentioned before a general weighted sum of squares

$$\sum_{n=1}^{N} \frac{(a_n \Delta_n)^2}{y_n^2} \tag{3.14}$$

is considered in this Section, where y_n is an arbitrary non-zero coefficient. The problem here is to find the set of element position perturbations Δ_n, that will locate the nulls at certain prescribed locations $u = u_m$, $m = 1,2..., M$ and at the same time minimizes Eq.(3.14) for the given set of non-zero coefficient y_n. The

constraints for nulls on the perturbed pattern at prescribed locations is given by Eq.(3.11). So that we wish to find the set of element position perturbations Δ_n satisfying (3.11) and minimizing (3.14). The mathematical expression of the previous problem can be written in the form

$$\sum_{n=1}^{N} \Delta_n a_n \sin[\, d_n (u_m - u_s)\,] = \frac{F_0(u_m)}{(u_m - u_s)} \qquad (3.15\text{-a})$$

$$\sum_{n=1}^{N} \Delta_n a_n \cos[\, d_n (u_m - u_s)\,] = 0 \qquad (3.15\text{-b})$$

$$\sum_{n=1}^{N} \frac{(a_n \Delta_n)^2}{y_n^2} = \min. \qquad (3.15\text{-c})$$

Let us obtain the solution for Eqs.(3.15-a) and (3.15-c) first. The problem can be expressed in terms of finding the vector of weighted position perturbations

$$X = [\, (a_1\Delta_1), (a_2\Delta_2), \ldots\ldots\ldots\ldots, (a_N\Delta_N),\,]^T$$

satisfying the equation system,

$$A\,X = B \qquad (3.16\text{-a})$$

and minimizing

$$X^T\,Y\,X \qquad (3.16\text{-b})$$

where A is the $M \times N$ matrix

$$A = \begin{bmatrix} \sin(d_1(u_1 - u_s)) & \ldots & \sin(d_N(u_1 - u_s)) \\ \sin(d_1(u_2 - u_s)) & \ldots & \sin(d_N(u_2 - u_s)) \\ . & \ldots & \\ . & \ldots & \\ \sin(d_1(u_M - u_s)) & \ldots & \sin(d_N(u_M - u_s)) \end{bmatrix}$$

Y is the $N \times N$ matrix

$$Y = \begin{bmatrix} y_1^{-2} & . & . & . \\ . & y_2^{-2} & . & . \\ . & . & . & . \\ . & . & . & . \\ . & . & . & y_N^{-2} \end{bmatrix}$$

and the vector B

$$B^T = [\ \frac{F_0(u_1)}{(u_1 - u_s)}, \frac{F_0(u_2)}{(u_2 - u_s)}, \ldots\ldots\ldots, \frac{F_0(u_M)}{(u_M - u_s)}\ ]^T$$

Using the result of the previous theorem and from the corresponding remark, the solution is given by

$$X = Y^{-1} A^T C \tag{3.17}$$

So that X is a linear combination of the columns of $Y^{-1}A^T$ with coefficients from the vector C. The elements of $(AY^{-1}A^T)$ matrix are given as (see Appendix B),

$$[(AY^{-1}A^T)]_{i,j} = \sum_{1}^{N} y_n^2 \sin[\ d_n (u_i - u_s)\ ] \sin[\ d_n (u_j - u_s)\ ] \tag{3.18}$$

But

$$Y^{-1} A^T = \begin{bmatrix} y_1^2\sin(d_1(u_1-u_s)) & y_1^2\sin(d_1(u_2-u_s)) & . & . & y_1^2\sin(d_1(u_M-u_s)) \\ y_2^2\sin(d_2(u_1-u_s)) & y_2^2\sin(d_2(u_2-u_s)) & . & . & y_2^2\sin(d_2(u_M-u_s)) \\ . & . & . & . & . \\ . & . & . & . & . \\ y_N^2\sin(d_N(u_1-u_s)) & y_N^2\sin(d_N(u_2-u_s)) & . & . & y_N^2\sin(d_N(u_M-u_s)) \end{bmatrix}$$

Therefore, the weighted (or relative) element position perturbations are given as,

$$a_n \Delta_n = y_n^2 \sum_{m=1}^{M} c_m \sin[\ d_n (u_m - u_s)\ ] \tag{3.19}$$

and the perturbed pattern

$$F(u) = F_0(u) + F_c(u)$$

where the cancellation pattern can be obtained by substituting (3.19) in (3.7) to get,

$$F_c(u) = j\,(u-u_s) \sum_{m=1}^{M} c_m \sum_{n=1}^{N} y_n^2 \sin[\, d_n\,(u_m-u_s)\,]\, e^{j\,d_n\,(u-u_s)}$$

$$= \frac{1}{2} \sum_{m=1}^{M} c_m \{ \sum_{n=1}^{N} y_n^2 [\, (u-u_s)\, e^{j\,d_n\,(u+u_m-2u_s)} - (u-u_s)\, e^{j\,d_n\,(u-u_m)}\,]\,\} \qquad (3.20)$$

Let the weighting coefficients have even symmetry with respect to the reference center; that is

$$y_n = y_{N-n+1}, \qquad n = 1, 2, ..., N.$$

Then the element position perturbations Δ_n, are odd symmetrical with respect to the center of the array as will be proven in the next Section. In addition, because the current amplitudes are even symmetry, and using the even property of the cosine function, then the solution (3.19) also satisfies (3.15-b) which means it is the complete solution of (3.15). And if the original pattern $F_0(u)$ is real as we assumed in our analysis, then the cancellation pattern must be real also. Therefore, the cancellation beam, as given by (3.20), is a sum of M pairs of cancellation beams. Each of these pairs of beams corresponds to an element amplitude taper proportional to the weighted square of the weight coefficient $[(u-u_s)y_n^2]$, with one member of the pair having a peak in the direction of null location and the other member of the beam pair having a peak in the symmetric direction on the other side of the original pattern look direction, u_s. Therefore, the parameter y_n, will determine the characteristics of the cancellation pattern

and hence the characteristics of the adaptive nulling.

The components of C vector are called the beam coefficients. If one null is imposed at the pattern then the beam coefficient has a value approximately equal to the initial pattern evaluated at u_1,

$$c_1 = \frac{2F_0(u_1)}{(u_1 - u_s)\sum_{n=1}^{N} y_n^2}$$

+ [contribution from the second pair having a peak at $(-u_1 + 2u_s)$] (3.21)

The above result can be verified from Eq.(3.20) with one prescribed null (M = 1). If more than one null at multiple locations are imposed at the pattern, then the beam coefficient values from their values for the same null locations taken one at a time give measure of the extent of coupling or interference between the component beams of the perturbed pattern.

3.4. Minimization of the sum of the squares of the total element position perturbations

The two specific types of approximation criterion mentioned in the introduction are special cases of the general result obtained in the previous Section. Minimizing the sum of the squares of the total element position perturbations are obtained by letting $y_n = a_n$ in (3.14) to get,

$$\sum_n (\Delta_n)^2 = \text{min.} \qquad (3.22)$$

and hence the element position perturbations of Eq.(3.19) will be as,

$$\Delta_n = \sum_{m=1}^{M} c_m \, a_n \sin[\, d_n \, (u_m - u_s) \,] \tag{3.23}$$

Because the amplitude coefficients $\{a_n\}$ are assumed even symmetrical and the element positions $\{d_n\}$ are odd symmetrical about the array center, it follows from (3.23) that the element perturbations $\{\Delta_n\}$ are odd symmetrical with respect to the array reference center; that is,

$$\begin{aligned} \Delta_{N-n+1} &= \sum_{m=1}^{M} c_m \, a_{N-n+1} \sin[\, d_{N-n+1} \, (u_m - u_s) \,] \\ &= \sum_{m=1}^{M} c_m \, a_n \sin[\, -d_n \, (u_m - u_s) \,] \\ &= -\Delta_n \end{aligned}$$

It is important to note that the values $\{\Delta_n\}$ calculated from (3.23) must be substituted in (3.3) to obtain the perturbed pattern. Since the values for the $\{\Delta_n\}$ were obtained using the approximation (3.6), this means that the resulting pattern nulls can not be expected to be theoretically perfect as they would be if the calculated values were substituted in approximation (3.5). In fact the values of the perturbed pattern at a prescribed null location u_m is given by subtracting (3.6) from (3.4),

$$\begin{aligned} \Delta F(u_m) &= \sum_{n=1}^{N} a_n [\, e^{j \Delta_n (u_m - u_s)} - (1 + j\Delta_n \, (u_m - u_s) \,] \, e^{j d_n (u_m - u_s)} \\ &\approx \sum_{n=1}^{N} a_n [\, \Delta_n \, (u_m - u_s)]^2 \, e^{j d_n (u_m - u_s)} \end{aligned} \tag{3.24}$$

with the value of the power pattern at the location given approximately by,

$$[\Delta F(u_m)]^2 \approx \sum_{k=1}^{N}\sum_{n=1}^{N} a_k a_n [\Delta_k (u_m - u_s)]^2 [\Delta_n (u_m - u_s)]^2 e^{j(d_k - d_n)(u_m - u_s)} \qquad (3.25)$$

Also, the cancellation pattern is obtained by substituting $y_n = a_n$ in (3.20) to get

$$F_c(u) = \frac{1}{2}\sum_{m=1}^{M} c_m \{\sum_{n=1}^{N} a_n^2 [(u-u_s) e^{j d_n (u + u_m - 2u_s)} - (u-u_s) e^{j d_n (u - u_m)}]\} \qquad (3.26)$$

Accordingly the perturbed pattern equals the original pattern plus the sum of M cancellation beam. The cancellation beam, as given by Eq.(3.26), is the sum of differences of M pairs of cancellation beams. Each of these pairs of beams corresponds to an element amplitude taper proportional to the square of the original amplitude taper $[(u-u_s) a_n^2]$, with one member of the pair having a peak in the direction of null location and the other member of the beam pair having a peak in the symmetric direction on the other side of the original pattern look direction, u_s.

If one null is imposed at the pattern then the beam coefficient has a value almost equal to the unperturbed pattern at the null location u_1,

$$c_1 = \frac{2F_0(u_1)}{(u_1 - u_s)\sum_{n=1}^{N} a_n^2}$$

+ [contribution from the second pair having a peak at $(-u_1 + 2u_s)$] (3.27)

Equation (3.27) can be obtained directly from Eq.(3.21) by letting $y_n = a_n$.

3.5 Minimization of the sum of the squares of the relative element position perturbations

Similarly, the second case corresponding to the requirement that the solution minimizes the sum of the squares of the relative element position perturbations are obtained by letting $y_n = 1.0$ in (3.14)

$$\sum_n (a_n \Delta_n)^2 = \min. \tag{3.28}$$

Hence, the element position perturbations of Eq.(3.19) will be

$$\Delta_n = \frac{1}{a_n} \sum_{m=1}^{M} c_m \sin[\, d_n (u_m - u_s)\,] \tag{3.29}$$

Because the factors $\{\frac{1}{a_n}\}$ have even symmetry and the element positions $\{d_n\}$ are odd symmetrical about the array center, it follows from (3.20) that the element perturbations $\{\Delta_n\}$ are odd symmetric with respect to the array reference center; that is,

$$\Delta_{N-n+1} = -\Delta_n$$

Eqs.(3.19) and (3.29) are to be used to calculate the element position perturbations, Δ_n. Using the same argument as in the previous case the resulting pattern nulls are not perfect since the values (Δ_n) were obtained using the approximation (3.6). The values of the perturbed pattern and the power pattern at a prescribed null location u_m is given by Eqs.(3.24) and (3.25) respectively.

In a similar way, the cancellation pattern can be obtained by substituting $y_n = 1.0$ in (3.20) to get,

$$F_c(u) = \frac{1}{2}\sum_{m=1}^{M} c_m \{ \sum_{n=1}^{N} [(u-u_s)\, c^{j d_n (u+u_m-2u_s)} - (u-u_s)\, c^{j d_n (u-u_m)}] \} \qquad (3.30)$$

Therefore, the cancellation pattern, as given by Eq.(3.30), is a sum of differences of M pairs of cancellation beams. Each of these pairs of beams corresponds to a uniform element amplitude distribution weighted by $(u-u_s)$, with one member of the pair having a peak in the direction of null location and the other member of the beam pair having a peak in the symmetric direction on the other side of the original pattern look direction, u_s. Assuming only one null imposed at the pattern then the beam coefficient has a value almost equal to the unperturbed pattern at the null location u_1,

$$c_1 = \frac{2F_0(u_1)}{N(u_1-u_s)}$$

$$+ [\text{ contribution from the second pair having a peak at } (-u_1+2u_s)] \qquad (3.31)$$

It is instructive to compare the approximate representations for small element position perturbations of the cancellation pattern given in Eqs.(3.26) and (3.30), with the cancellation pattern obtained when both the amplitude and phase or the phase-only are allowed to vary. Minimizing the sum of the squares of the absolute values of the phase perturbations $\sum|\varphi_n|^2$ for the phase only and the relative (to the original amplitude weight) perturbations $\sum|\delta_n+j\varphi_n|^2$ for combined amplitude and phase perturbations, leads to a representation of the

cancellation pattern in terms corresponding to an element amplitude taper proportional to the square of the original amplitudes; where as minimizing the sum of the absolute values of the total element position perturbations $\sum|\Delta_n|^2$ leads to a representation of the cancellation pattern in terms corresponding to an element amplitude taper proportional to the square of the original amplitudes multiplies with the factor $(u-u_s)$.

However, minimizing the sum of the squares of the absolute values of the relative element position perturbations $\sum|a_n\Delta_n|^2$ leads to a representation of the cancellation pattern in terms corresponding to uniform element amplitude distribution weighted by the factor $(u-u_s)$, as given in (3.30). Where as minimizing the sum of squares of the absolute values of the total weight perturbations $[\approx ja_n\varphi_n, a_n(\delta_n+j\varphi_n)$ for the phase-only and the phase and amplitude respectively] leads to a representation of the cancellation pattern in terms corresponding to a uniform distribution.

3.6 Symmetric nulling property

Null steering in adaptive arrays by means of phase only variations results in a nonlinear problem. However, the problem can be linearized by assuming small phase perturbations to avoid the computational difficulties associated with the nonlinear problem. A consequence of this assumption is that the imposing of a null in the pattern of a linear array is accompanied by the reinforcement of the pattern at the location symmetric with respect to the main beam. Thus, it is

impossible to impose nulls at symmetric locations around the main beam with small phase perturbations [12,14].

One of the main advantages of using element position perturbations is that imposing a null in the pattern of an isotropic linear array is accompanied by another null at the location symmetric with respect to the main beam, thus making it possible to impose nulls at symmetric locations with small element position perturbations. The purpose of this section is to prove that if small element position perturbations is assumed to impose nulls in the pattern of a linear array of isotropic equispaced elements while minimizing the weighted sum of squares given by Eq.(3.14), then symmetrical nulls with respect to the main beam will be created. This result is of considerable value when two symmetrical nulls around the main beam are required or with the main beam steering as will be seen in chapter four. Let us rewrite the perturbed pattern for the null steering by element position perturbations given by Eq.(3.3),

$$F(u) = \sum_{n=1}^{N} a_n e^{j x_n (u - u_s)}$$

Assuming small element position perturbations, the solution which is given by Eq.(3.19), will find the set of perturbations, Δ_n, that will impose the nulls at the prescribed locations u_m, and that will minimize the sum of Eq.(3.14). Because the element positions d_n, and the element position perturbations Δ_n, obtained from Eq.(3.19) are odd symmetric and, in addition, if the given set of y_n, are even symmetric, then the perturbed element positions x_n, are odd symmetric, i.e

$$x_n = -x_{N-n+1}$$

Generally, we are interested in the case of real symmetric pattern $F_0(u)$, and hence to real symmetric coefficients $a_n = a_{N-n+1}$. Substituting the above results in Eq.(3.3), then

$$F(u) = \sum_{n=1}^{N} a_{N-n+1}\, e^{-j x_{N-n+1}(u-u_s)}$$

Let $i = N-n+1$, then the above summation can be written as,

$$F(u) = \sum_{i=1}^{N} a_i\, e^{j x_i(-u+u_s)}$$

Therefore, from Eqs.3.5 and 3.32, if the imposed null is at u_m, then,

$$F(u_m) = F(-u_m + 2u_s) \tag{3.32}$$

Thus, imposing a null at the initial pattern will locate another null at the symmetric location with respect to the main beam or

$$\bar{u}_m = -u_m + 2u_s \tag{3.33}$$

where $\bar{u}_m$ is the symmetric null location of the imposed null.

3.7 Mean square of the pattern difference (MSD)

It is known that minimizing the sum of the square of the total weight perturbations, $\sum|\Delta w_n|^2$ is equivalent to minimizing the the mean square of the pattern perturbation, $[F(u)-F_0(u)]$, (MSD), for half wavelength element spacing, [24,26]. This result can be written as,

$$\text{MSD} = \frac{1}{2k}\int_{-k}^{k}|F(u)-F_0(u)|^2\,du = \frac{1}{2k}\int_{-k}^{k}|F_c(u)|^2\,du$$

$$= \sum_{n=1}^{N} |\Delta w_n|^2 \tag{3.34}$$

where the derivation is given in appendix A. In the case of small phase-only perturbations, half wavelength element spacing, we have

$$MSD = \frac{1}{2k}\int_{-k}^{k} |F(u) - F_0(u)|^2 du = \sum_{n=1}^{N} |\Delta w_n|^2 = \sum_{n=1}^{N} |a_n(e^{j\varphi_n} - 1)|^2 du$$

$$\approx \sum_{n=1}^{N} |a_n \varphi_n|^2 \tag{3.35}$$

so that minimizing the relative phase perturbations, is approximately equivalent to minimizing the mean square pattern perturbation (MSD). In the above results, the mean is taken to be in the visible region defined in the interval $(-\frac{\pi}{2} \le 0 \le \frac{\pi}{2})$.

We now ask whether there is a similar pattern minimization that corresponds to minimizing the sum of the square of the relative element position perturbations. In fact there is, and to answer this question let us first obtain the MSD for the case of the element position perturbations.

In general, the problem can be stated as follows:
Given a linear array of N equispaced isotropic elements with an initial set of element positions d_n, n = 1,2,.....,N and a set of new perturbed element positions x_n, n = 1,2,.....,N which produces the array pattern with nulls at a set of M prescribed pattern locations, u_m, m = 1,2,.....,M, M < N, determine the mean square difference (MSD) between the perturbed and the the initial pattern. The

mean is taken to be in the visible region. So that the variable $u = k\sin\theta$, is to be integrated from -k to k.

The initial and the perturbed patterns are given by Eqs.(3.1) and (3.3), respectively. The MSD can be expressed as,

$$MSD = \frac{1}{2k}\int_{-k}^{k}|F(u)-F_0(u)|^2du$$

$$= \frac{1}{2k}\int_{-k}^{k}\{\sum_{n=1}^{N}a_n[e^{jx_n(u-u_s)}-e^{jd_n(u-u_s)}]\}\{\sum_{n=1}^{N}a_n[e^{-jx_n(u-u_s)}-e^{-jd_n(u-u_s)}]\}du \qquad (3.36)$$

After the simplification and interchanging the integration with the summations, we get,

$$MSD = \sum_{n=1}^{N}\sum_{v=1}^{N}a_na_v\{\frac{1}{2k}\int_{-k}^{k}[e^{j(x_n-x_v)(u-u_s)}-e^{j(x_n-d_v)(u-u_s)}-e^{j(d_n-x_v)(u-u_s)}+e^{j(d_n-d_v)(u-u_s)}]du\}$$

$$= \sum_{n=1}^{N}\sum_{v=1}^{N}a_na_v\{e^{-j(x_n-x_v)u_s}\,\mathrm{sinc}[(x_n-x_v)k]-e^{-j(x_n-d_v)u_s}\,\mathrm{sinc}[(x_n-d_v)k]$$

$$-e^{-j(d_n-x_v)u_s}\,\mathrm{sinc}[(d_n-x_v)k]+e^{-j(d_n-d_v)u_s}\,\mathrm{sinc}[(d_n-d_v)k]\} \qquad (3.37)$$

Eq.(3.37) computes the MSD without any restriction on the element spacing neither on the element position perturbations. For simplification, let the main beam steering angle pointed at broad side, i.e; $u_s=0$. And by substituting Eq.(3.2) in (3.37), the above Equation is going to be as,

$$MSD = \sum_{n=1}^{N}\sum_{v=1}^{N}a_na_v\{\mathrm{sinc}[(d_n-d_v)k+(\Delta_n-\Delta_v)k]-\mathrm{sinc}[(d_n-d_v)k+\Delta_nk]$$

$$-\mathrm{sinc}[(d_n-d_v)k-\Delta_vk]+\mathrm{sinc}[(d_n-d_v)k]\} \qquad (3.38)$$

Assuming half wavelength element spacing, then

$$(d_n-d_v)k = d_0k(n-v) = (n-v)\pi \qquad (3.39)$$

Also, using the trigonometric property, the following relation

$$\text{sinc}(x+y) = \frac{\sin(x)\cos(y) + \cos(x)\sin(y)}{x+y}$$

is true. Letting $x = (n-\nu)\pi$, in the above relation

$$\text{sinc}[(n-\nu)\pi + y] = \frac{(-1)^{n-\nu}\sin(y)}{(n-\nu)\pi + y} \tag{3.40}$$

Further more, since in our case y can be any element position perturbation Δ_n, or $(\Delta_n - \Delta_\nu)$, as can be seen from Eq.(3.37), then it can be generally assumed to be very small. Note that the maximum possible value of y is twice the largest magnitude value of the element position perturbations. So that Eq.(3.40) can be written as,

$$\text{sinc}[(n-\nu)\pi + y] = \frac{(-1)^{n-\nu} y}{(n-\nu)\pi} \qquad n \neq \nu \tag{3.41-a}$$

$$= \text{sinc}(y) \qquad n = \nu \tag{3.41-b}$$

It is important to note that Eq.(3.41-b) is valid for any y. Consider first the term values of the double summation where $n \neq \nu$, then the MSD will be,

$$\text{MSD}\,|_{n\neq\nu} = \sum_{n=1}^{N}\sum_{\nu\neq n}^{N} a_n a_\nu \left\{ \frac{(-1)^{n-\nu}}{(n-\nu)\pi} [\,(\Delta_n - \Delta_\nu)k - \Delta_n k + \Delta_\nu k + 0\,]\right\} \tag{3.42}$$

Using the above result with Eqs.(3.41-b) and (3.38), the double summation can be reduced to single summation as,

$$\text{MSD} = \sum_{n=1}^{N} a_n^{\,2}[\,2 - 2\text{sinc}(\Delta_n k)\,] \tag{3.43}$$

The above Equation can be simplified more using the series expansion of the sinc function

$$\text{sinc}(y) = 1 - \frac{y^2}{3!} + \frac{y^4}{5!} - \ldots\ldots \tag{3.44}$$

Because y is assumed to be small, the above sinc function can be approximated by the first two terms of Eq.(3.44). So by substituting the first two terms of Eq.(3.44) into (3.43), the MSD will be given as,

$$\therefore \text{MSD} = \sum_{n=1}^{N} a_n^2 \left[\frac{(\Delta_n k)^2}{6} \right]$$

$$= \frac{k^2}{6} \sum_{n=1}^{N} (a_n \Delta_n)^2 \tag{3.45}$$

From the above result, we can see that minimizing the square of the relative element position perturbations is equivalent to minimizing the pattern perturbation (MSD). This result is valid for half wavelength spacing and when the perturbations, Δ_n, is small. Otherwise, the MSD is computed numirecally using Eq.(3.30) directly.

3.8 Normalized beam coefficients

Before proceeding to chapter four for discussing numerical results, let us introduce a useful normalization of the beam coefficients. it is desirable to normalize the beam coefficients so that the extent of coupling between component beams as well as comparing differences in coupling corresponding to different types of beams can established easily. Also, this normalized beam coefficient may be compared with the values obtained using other techniques such as full amplitude and/or phase only. This is equivalent to say that the beam coefficient value equals to the unperturbed pattern value at the null

location when there is only one null imposed at the pattern.

To illustrate the concept, consider first Eqs.(2.9) and (2.12) obtained when both amplitude and phase of the weight perturbations are allowed to vary. And suppose there is only one null imposed in the pattern (that is M = 1). When the cancellation pattern given by (2.9) is substituted, then Eq.(2.6) can be written as,

$$-F_0(u_1) = F_c(u_1) = c_1 \sum_{n=1}^{N} a_n^2$$

so that

$$c_1 = \frac{-F_0(u_1)}{\sum_{n=1}^{N} a_n^2} \tag{3.46}$$

Where as, for minimum total weight perturbations, substituting Eq.(2.12) in (2.6) gives

$$-F_0(u_1) = F_c(u_1) = N\, c_1$$

or

$$c_1 = \frac{-F_0(u_1)}{N} \tag{3.47}$$

The beam coefficients in the two cases can have widely different values depending on the amplitude taper, a_n, and the number of elements in the array, N.

Thus, for minimizing the squares of the total element position perturbations, the normalized beam coefficients $[c_m]_n$, may be written as

$$[c_m]_n = \frac{(u_m - u_s)\sum_{n=1}^{N} a_n^2}{2\sum_{n=1}^{N} a_n} c_m \tag{3.48}$$

Where as, for minimizing the squares of the relative element position perturbations, the normalized beam coefficients $[c_m]_n$, may be written as

$$[c_m]_n = \frac{(u_m - u_s)\, N}{2\sum_{n=1}^{N} a_n} c_m \tag{3.49}$$

The above results can easily verified by referring to Eqs.(3.27) and (3.31), respectively.

CHAPTER 4

RESULTS AND COMPUTER SIMULATIONS OF THE ELEMENT POSITION PERTURBATIONS

In this Chapter we present the simulation results of null steering by controlling the element positions. The derived solutions are tested to validate the capability of null steering and to discuss and display the basic features. In Section 4.2, the performance and the basic features of the element position perturbations are compared with main features of the full weight and the small phase only perturbations. Because the small element position perturbations and the small phase-only perturbations have similar analysis the results show that they have some common characteristics. Also, the capability of the new method was studied from the simulation results in Sections 4.3 and 4.4 as far as,

a) the effect of varying the number of nulls

b) utilization of different types of patterns

c) generating two nulls, one very close to the main beam and the other very far.

In Section 4.5, the performance of null steering while varying the direction of the main beam is studied. The new method show the ability to impose nulls in the sidelobe region when the main beam direction had been steered from the

broadside independent of the null direction. We investigate the capability and the performance of the element position perturbations to suppress wideband interference signals and sidelobe cancellation. A practical scheme is suggested to achieve the null steering by element position perturbations in Section 4.7. In the last Section, the new method of element position perturbations was tested to examine the sensitivity performance as a consequence of the suggested practical scheme.

4.1 Basic features of the small element position perturbations method

To demonstrate the basic features of null steering by controlling the element positions method, the computations were done for an array with 20 isotropic elements of half wavelength element spacing. The initial (original or unperturbed) pattern corresponds to a 30 dB chebyshev taper of the element excitations (see Appendix D). We begin by simulating the simplest case when a single null is imposed at a location of 20° which corresponds to the approximate location of the peak of the third sidelobe of the initial pattern. Figures 4.1a-c show the patterns corresponding to the element position perturbations by using Eq.(3.23), the solution of minimizing the sum of the squares of the total element position perturbations $\sum(\Delta_n)^2$. And Figs.4.2a-c show the patterns using Eq.(3.29) where the sum of the squares of the relative element position perturbations is minimized, $\sum(a_n\Delta_n)^2$. Appendix B list the computer program which computes the element position perturbations for the general solution given by Eq.(3.19). For each of these two cases we show three graphs. The first with perturbed pattern

for 0 in the range from -90° to 90°, and the second with the cancellation pattern in the range from -90° to 90°, and the third with both the initial and the perturbed patterns in the range from 0° to 50°. Note that since the cancellation pattern of Figs.4.1b and 4.2b have even symmetry for both methods (as will be shown), the nulls occur also on the other side of the main beam. The corresponding position perturbations and the new element positions (in wavelength) are listed in Table 4-1. From the Table, it is seen that the element position perturbations values, Δ_n, are odd symmetrical around the array center and the new element positions, x_n, are symmetrical around the array center which yields an even symmetry cancellation pattern.

We see that the cancellation pattern in Fig.4.1b for minimizing the total position perturbations consists of a pair of cancellation beam. With one member of the pair having a peak at 20° and the other member of the pair having a peak in the symmetric direction, $-20°$. Because each of these members of the beam corresponds to an element amplitude taper proportional to the square of the original amplitude taper weighted by a directional factor $[a_n(u-u_s)]$, the cancellation beam has a much broader main beam and much lower sidelobes than the cancellation pattern of Fig.4.2b which corresponds to a uniformly amplitude distribution weighted by $(u-u_s)$. This means that the perturbed pattern is distorted more strongly in the vicinity of the null location for minimizing the total position perturbations (Fig.4.1c) than it is for minimizing the relative position perturbations (Fig.4.2c). However, it is true that the initial

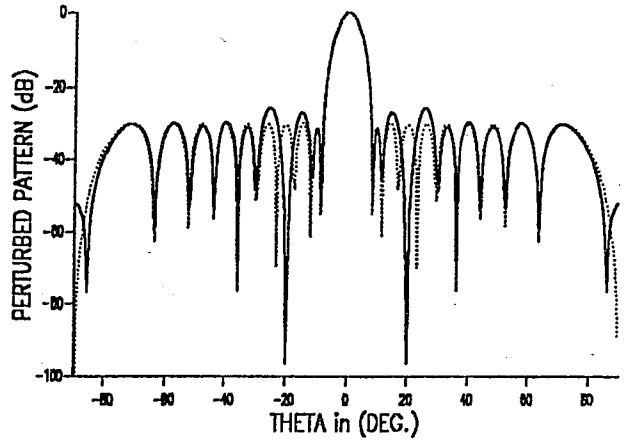

(a)

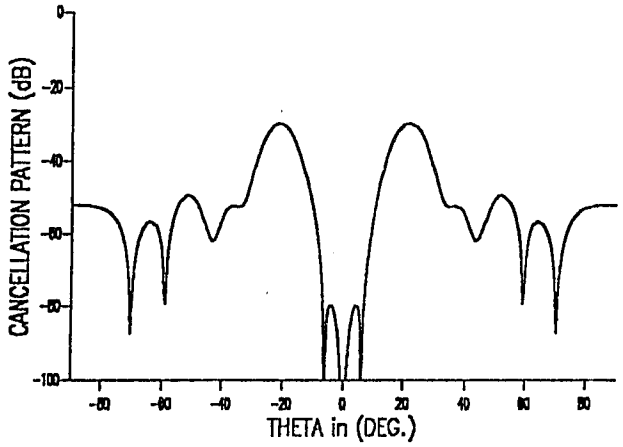

(b)

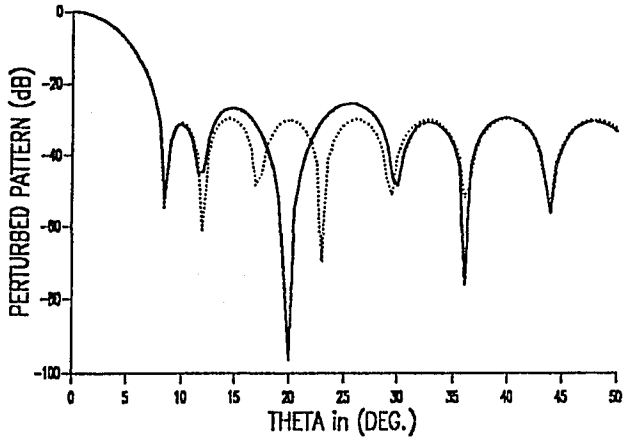

(c)

Fig.4.1 : Total element position perturbations. $\sum|\Delta_n|^2 = Min.$
a) Perturbed pattern (solid) with one null imposed at 20°.
b) Cancellation pattern. c) Perturbed pattern, $0 = 0°$ *to* 50°.
Initial 30-dB Chebyshev pattern (dotted), $N = 20$, $d_0 = \frac{\lambda}{2}$.

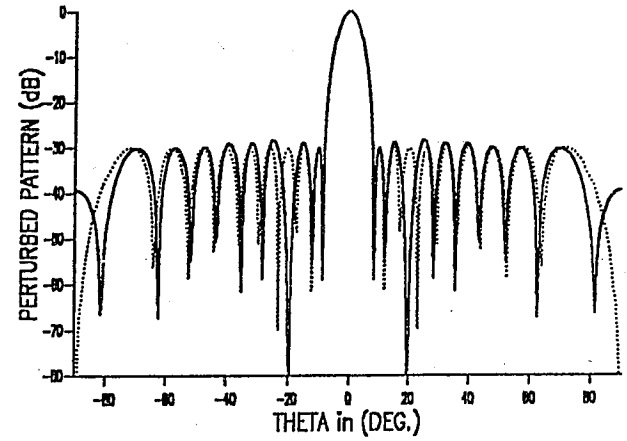

(a)

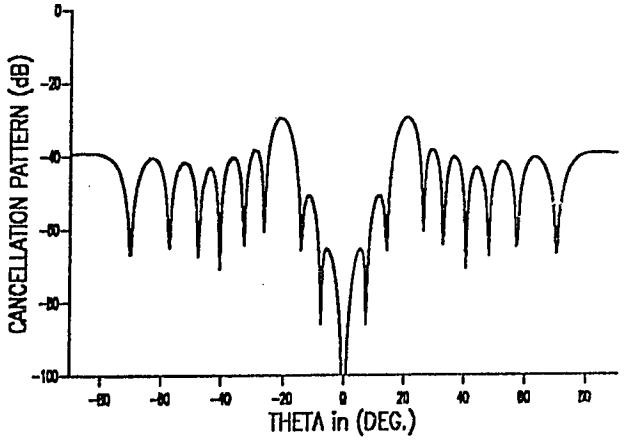

(b)

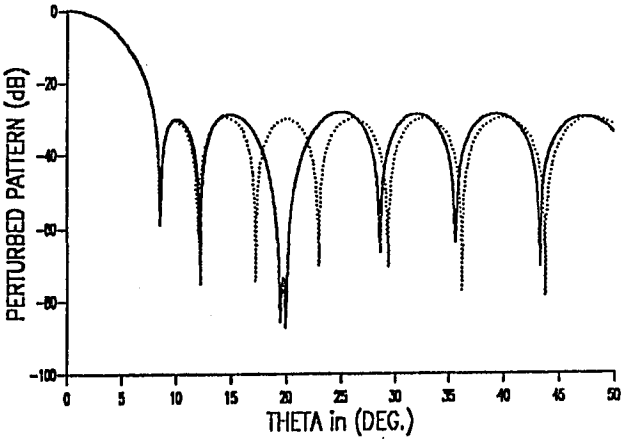

(c)

Fig.4.2 : Relative element position perturbations. $\sum|a_n \Delta_n|^2 = Min.$
a) Perturbed pattern (solid) with one null imposed at 20°.
b) Cancellation pattern. c) Perturbed pattern, $0 = 0°$ *to* 50°.
Initial 30-dB Chebyshev pattern (dotted), $N = 20$, $d_0 = \frac{\lambda}{2}$.

Table 4-1

Computed element position perturbations for Figs.(4.1,4.2) and the perturbed element positions of Fig.(4.1) in wavelength.

ELEMENT NO.	FIG.4.1		FIG.4.2
	Δ_n	x_n	Δ_n
1	-0.008729	-4.758729	-0.042550
2	0.003121	-4.246879	0.017346
3	0.014554	-3.735446	0.059069
4	0.012373	-3.237627	0.038910
5	-0.008608	-2.758608	-0.022013
6	-0.027635	-2.277635	-0.059874
7	-0.018391	-1.768391	-0.035009
8	0.015345	-1.234654	0.026532
9	0.037177	-0.712823	0.060278
10	0.019669	-0.230331	0.030874
11	-0.019669	0.230331	-0.030874
12	-0.037177	0.712823	-0.060278
13	-0.015345	1.234654	-0.026532
14	0.018391	1.768391	0.035009
15	0.027635	2.277635	0.059874
16	0.008608	2.758608	0.022013
17	-0.012373	3.237627	-0.038910
18	-0.014554	3.735446	-0.059069
19	-0.003121	4.246879	-0.017346
20	0.008729	4.758729	0.042550

pattern is distorted less strongly far a way from the null location for minimizing the total position perturbation than it is for minimizing the relative position perturbations . The MSD for Figs.4.1 and 4.2 are 0.0026 and 0.0021 respectively, which means that the solution of minimizing the sum of the relative position perturbation has less MSD than the solution corresponding to minimizing the sum of the square of the total position perturbations (compared with the initial pattern). Indeed the effect of the main beam of the cancellation pattern shown in Fig.4.1b extends even to the second and fourth sidelobes of the initial pattern which are lowered slightly for their initial values. However, the time the first and fifth sidelobes are reached, the effect of the cancellation pattern of Fig.4.1b is no longer felt and the perturbed and the initial pattern are virtually indistinguishable. In contrast, the cancellation pattern of Fig.4.2b, which taper much slowly than does the cancellation pattern of Fig.4.1b, can be seen to have a small effect as far as the first sidelobe of the initial pattern.

In Table 4-2 we have tabulated the values of the antenna parameters for the initial and the perturbed patterns for both cases. Fortran subroutines for computing the antenna parameters are listed in Appendix C, which were used to compute the values of Table 4-2. From the Table we can see that the main beam for both perturbed patterns are almost unaffected compared to the initial main beam. But the SLL for the perturbed pattern of the total position perturbations is affected more than the perturbed pattern for the relative position perturbations which is expected. Also it is apparent that the directivity decreases as the SLL increases. Note also that the depth of the null achieved

Table 4-2

The values of the MSD, directivity, half power beamwidth (BW), and SLL of the perturbed pattern when the imposed nulls are located at θ_m.

	$\sum(a_n\Delta_n)^2 = min.$				$\sum(\Delta_n)^2 = min.$			
θ DEG.	MSD	DIR.	BW DEG.	SLL dB	MSD	DIR.	BW DEG.	SLL dB
20	0.0021	17.33	6.33	-28.43	0.0026	17.32	6.33	-25.59
18.6 21.5	0.0011	17.34	6.33	-28.21	0.0013	17.33	6.33	-26.84
21.5 24.5	0.0077	17.28	6.34	-25.84	0.0100	17.21	6.32	-21.83
20.0 21.5	0.0026	17.30	6.35	-26.65	0.0030	17.30	6.33	-24.31
INITIAL		17.36	6.33	-29.71				

when minimizing the total position perturbations is much deeper than the depth of the null when minimizing the relative position perturbations.

The normalized values of the beam coefficients of the element position perturbations c_m, the initial and the perturbed patterns at the null locations are tabulated in Table 4-3. For one null at 20°, it is given in Table 4-3 that the value of the beam coefficient is slightly larger from the value of the initial pattern value at the null location. This deviation can be explained from Eqs.(3.27) and (3.31) where the beam coefficient is equal to the normalized unperturbed pattern value plus a small contribution from the other member of the pair of the cancellation pattern.

We now look at the case of two nulls imposed symmetrically at the -3 dB points of the third sidelobe of the initial pattern. Figures 4.3a-c and 4.4a-c show the patterns corresponding to minimizing sum of the total and the relative element position perturbations respectively. We see that the two pair of beams composing the cancellation pattern appear to add constructively to form one resultant beam pair. Thus, the qualitative features of the patterns shown in Figs.4.3 and 4.4, are the same of those noted before in the case of only one prescribed null for Figs.4.1 and 4.2 respectively.

From Table 4-3, we note that unlike the case of one null, the beam coefficients for both minimization types are considerably smaller than the corresponding values of the magnitude of the initial pattern at the null locations.

Table 4-3

Normalized values of the beam coefficient c, initial pattern F0,
for the element position perturbations method.

0 DEG.	F0 VALUE	$\sum(\Delta_n)^2=min.$ c	$\sum(a_n\Delta_n)^2=min.$ c
20.0	-0.0311	-0.0312	-0.0320
18.6	-0.0221	-0.0223	-0.0189
21.5	-0.0219	-0.0001	-0.0075
21.5	-0.0219	-0.1368	-0.0651
24.5	-0.0221	0.1558	0.0761
20.0	-0.0311	-0.1505	-0.0797
21.5	-0.0219	0.1320	0.0541

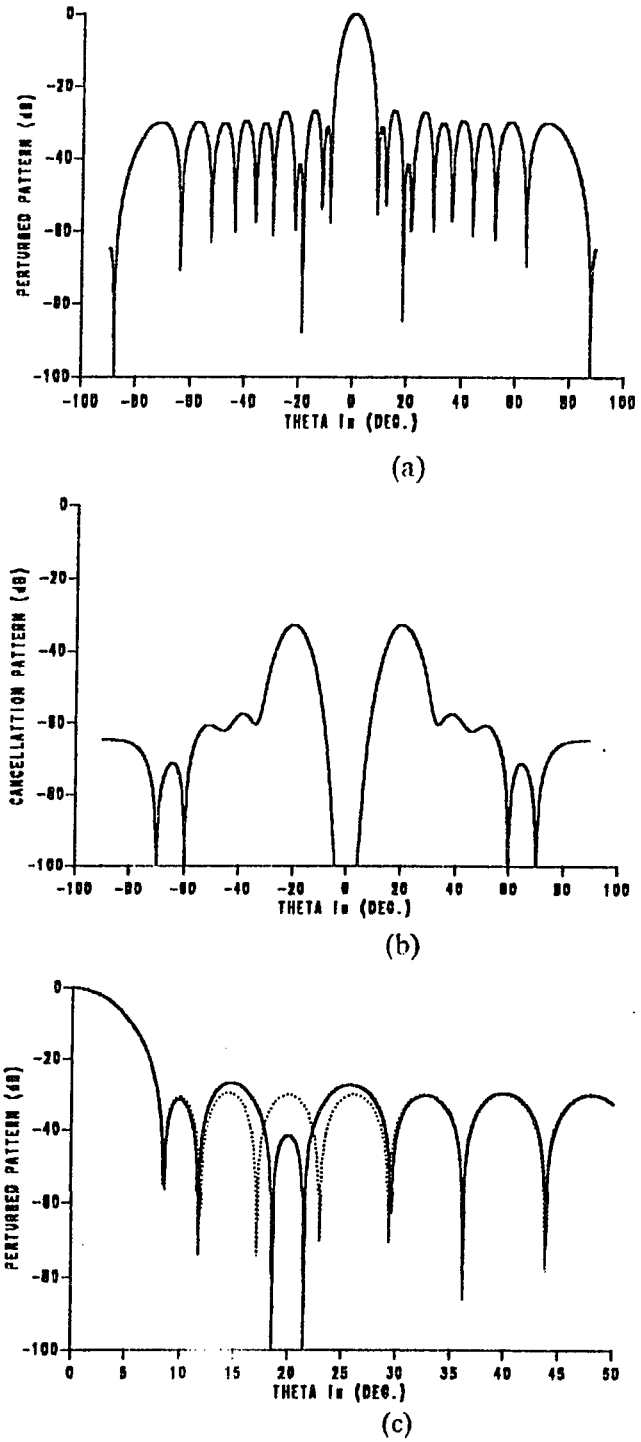

Fig.4.3 : Total element position perturbations. $\sum|\Delta_n|^2 = Min.$
a) Perturbed pattern (solid) with two nulls imposed at 18.6° *and* 21.5°.
b) Cancellation pattern. c) Perturbed pattern, $\theta = 0°$ *to* 50°.
Initial 30-dB Chebyshev pattern (dotted), $N = 20$, $d_0 = \frac{\lambda}{2}$.

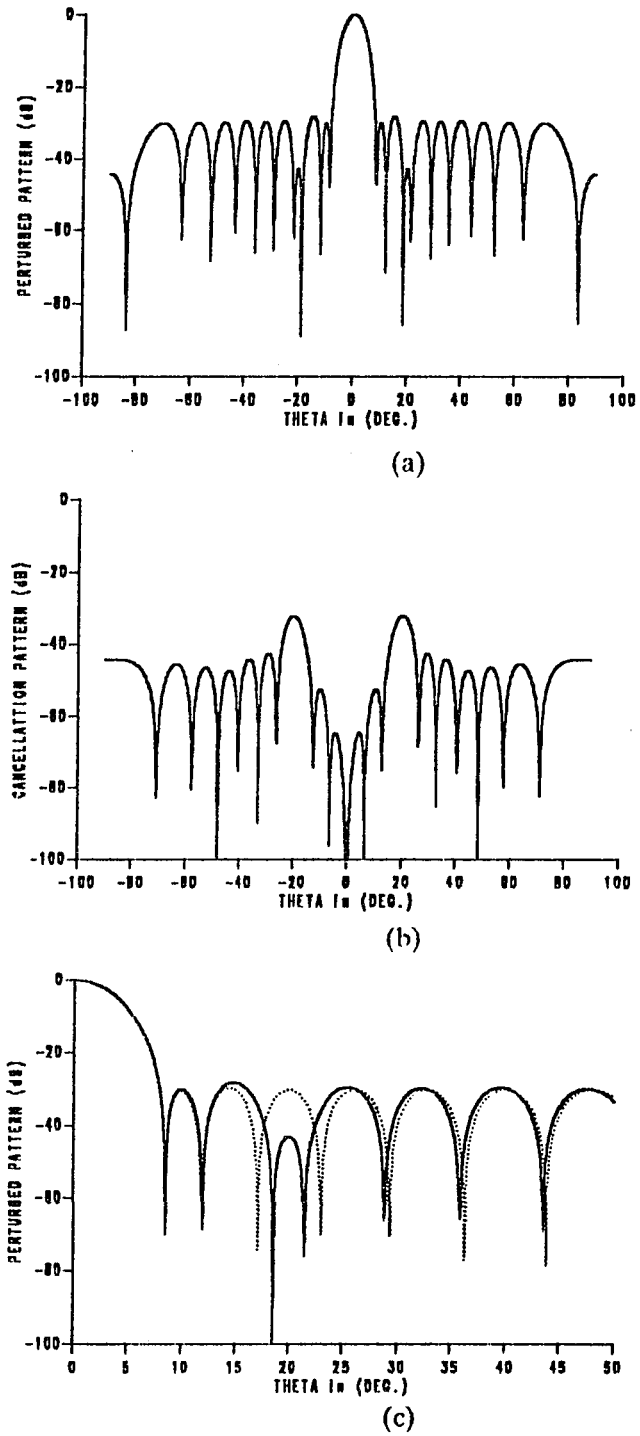

Fig.4.4 : Relative element position perturbations. $\sum |a_n \Delta_n|^2 = Min.$

a) Perturbed pattern (solid) with two nulls imposed at 18.6° *and* 21.5°.
b) Cancellation pattern. c) Perturbed pattern, $\theta = 0°$ *to* 50°.
Initial 30-dB Chebyshev pattern (dotted), $N = 20$, $d_0 = \frac{\lambda}{2}$.

This result of the fact that the cancellation of the initial pattern at the null location is affected by the peak of the cancellation beam directed at one null position along with the main lobe of the cancelling beam directed at the other null position so that the two beams help one another. Some of features noted above for the case of one are seen here as well. Minimizing the sum of the total element position perturbations give deeper nulls than do the case of minimizing the relative element position perturbations.

We next examine the case of two nulls imposed symmetrically on either side of a null, say the fourth null, of the initial pattern. The null locations at 21.5 and 24.5 are the -3 dB point of the initial pattern of the third and the fourth sidelobes and they are symmetrically placed of the null between the third and the fourth sidelobes of the initial pattern. Since the points at which the nulls are imposed belong to the adjacent and almost sidelobes, and are approximately symmetrically with respect to the null between the sidelobes, the beam coefficients are approximately equal in magnitude but opposite in sign (see Table 4-3). Unlike the previous case where the mainlobes of the two component beams of the cancellation patterns added in phase to form a single mainlobe, here the cancellation pattern in the vicinity of the null positions is split into two lobes of opposite sign as shown in Figs.4.5 and 4.6. The fact that the beam coefficients are of opposite sign means that each of the beams must do considerable amount of work to cancel the effect of the other beam. As a result, unlike the previous case (Fig.4.3), where the beams are helping each other, the beam coefficients are considerably larger in magnitude than the values of the

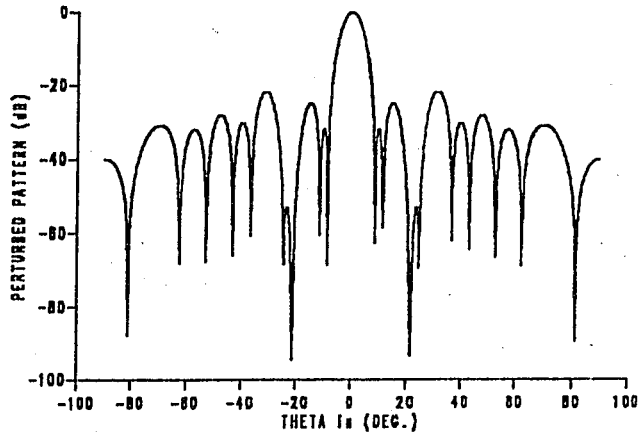

(a)

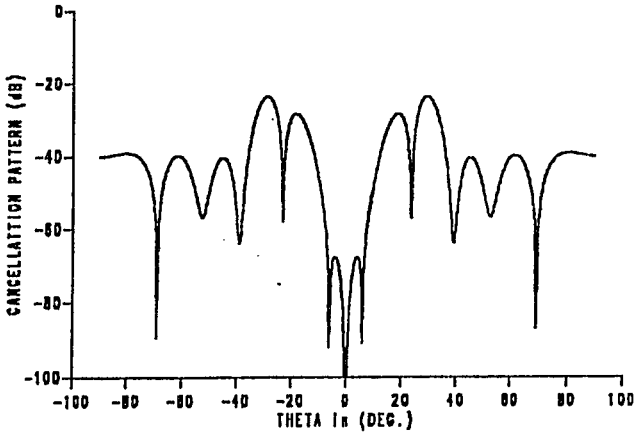

(b)

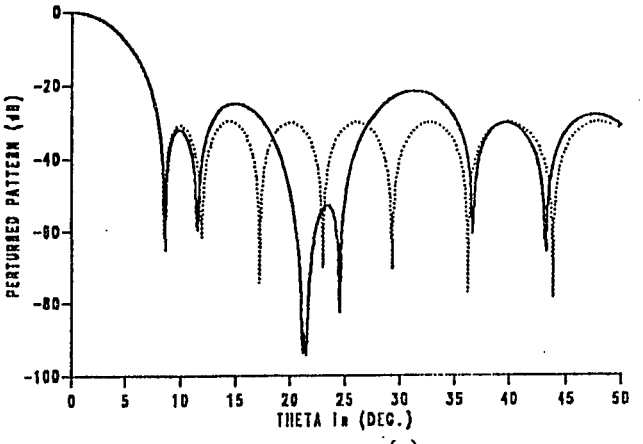

(c)

Fig.4.5 : Total element position perturbations. $\sum|\Delta_n|^2 = Min.$

a) Perturbed pattern (solid) with two nulls imposed at 21.5° *and* 24.5°.
b) Cancellation pattern. c) Perturbed pattern, $0 = 0°$ *to* 50°.
Initial 30-dB Chebyshev pattern (dotted), $N = 20$, $d_0 = \frac{\lambda}{2}$.

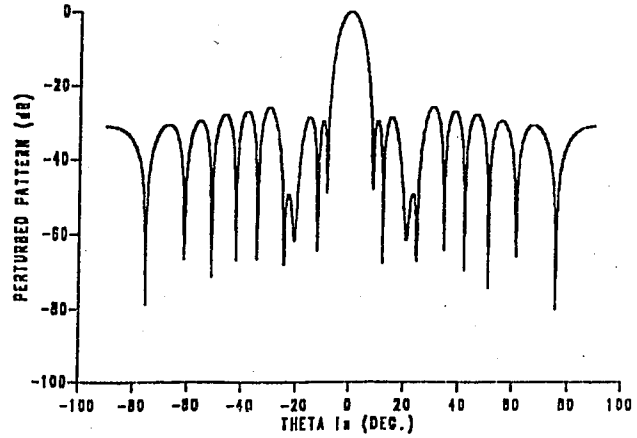

(a)

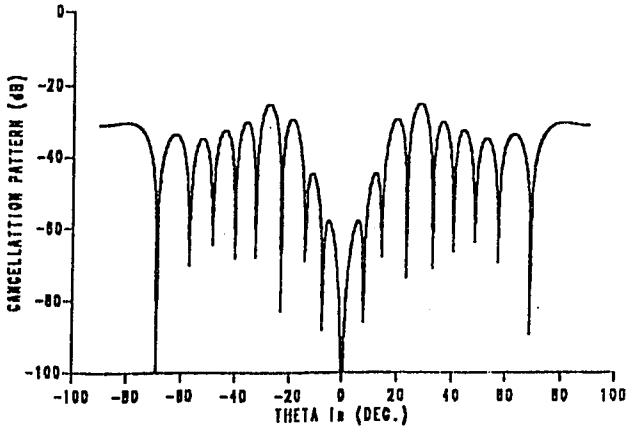

(b)

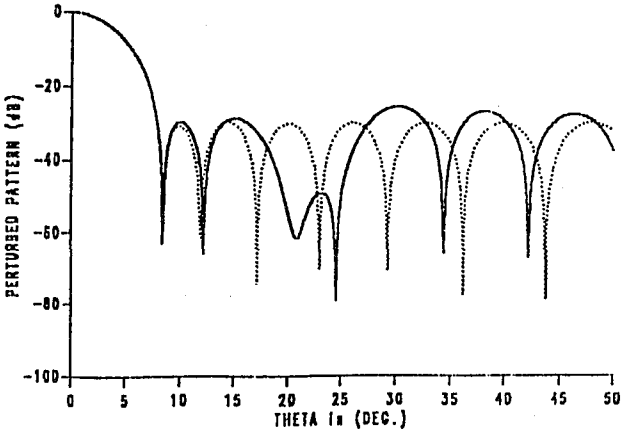

(c)

Fig.4.6 : Relative element position perturbations. $\sum|a_n \Delta_n|^2 = Min.$
a) Perturbed pattern (solid) with two nulls imposed at 21.5° *and* 24.5°.
b) Cancellation pattern. c) Perturbed pattern, $0 = 0°$ *to* 50°.
Initial 30-dB Chebyshev pattern (dotted), $N = 20$, $d_n = \frac{\lambda}{2}$.

initial pattern at the null locations (see Table 4-3).

Finally the case of two nulls imposed within a sidelobe are shown in Figs.4.7 and 4.8. The null location of $\theta = 20°$ and $21.5°$ were examined corresponding to the peak and the right -3 dB point of the third sidelobe of the initial pattern. Figures 4.7a-c show the pattern when the sum of the square of the total element position perturbations is minimized while Figs.4.8a-c show the pattern when the sum of the square of the relative element position perturbations is minimized. In contrast to the case of two nulls imposed symmetrically with respect to the sidelobe maximum, Figs.4.1 and 4.2, here the mainlobe of the cancellation pattern for minimizing the total element position perturbations is seen to be split into two lobes. This behavior of the cancellation pattern may be explained qualitatively as follows.The mainlobe of the beam directed at the location of the peak of the sidelobe at 20 is much broader than the sidelobe of the initial pattern. Hence, if the beam directed at 20 was exactly matched in magnitude to the initial pattern there it would have a component considerably larger in magnitude than the value of the initial pattern at 21.5. To counter this unwanted "overshoot" of the beam directed at 20, the beam at 21.5 must be of opposite sign. Because the component at 20 of the mainlobe of the beam directed at 21.5 is opposite the sign of the peak of the beam directed at 20, then the magnitude of the beam directed at 20 is forced to exceed the magnitude of the initial pattern. Referring to Table 4-3 we see that the coefficients of the two beams are of opposite sign and have magnitudes more than five times larger than the corresponding initial pattern values, indicating that the two beams are

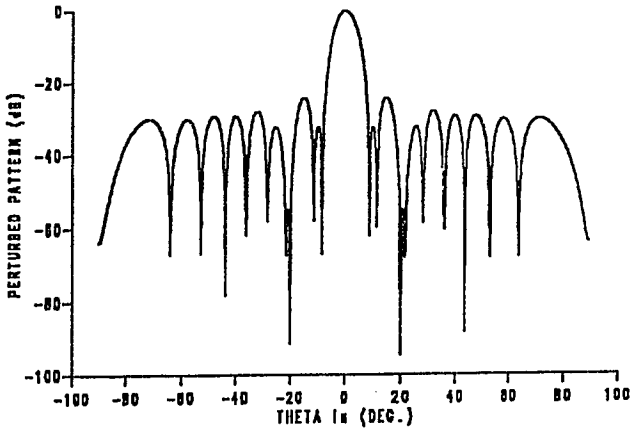

(a)

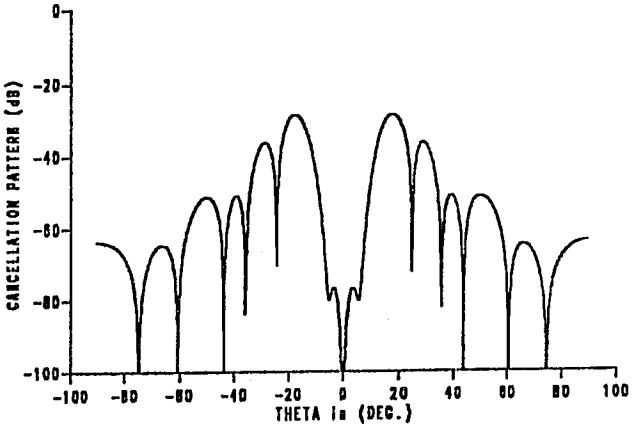

(b)

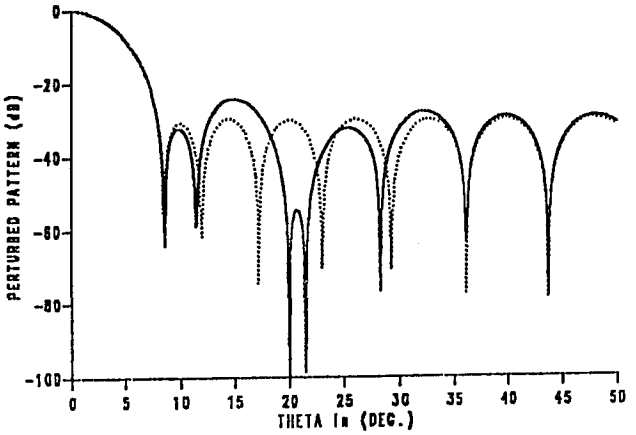

(c)

Fig.4.7 : Total element position perturbations. $\sum|\Delta_n|^2 = Min.$

a) Perturbed pattern (solid) with two nulls imposed at 20° *and* 21.5°.
b) Cancellation pattern. c) Perturbed pattern, $\theta = 0°$ *to* 50°.
Initial 30-dB Chebyshev pattern (dotted), $N = 20$, $d_0 = \frac{\lambda}{2}$.

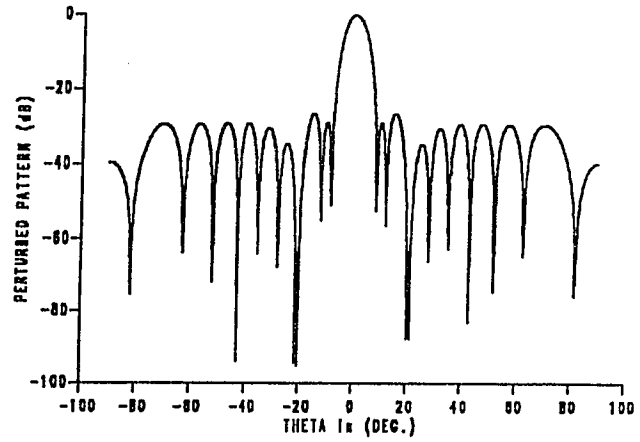

(a)

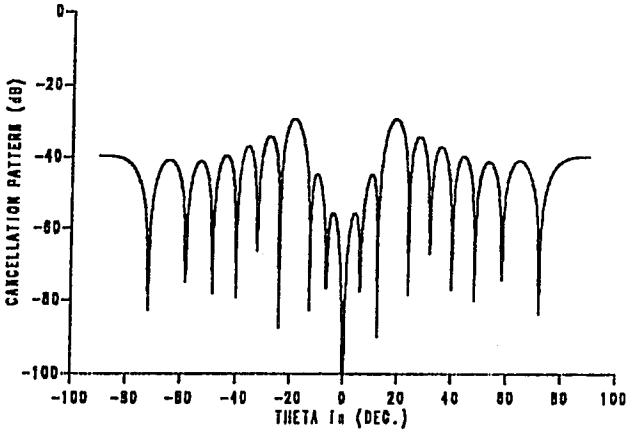

(b)

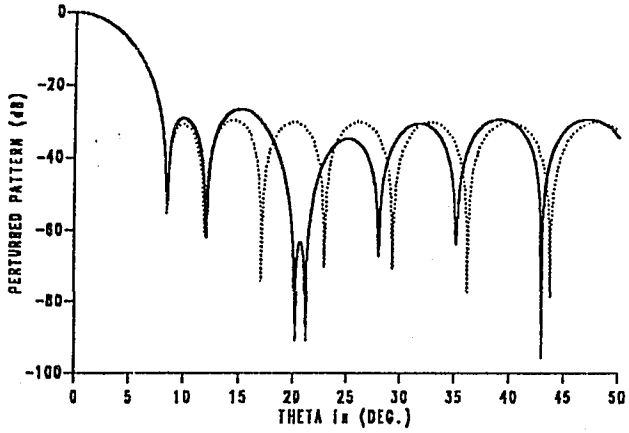

(c)

Fig.4.8 : Relative element position perturbations. $\sum|a_n \Delta_n|^2 = Min.$

a) Perturbed pattern (solid) with two nulls imposed at 20° *and* 21.5°.
b) Cancellation pattern. c) Perturbed pattern, $\theta = 0°$ *to* 50°.
Initial 30-dB Chebyshev pattern (dotted), $N = 20$, $d_0 = \frac{\lambda}{2}$.

doing considerably work in cancelling the effect of each other in addition to cancelling the initial pattern.

Similarly the case for minimizing the relative element perturbations is examined. The mainlobe of the beam directed at 20 is less wide than the mainlobe of the minimized total element position perturbations but still twice as wide as the sidelobe of the initial pattern. Thus the "overshoot" at 21.5 due to the main lobe at 20 is smaller than the first case which requires less compensation by the beam directed at 21.5. Consequently, the beam coefficients of the corresponding cancellation pattern are smaller than the first case but still much larger than the value of the initial pattern as given by Table 4-3.

In summary, imposing two nulls symmetrically on either side of a null is more difficult than any other null locations as the cancellation pattern in the vicinity of the null is split into two lobes of opposite sign which means that each member of the beams must do considerable a mount of work to cancel the effect of the other member of beam. Similarly, the case of two nulls imposed within a sidelobe will yield a more perturbed pattern compared to the case when the imposed nulls are far from each other. The above results can be verified from Table 4-2, where the MSD and SLL of the two nulls imposed at 21.5 and 24.5 are affected much more than the others.

4.2 Comparison of element position results with full weight and phase-only methods

It is valuable to compare the results of the basic features of the approximate representations for small element position perturbations discussed in the previous Section, with the results of the basic features discussed in Chapter two for the phase-only method. Referring to Eqs.(3.26) and (3.30), we see that minimizing the sums $\sum(\Delta_n)^2$ and $\sum(a_n\Delta_n)^2$ for the total and relative element position perturbations, leads to a representation of the cancellation pattern in terms corresponding to an element amplitude taper proportional to $[(u-u_s)a_n]$ and $[(u-u_s)]$ respectively. However, when referring to Eqs.(2.19) and (2.22), we can see that minimizing the sums $\sum(\varphi_n)^2$ and $\sum(a_n\varphi_n)^2$ for the total and relative element phase-only perturbations, leads to a representation of the cancellation pattern in terms corresponding to an element taper proportional to a^2 and to a uniform amplitude distribution respectively. Although, for both methods, the element position and the phase-only perturbations, the cancellation pattern is the superposition of M pairs of cancellation beams with some common features as discussed above, they also have some different characteristics.

The principal change in those cancellation patterns of the element position perturbations is that now one member of the pair has a peak in the direction of the null and the other member with a peak of the same magnitude and sign in the symmetric direction of the main beam. Hence any change on the pattern on

the null side of the main beam is accomplished by an equal change on the other side of the main beam. Thus, imposing a null on one side automatically creating another null in the symmetric direction of the main beam as shown in Figs.4.1-4.8. However, The first member of the pair of cancellation pattern, for the phase only perturbations, has a peak in the direction of the null but the other member of the pair has a peak of opposite phase in the symmetric direction of the main beam as shown in Figs.2.3 and 2.4. Hence any change in the pattern on the null side of the main beam is accomplished by an equal change but opposite sign on the other side of the main beam.Therefor, it can not possible to impose two nulls symmetrical around the main beam as proven by Shore [13].

Table 4-4 shows a tabulation of the normalized values of the beam coefficients c_m, of the element position perturbations compared to the normalized beam coefficients of the full weight and phase only methods. From the Table, the beam coefficients values for the element position perturbations are generally similar to the corresponding values of the phase only method which is expected from the previous discussions of the cancellation patterns. However, Table 4-5 give the values of the cancellation pattern at the null locations and at the corresponding symmetric locations around the main beam of the element position and the phase only perturbations. It can be seen that the values of the cancellation pattern at the null locations and at the symmetric locations around the main beam of the element position perturbations are equal in magnitude and

Table 4-4

Normalized values of the beam coefficient c, initial pattern F0, for the element position, full weight and phase-only perturbations.

0 DEG.	F0 VALUE	c FULL c y=a	y=1.0	c PHASE c y=a	y=1.0	c POSITION c y=a	y=1.0
20.0	-0.0311	-0.0311	-0.0311	-0.0312	-0.0320	-0.0312	-0.0320
18.6	-0.0221	-0.0125	-0.0135	-0.0138	-0.0157	-0.0223	-0.0189
21.5	-0.0219	-0.0112	-0.0128	-0.0100	-0.0112	-0.0001	-0.0075
21.5	-0.0219	-0.1415	-0.0645	-0.1446	-0.0685	-0.1368	-0.0651
24.5	-0.0221	0.1417	0.0647	0.1471	0.0723	0.1558	0.0761
20.0	-0.0311	-0.1228	-0.0624	-0.1326	-0.0720	-0.1505	-0.0797
21.5	-0.0219	0.0958	0.0346	0.1047	0.0423	0.1320	0.0541

y=a : $\sum(\Delta_n)^2 = MIN.$

y=1.: $\sum(a_n\Delta_n)^2 = MIN.$

Table 4-5

Normalized values of the initial pattern F0, perturbed pattern F, and the cancellation pattern value Fc, with one null located at 20°.

APPROX. CRITERIA	F0(20)	Fc(20)	Fc(-20)	F(20)
POS. $\sum(\Delta_n)^2$	-0.0311	0.0311	0.0311	-96 dB
POS. $\sum(a_n\Delta_n)^2$	-0.0311	0.0312	0.0312	-86 dB
PHASE $\sum(\varphi_n)^2$	-0.0311	0.0311	-0.0311	-96 dB
PHASE $\sum(a_n\varphi_n)^2$	-0.0311	0.0312	-0.0309	-79 dB

phase, where as the corresponding cancellation pattern values for the phase only method are equal in magnitude but opposite in sign.

Finally, let us examine the mean square difference (MSD) between the perturbed and the initial patterns for the element position, phase only and full weight perturbations. For half wavelength element spacing, it is known that minimizing the MSD is equivalent to minimizing the sum of the square of the total weigh perturbations $\sum|\Delta w_n|^2$ [24]. In the case of small phase only perturbations, minimizing sum of the square of the relative phases $\sum(a_n\varphi_n)^2$ will also approximately minimize the MSD as given in the previous reference. Similarly, from the results of Section 3.7, it can be concluded that minimizing the sum of the square of the relative element position perturbations $\sum(a_n\Delta_n)^2$ is approximately equivalent to minimizing the MSD for half wavelength spacing. Figures 4.9a-c show the MSD for the three methods when the imposing null was scanned in the sidelobe region with half wavelength spacing and with the main beam directed to the broadside. The MSD of the element position perturbations for minimizing the both approximation criteria $\sum(\Delta_n)^2$ and $\sum(a_n\Delta_n)^2$, are shown in Fig.4.9a. Note that the maximum MSD value is achieved when the null was imposed at a peak of a sidelobe and it is minimum when the imposed null coincides with an initial pattern null. Because the sidelobes level of the initial pattern are equal, the peaks of Fig.4.9a has equal MSD values too. Also, the figure shows that the MSD values for minimizing the relative element position perturbations are always smaller than the corresponding values with minimizing

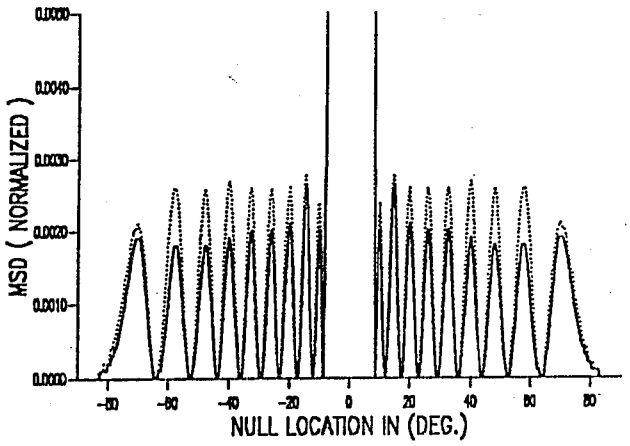

(a)

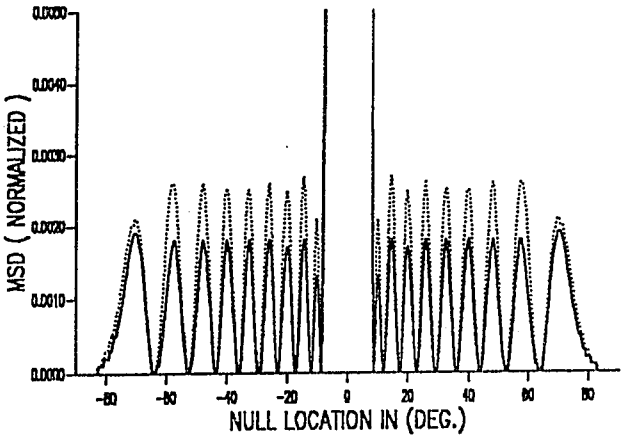

(b)

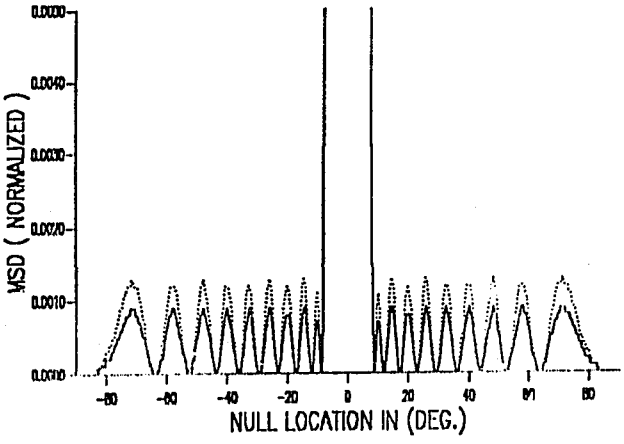

(c)

Fig.4.9 : Mean square difference (MSD) between the perturbed and the initial patterns when one null was scanned in the sidelobe region.
a) Element position method. b) Phase only method. c) Full weight method.
Dotted : Minimizing the sum of total perturbations.
Solid : Minimizing the sum of relative perturbations.
Initial 30-dB Chebyshev pattern, $N = 20$, $d_0 = \frac{\lambda}{2}$.

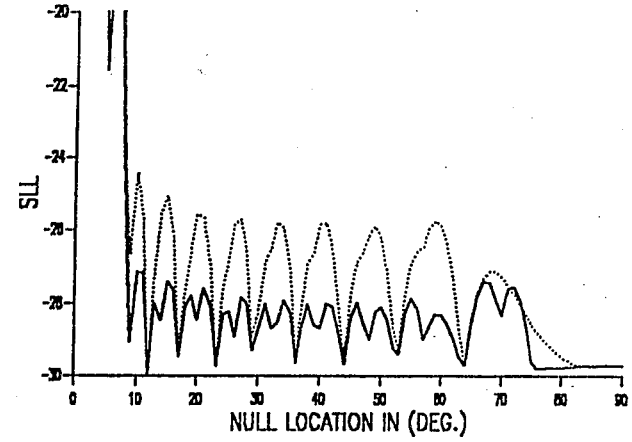

(a)

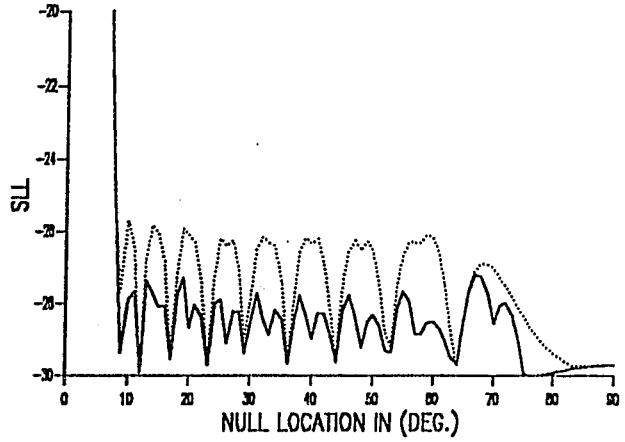

(b)

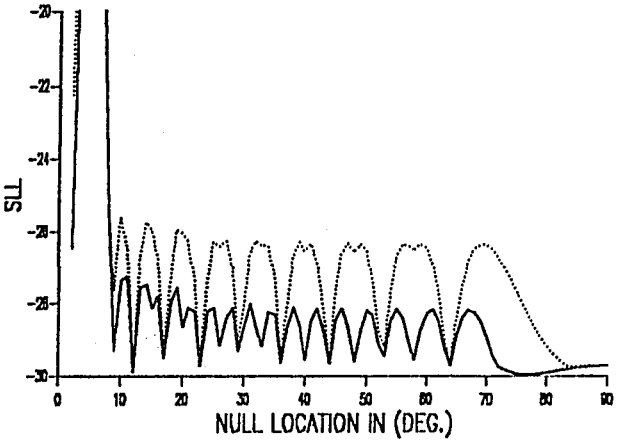

(c)

Fig.4.10 : Sidelobe level (SLL) of the perturbed pattern when one null was scanned in the sidelobe region.
a) Element position method. b) Phase only method. c) Full weight method.
Dotted : Minimizing the sum of total perturbations.
Solid : Minimizing the sum of relative perturbations.
Initial 30-dB Chebyshev pattern, $N = 20$, $d_0 = \frac{\lambda}{2}$.

the total element position perturbations. From Figs.4.9a-c, it can be seen that the MSD performance for the element position perturbations is similar to the performance of the phase only method, but not as well as the full weight perturbations method.

On the other hand, the SLL value is more important from the view point of antenna synthesis. Figures 4.10a-c show the SLL of the perturbed pattern when one null was scanned in the sidelobe region for the element position, phase-only, and full weight perturbations methods, respectively. From the Figures, it can be seen that the SLL performance with null steering is similar to MSD performance shown in Figs.4.9a-c, where the element position perturbations was performed similar to the phase-only but not as good as the full weight method. Note also that the SLL for the relative minimizations (solid) is always less than the total minimizations (dotted).

4.3 Effects of varying the number of imposed nulls on the array performance

The method for null steering by controlling the element positions which is described in Chapter three, is based on an approximation. The element position perturbations are considered small compared to the initial element spacing. Thus, two term Taylor expansion was proposed to obtain equation 3.6. To examine the effect of increasing the number of nulls, Figs.4.11a-c show the perturbed patterns with 2, 3, 4 and 5 nulls imposed at the top of the 3rd, 4th, 5th, and the 6th sidelobes respectively.

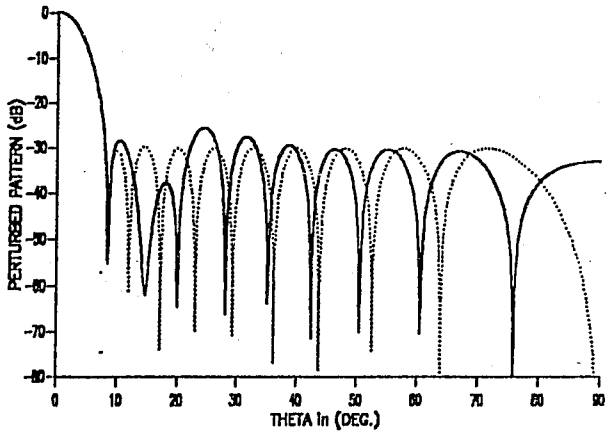

(a)

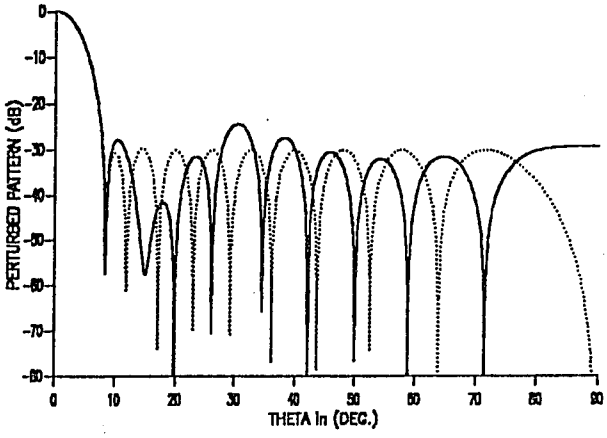

(b)

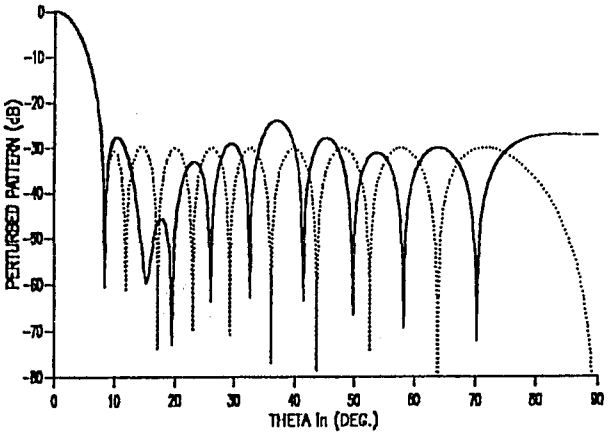

(c)

Fig.4.11 : Perturbed pattern (solid) with nulls imposed at
a) 14.5, 20.0, b) 14.5, 20.0, 26.1, c) 14.5, 20.0, 26.1, 32.7,
d) 14.5, 20.0, 26.1, 32.7, 39.9 and e) 14.5, 20.0, 26.1, 32.7, 39.9, 48.0.
Initial (dotted) 30-dB Chebyshev-pattern, $N=20$, $d_0=\frac{\lambda}{2}$. $\sum(a_n\Delta_n)^2=min.$

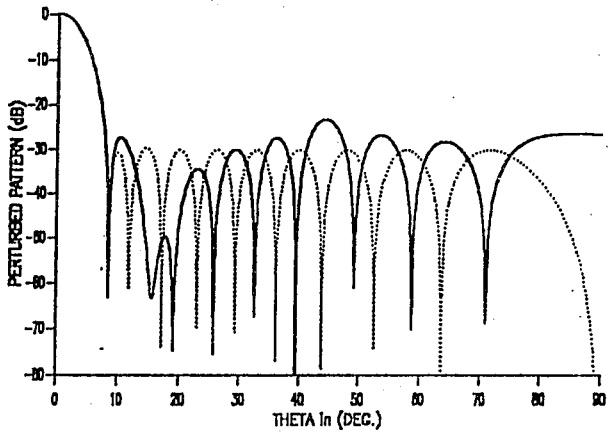

(d)

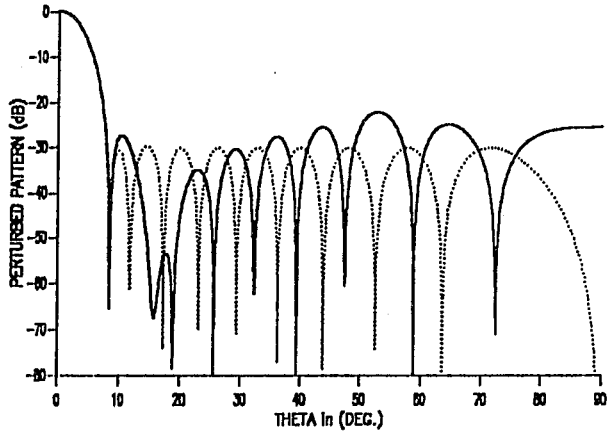

(c)

Fig.4.11 : \ Continued..

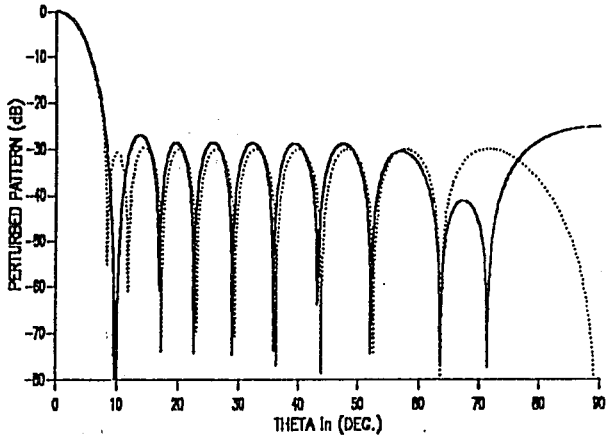

Fig.4.12 : Perturbed pattern (solid) with two nulls imposed at 10°and71.5°. $\sum(a_n\Delta_n)^2 = Min.$ Initial (dotted) 30-dB Chebyshev pattern, $N = 20$, $d_0 = \frac{\lambda}{2}$.

Table 4-6 gives the antenna array parameters for each of the Figures. From the Table, we can see that the SLL for each perturbed pattern is changed compared with the initial SLL value. The SLL degrades more as the number of the imposed nulls increases for both minimization criteria. However, it is seen that the mainlobe characteristics is almost unchanged compared to the initial main beam. Also, the antenna array directivity value is very close to the value of the initial array. In general the SLL value with minimized total element position perturbations is affected more than with minimized relative element position perturbations, which is consistent with the result obtained in Section 4.1.

When the number of nulls increases the pattern values at the null locations are almost changing randomly while the null location may shift as shown in Figs.4.11a-c. The above result may be explained as following. The method derived in Chapter three is based on an approximation where a small element position perturbations are assumed during our analysis. As the number of nulls increases the element positions must perturbed more to allocate the required null at the pattern which opposes the assumption of small element position perturbations. As the element position perturbations become large the results given by Eqs.(3.26) and (3.30) do not represent the solution of Eq.(3.6) any more. Table 4-7 gives element position perturbations for different selected set of prescribed nulls. It can be easily seen that the element position perturbation values are generally larger as the number of nulls increases.

It is interested to examine the capability of the algorithm to impose two null

Table 4-6

The values of the MSD, directivity, half power beamwidth (BW) and SLL for the perturbed patterns of Figs.4.11a-e and 4.12.

	MSD	DIR.	BW DEG.	SLL dB
Fig.4.11a	0.0063	17.30	6.33	-25.63
Fig.4.11b	0.0108	17.28	6.34	-24.54
Fig.4.11c	0.0151	17.26	6.34	-24.04
Fig.4.11d	0.0192	17.22	6.34	-23.31
Fig.4.11e	0.0241	17.15	6.34	-22.14
Fig.4.12	0.0039	17.33	6.30	-27.11
INITIAL		17.36	6.33	-29.71

TABLE 4-7

Computed element position perturbations for Figs.4.11a, 4.11c and 4.11e in wavelength.

ELEMENT NO.	FIG.4.11a Δ_n	FIG.4.11c Δ_n	FIG.4.11e Δ_n
1	-0.1344	-0.1970	-0.2212
2	-0.0179	0.0837	0.1657
3	0.0858	0.1398	0.0967
4	0.0836	0.0425	0.0417
5	0.0310	0.0052	0.0317
6	-0.0152	0.0062	-0.0136
7	-0.0294	-0.0148	-0.0136
8	-0.0190	-0.0292	-0.0215
9	-0.0048	-0.0137	-0.0198
10	0.0003	-0.0004	-0.0013

one very close and the the other very far from the main beam. Figure 4.12 shows two nulls imposed at the pattern the first at 10° and the other at 71.5° which are the top of the first and the last sidelobes respectively. From the figure, the null value of the first null is more than 90 dB and 80 dB for the second null. The antenna array parameters corresponding to this figure are given in Table 4-6. AS a result from the figure and the values given in the Table, the algorithm is able to impose two nulls one very close and the other very far from the main beam.

4.4 Effects of varying the pattern type on the array performance

The solution as given by Eqs.(3.23) and (3.29) is independent of the initial pattern type. Thus, the solution for both cases with the most common current distributions are tested. Figures 4.1-11 show the capability of the algorithm to steer the nulls when the chebyshev current distribution was applied. Figures 4.13a and 4.14a show three nulls imposed at 14.5°,20° and 26.1°, for the uniform and Taylor current distributions respectively. Since the chebyshev current distribution is optimum in the sense of minimax criterion, where a uniform sidelobes are achieved, a wide main beam will be obtained. Also, the uniform current distribution yields a taper sidelobes with sharp main beam. Therefore, we can conclude that the algorithm can steer the nulls independent of pattern type. In fact all the results for one pattern type are applicable to any other type. The element position perturbations of Figs.4.11b, 4.13, and 4.14 are given in Table 4-8. From the Table, it can be seen that the element position

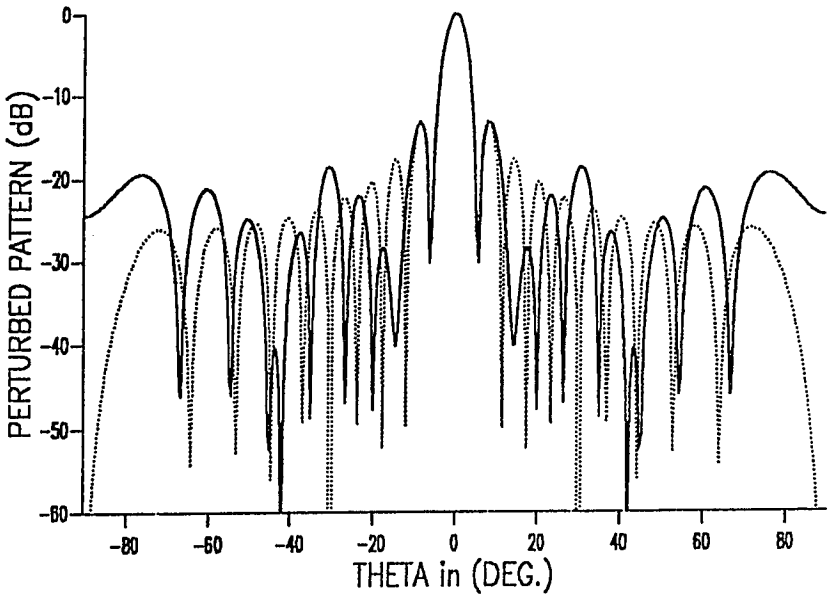

(a)

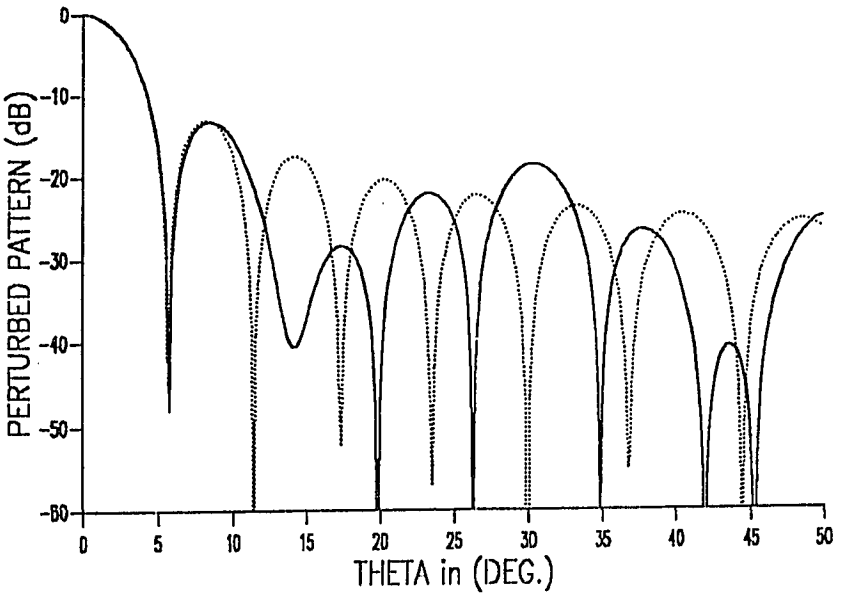

(b)

Fig.4.13 : a) Perturbed pattern with three nulls imposed at 14.5°, 20.0° and 26.1°.
b) Perturbed pattern (solid), $\theta = 0°$ *to* 50°.
Initial uniform distribution pattern (dotted), $N = 20$, $d_0 = \frac{\lambda}{2}$.

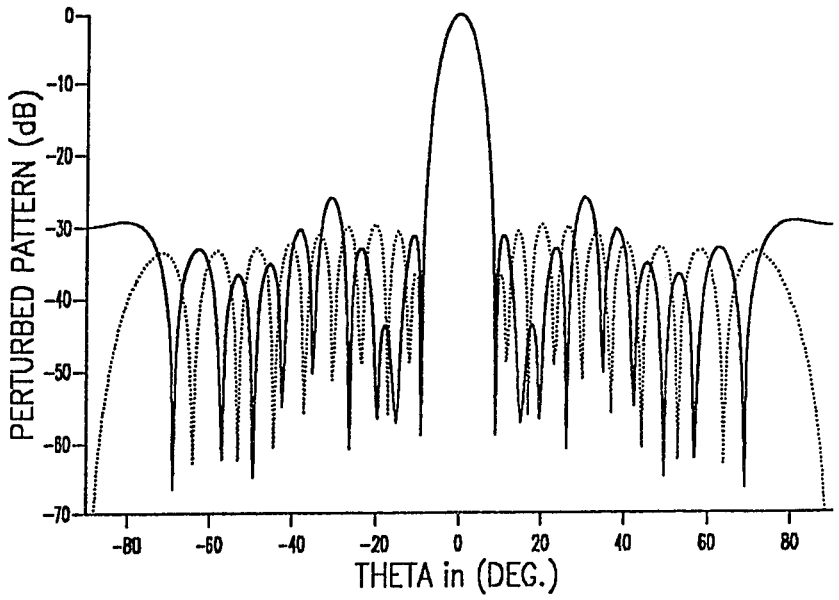

(a)

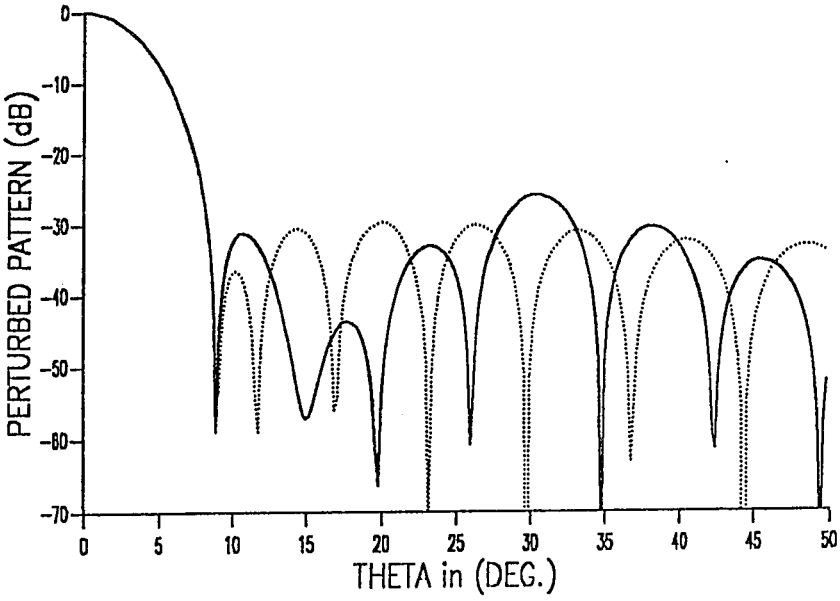

(b)

Fig.4.14 : a) Perturbed pattern with three nulls imposed at 14.5°, 20.0° and 26.1°.
b) Perturbed pattern (solid), $0 = 0°$ *to* 50°. Minimizing $\sum(a_n\Delta_n)^2$.
Initial 30-dB Taylor pattern (dotted), $N = 20$, $d_0 = \frac{\lambda}{2}$.

Table 4-8

Computed element position perturbations for Figs.4.11b, 4.13 and 4.14 in wavelength.

ELEMENT NO.	FIG.4.11b Δ_n	FIG.4.14 Δ_n	FIG.4.13 Δ_n
1	-0.1725	-0.1966	-0.2904
2	0.0301	0.0327	0.0159
3	0.1295	0.1399	0.2410
4	0.0716	0.0732	0.2101
5	0.0028	-0.0012	0.0552
6	-0.0143	-0.0168	-0.0376
7	-0.0082	-0.0078	-0.0611
8	-0.0135	-0.0104	-0.0954
9	-0.0221	-0.0181	-0.1208
10	-0.0117	-0.0099	-0.0595

perturbations for the sinc pattern is the largest.

4.5 Effects of main beam steering on the array performance

One of main advantages of null steering using the element position perturbations is that the phase shifters are used solely for steering the main beam. Thus, if the interference direction is known exactly then the complete nulling of the noise source can be achieved despite the coarseness of the phase increments. In other words, the main beam is steered by changing the phase shifters only, while the desired nulls are created solely by changing the element positions. In general, the element spacing must be less or equal half the operating wavelength to avoid the grating mainlobe. The null steering capability by controlling the element positions is discussed in this Section when the main beam is steered from broadside. But before that, let us verify the results given in Section 3.6 where the discussion show that imposing a null at the sidelobe of the initial pattern will automatically locate another null symmetric with respect to the main beam. To simplify the following discussions, let us define the variable u, given previously by Eq.(3.1), to be

$$u = \sin(\theta)$$

where θ: the angle from broadside. In fact, from the above definition, the wavenumber k was only dropped from the old variable u given by Eq.(3.1). Then Eq.(3.33) remains also true with the new definition given above; that is, if the imposed null location is at u_l, then,

$$\bar{u}_l = -u_l + 2u_s \tag{4.1}$$

where, $u_1 = \sin(\theta_1)$, θ_1 : imposed null angle

$\bar{u}_1 = \sin(\bar{\theta}_1)$, $\bar{\theta}_1$: the angle of the symmetric null accompanied with the imposed null.

$u_s = \sin(\theta_s)$, θ_s : steering angle of the main beam.

Because the visible region is defined as $\frac{-\pi}{2} \le \theta \le \frac{\pi}{2}$ or $-1 \le u \le 1$, then the symmetric location of the imposed null will be inside the visible region when

$$-1 \le \bar{u}_1 \le 1$$

or

$$\frac{\sin(\theta_1) - 1}{2} \le \sin(\theta_s) \le \frac{1 + \sin(\theta_1)}{2} \tag{4.2}$$

Figures 4.15a-c show the perturbed pattern with one null imposed at -10° (u_1=-0.1736) for a 30-dB Chebyshev initial pattern of half wavelength element spacing. The perturbed pattern with the main beam steering angle at θ_s=20° (u_s=0.342) is shown in Fig.4.15a. The location of the corresponding symmetric null is at ($\bar{u}_1$=0.8577), which is agreed with expected location obtained by Eq.(4.1). The symmetric null location of the imposed null -10° is in the invisible region when the main beam steering angle θ_s> 24.4°. The perturbed pattern with the main beam steering angle at θ_s=30° (u_s=0.5) is shown in Fig.4.15b. The location of the corresponding symmetric null is at ($\bar{u}_1$=1.1736) which is in the invisible region.

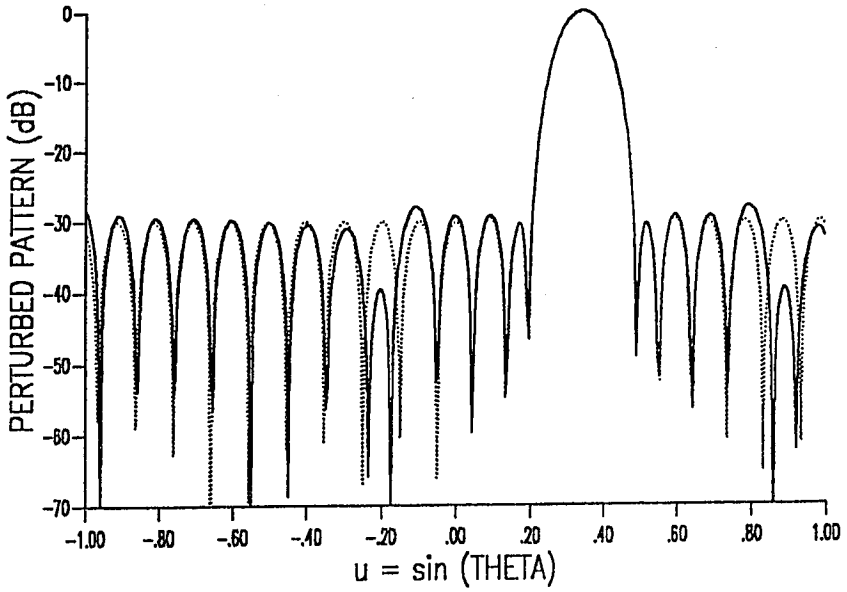

(a)

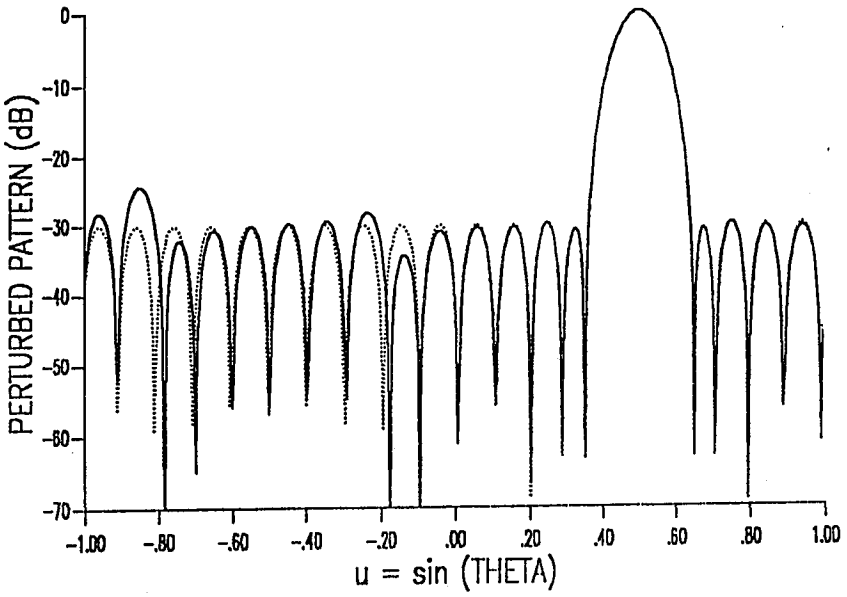

(b)

Fig.4.15 : Perturbed pattern (solid) with one null imposed at $u_1 = -0.1736$ (-10°)
a) $u_s = 0.342$, ($\theta_s = 20°$), b) $u_s = 0.5$, ($\theta_s = 30°$). $\sum(a_n\Delta_n)^2 = Min.$
Initial (dotted) 30-dB Chebyshev pattern, $N = 20$, $d_n = \frac{\lambda}{2}$.

Now let us study the null steering capability by controlling the element positions where a 30-dB Chebyshev initial pattern of 20 element isotropic linear array is considered. Figures 4.16a-c show the main beam bandwidth (BW), directivity and the sidelobe level (SLL) of the perturbed pattern with one null imposed at -10°, versus the main beam steering angle from broadside, when the element spacing was half wavelength. It is seen that the BW increases and the directivity value stay constant (17.36) as the main beam steering angle increases for the initial pattern (dotted) as shown in Figs.4.16a and 4.16b respectively. The BW of the perturbed pattern (solid) is almost unchanged compared with the BW of initial pattern as shown in Fig.4.16a. Also, the directivity of the perturbed pattern is changed slightly compared with initial value. However, the SLL performance degrades when the main beam steering angle exceeds 24.4°, as shown in Fig.4.16.c, which means that the symmetric null location is in the invisible region, ($\bar{u}_1 > 1$).

Since the array pattern for an equispaced linear array is periodic with 2π in the variable $d_0 k\sin(\theta)$, it is possible to improve null steering performance with the main beam steering angle larger than 24.4° by reducing the element spacing d_0, and hence shift the symmetric null location outside the visible region. Note that in the special case of half wavelength spacing $d_0 = \frac{\lambda}{2}$, the period $-\pi \le kd_0\sin(\theta) \le \pi$ coincides with visible region. To verify the above results, Figs.4.17a-c show the BW, directivity and the SLL of the perturbed pattern but

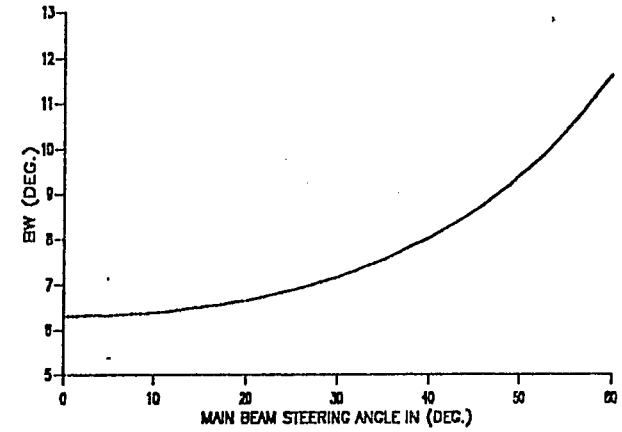

(a)

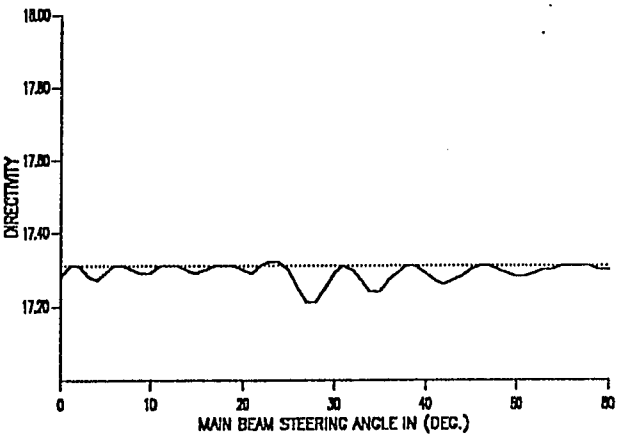

(b)

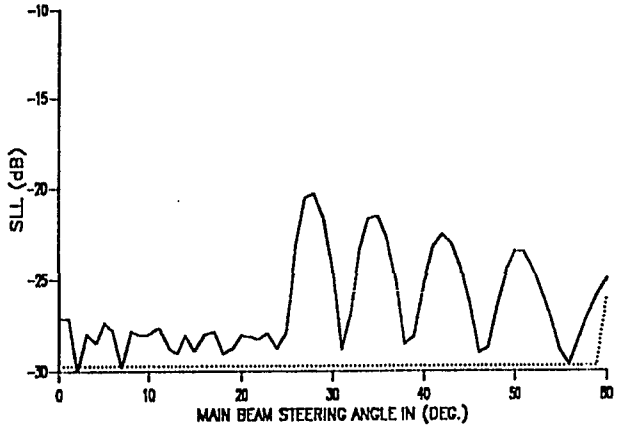

(c)

Fig.4.16 : Perturbed (solid) and initial (dotted) pattern parameters with one null imposed at -10°, when the main beam steering angle in the range, $\theta_s = 0°$ *to* $60°$. $\sum(a_n\Delta_n)^2 = min.$

a) Main beam width (BW). b) Directivity. c) Sidelobe level (SLL).

Initial (dotted) 30-dB Chebyshev pattern, $N = 20$, $d_0 = \frac{\lambda}{2}$.

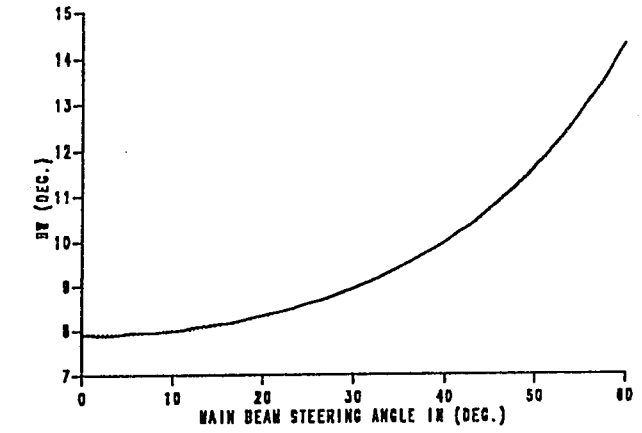

(a)

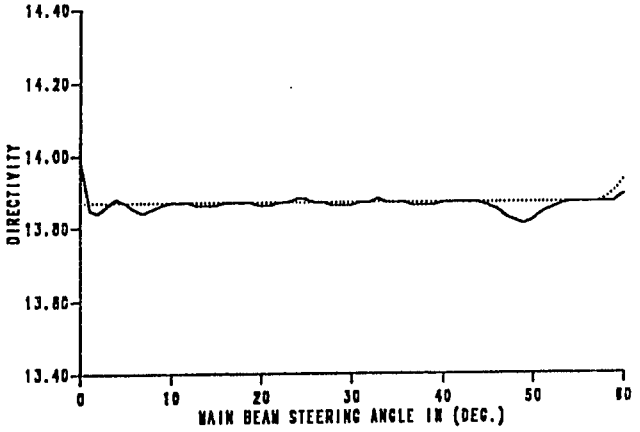

(b)

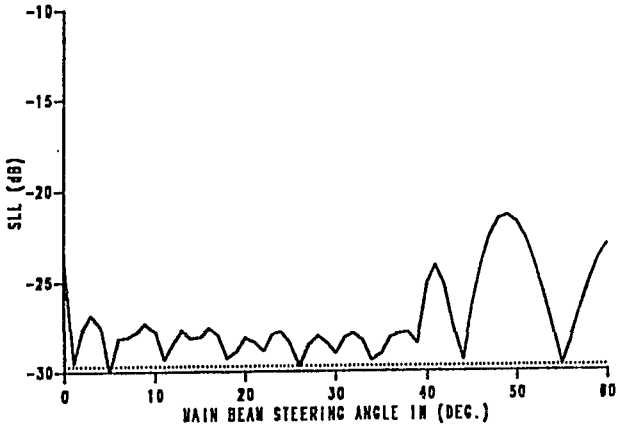

(c)

Fig.4.17 : Perurbed (solid) and initial (dotted) pattern parameters with one null imposed at -10°. when the main beam steering angle in the range, 0_s = 0° *to* 60°. $\sum(a_n\Delta_n)^2 = min.$
a) Main beam width (BW). b) Directivity. c) Sidelobe level (SLL).
Initial (dotted) 30-dB Chebyshev pattern, N = 20, d_0 = 0.4 λ.

with element spacing of 0.4 λ. Notice that, as the element spacing d_0, decreases the BW will increase and the directivity will decrease (initial 13.88) as shown in Figs.4.17a and 4.17b. However, the BW and directivity performance are similar to the corresponding BW and directivity shown in Figs.4.16a and 4.16b. Fig.4.17c show that the SLL performance is improved than the previous case when the element spacing was .5 λ. Here the main beam angle can be steered up to 39° and the SLL of the perturbed pattern is slightly changed from the initial value (dotted).

Similarly, Figs.4.18a-c show the BW, directivity and the SLL of the perturbed pattern with element spacing of 0.25 λ. The SLL performance of null steering when the main beam scanned from broadside is improved as shown in Fig.4.17c. In this case the main beam steering angle can be any angle in the given range, while the SLL may slightly changed from the initial value, with one null imposed at -10°.

Before finishing this discussion, Figs.4.19a-c illustrate some of the basic concepts mentioned above. Figure 4.19a show the perturbed pattern with one null imposed at -10° (u_1 = -0.1736), for element spacing $d_0 = 0.4\lambda$ and main beam steering angle 0_s = 30°. The symmetric null is located at (u = 1.1736), which can be verified from the Figure, unlike the case of element spacing of 0.5 λ where no symmetric null can be located in the period of 2π for the variable $[d_0 k \sin(0)]$ as was shown in Fig.4.15b. The case where the symmetric null can not be located in the period of 2π for the 0.4λ element spacing is shown in

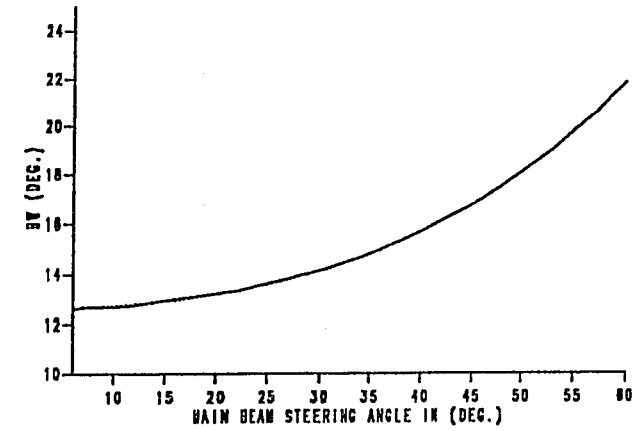

(a)

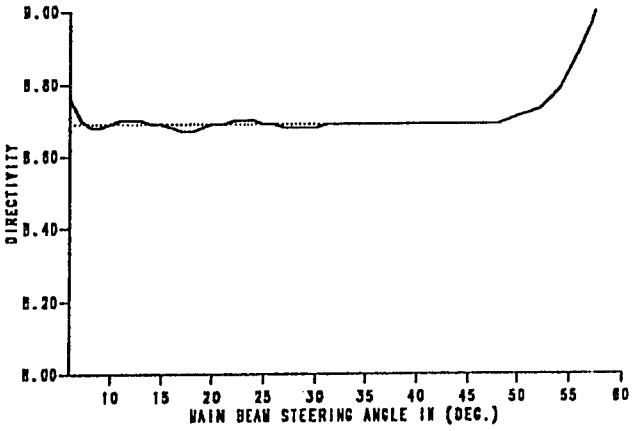

(b)

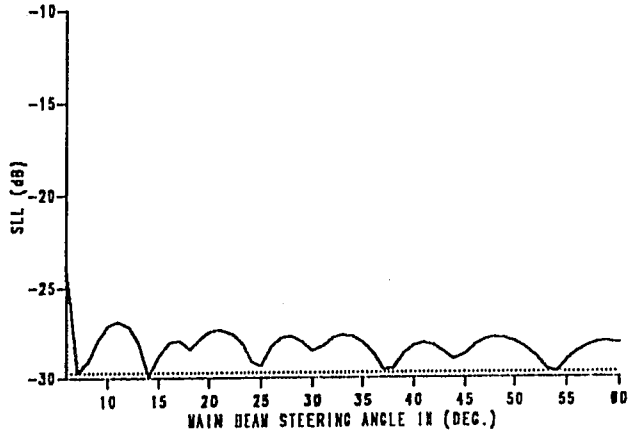

(c)

Fig.4.18 : Perturbed (solid) and initial (dotted) pattern parameters with one null imposed at -10°. when the main beam steering angle in the range, θ_s = 0° *to* 60°. $\sum(a_n\Delta_n)^2$ = *min.*
a) Main beam width (BW). b) Directivity. c) Sidelobe level (SLL).
Initial (dotted) 30-dB Chebyshev pattern, N = 20, d_0 = 0.25 λ.

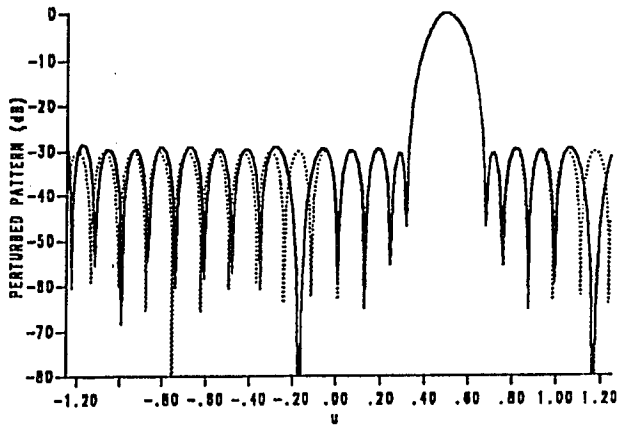

(a)

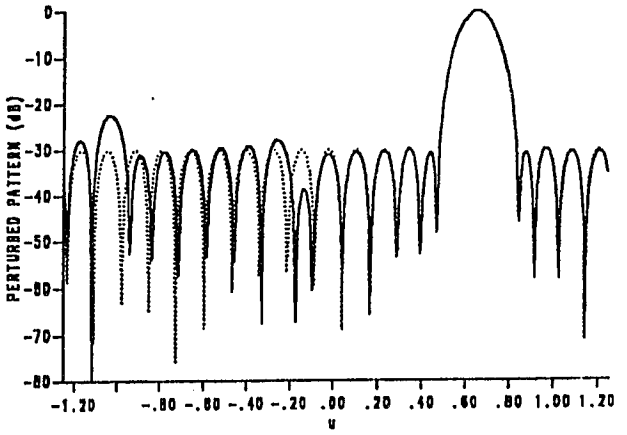

(b)

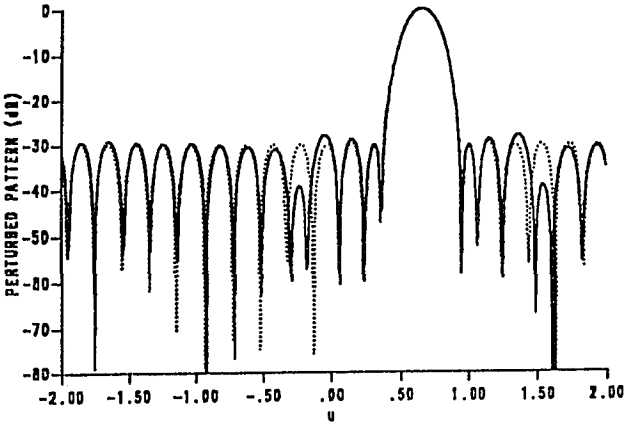

(c)

Fig.4.19 : Perturbed pattern (solid) with one null imposed at -0.1736 (-10°). $\sum(a_n\Delta_n)^2 = Min.$

a) $u_s = 0.5$, ($\theta_s = 30°$), $d_0 = 0.4\lambda$.

b) $u_s = 0.656$, ($\theta_s = 41°$), $d_0 = 0.4\lambda$.

c) $u_s = 0.656$, ($\theta_s = 41°$), $d_0 = 0.25\lambda$.

Initial (dotted) 30-dB Chebyshev pattern, N = 20.

Fig.4.19b, where the main beam steering angle $\theta_s = 41°$. In this case, the symmetric will be located at (u = 1.4857), which is outside the period of the array pattern. The SLL value for the perturbed pattern is much higher than the previous case of Fig.4.19a. The same imposed null with main beam steering angle but with element spacing of 0.25λ is shown in Fig.4.19c. Now the symmetric null is located inside the period of the array pattern as shown in the Figure. It can be seen that the SLL is much less than the SLL of the perturbed pattern shown in Fig.4.19b. As conclusion, the main beam steering angle will be improved as the element spacing reduced but the BW and the directivity value will degrade.

4.6 Wideband interference suppression

In recent years there has been considerable interest in designing antenna arrays with broad null sectors to suppress wideband interference signal [34,45]. Since the pattern is frequency dependent, a narrow angular null is effective only over a narrow frequency band. Therefore, wideband interference suppression requires that the pattern be nulled over an extended sector. Also, the need for broad null often arises when the direction of the undesired signal may be vary slightly with time or may be not known exactly.

One of the well known method to achieve broad null is by forming several closely spaced nulls. Clearly, the nulling performance of an adaptive antenna system depends not only on the available number of degrees of freedom but also

on the adaptive architecture. When a sufficient number of degrees of freedom, say M, has been imposing to obtain a broad null, then the remaining N/2-M degrees are used to approximate, in some sense, the initial pattern, independent of a particular architecture. In this Section, broad sector nulling by element position perturbations will be considered to suppress wide band interference signal.

Let us consider a linear array of N isotropic elements with equispaced distance d_0, as shown in Fig.1.5. The initial and the perturbed array patterns can be written as given by Eqs.(3.1) and (3.3). Simplification will be made when if we set the variable $u = \sin(0)$, and with the main beam steering angle at broadside, then Eq.(3.3) can be rewritten as,

$$F(u) = \sum_{n=1}^{N} a_n e^{j x_n k u} \tag{4.3}$$

Since the pattern is frequency dependent, therefore the dependence of the pattern on both angle and frequency is described by the product ku. Thus, a small change Δu, in angle has the same effects as a change Δf, in frequency. The relation between Δu and Δf can be found in [34], where the pattern differential obtained from (4.3) is set to zero,

$$dF = \frac{\partial F}{\partial f} df + \frac{\partial F}{\partial u} du = 0 \tag{4.4}$$

The partial derivatives can be obtained directly from (4.3) which gives,

$$\frac{\partial F}{\partial f} = u.G \quad \text{and} \quad \frac{\partial F}{\partial u} = f.G \tag{4.5}$$

where, by setting c to be the velocity of light,

$$G = \frac{j2\pi}{c} \sum_{n=1}^{N} a_n x_n e^{j x_n k u}$$

Substituting (4.5) into (4.4) to get

$$\frac{du}{u} = -\frac{df}{f} \tag{4.6}$$

The above differential can be approximated by increments as,

$$\frac{\Delta u}{u} \approx -\frac{\Delta f}{f} \tag{4.7}$$

From the above relation, a wide band interference with relative bandwidth $\frac{\Delta f}{f_0}$ located at $u = u_j$ will thus appear to cover an angular pattern sector which is centered at $u = u_j$ and has the width

$$\Delta u \approx u_j \frac{\Delta f}{f_0} \tag{4.8}$$

As mentioned in Section 3.2, the resultant pattern can be expected to more or less resemble the initial pattern, with local perturbations around the interference direction, if the number of imposed null M, is much less than the number of degrees of freedom N/2. Therefore, in the following we confine our interest to compare the initial pattern F(u) over the desired nulling sector Δu, only. The broad nulling performance can be studied easily if we follow the procedure of Steyskal [34], where the the measure of the sidelobe-peak cancellation ratio C, defined by the square of the maximum magnitude of F within a sector Δu, normalized to the maximum value of the sidelobe envelope

F_0, of the initial pattern is obtained,

$$C = \frac{\max_{u \in \Delta u} F(u)^2}{\max_{u \in \Delta u} F_0(u)^2} \tag{4.9}$$

The problem of wideband nulling for an array antenna using multiple nulling over a narrow angular sector with full weight perturbations was studied in the previous reference. Here, the element position perturbations will be suggested to achieve wideband interference nulling. To validate the above suggestion, Figs.4.20a-c show a 11.3,33.2 and 28.6 dB sidelobe cancellation ratio which are achieved over a sector $\Delta u = 0.0263$, corresponding to relative bandwidth spread of 5 % when 2, 3 and 4 equispaced nulls was imposed over the sector, respectively. It can be seen that the sidelobe cancellation ratio for $M = 3$ is better than the sidelobe cancellation ratio for $M = 2,4$ as shown in Figs.4.20a-c. Therefore, it is not true that the sidelobe cancellation ratio always gets better as the number of the imposed nulls increases, due to the approximation inherent in the method. Hence, for a specified sector width, there is an optimum number of imposed null to achieve the largest sidelobe cancellation ratio. The relation between the number of imposed nulls and the sidelobe suppression can be found in Table 4-9. From the Table, the optimum number of nulls to obtain broad sector nulling corresponds to a relative bandwidth of 5 % ,10 % ,and15 % are 3, 3 and 4 nulls, respectively.

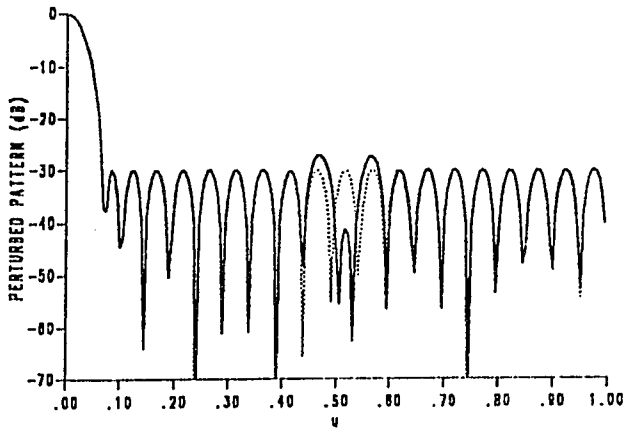

(a)

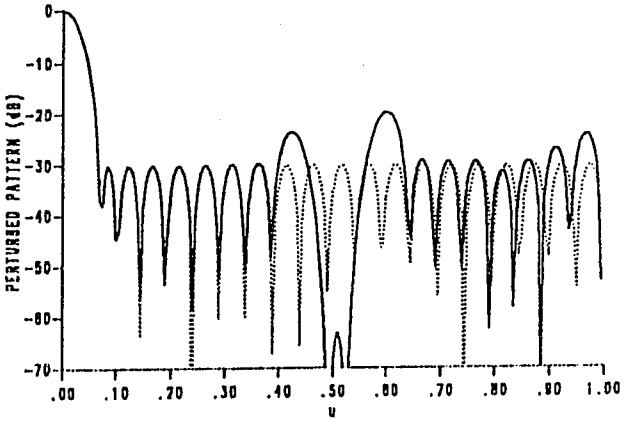

(b)

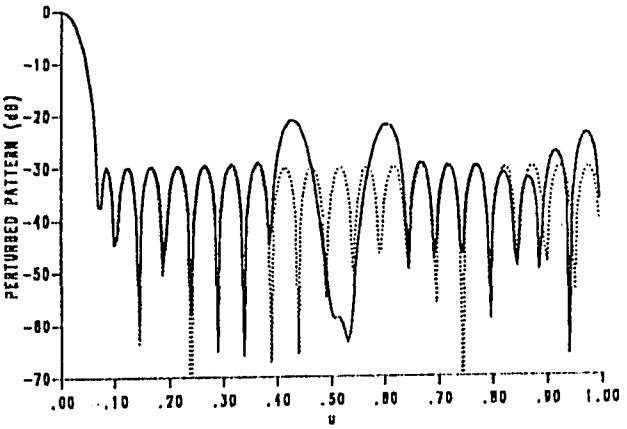

(c)

Fig.4.20 : Sector nulling centered at $u_j = 0.5165$ and with width $\Delta u = 0.0263$ (B = 5 %).
a) Two equispaced nulls, b) Three equispaced nulls, and
c) Four equispaced nulls imposed over the sector. $\sum(\Delta_n)^2 = Min.$
Initial 30-dB Chebyshev pattern . N = 40, $d_0 = \frac{\lambda}{2}$.

TABLE 4-9

Sidelobe peak cancellation ratio C, for different sector nulling widths centered at u_j=0.5165. when the number of imposed nulls M, are varied. Initial 30-dB Chebyshev pattern with half wavelength spacing.

		CANCELLATION RATIO C			
u	B%	M=2	M=3	M=4	M=5
.0263	5	41.3	63.2	58.6	
.0516	10	30.2	53.7	58.0	40.0
.0774	15	25.0	42.0	50.2	41.5

$\sum(\Delta_n)^2 = MIN.$

		CANCELLATION RATIO C			
u	B%	M=2	M=3	M=4	M=5
.0263	5	42.7	46.0	45.0	
.0516	10	30.0	46.0	45.5	31.0
.0774	15	26.2	41.5	45.0	30.0

$\sum(a_n\Delta_n)^2 = MIN.$

4.7 Practical considerations

In practice, servomechanism devices that are used extensively in automatic control systems, may be used to achieve the new element positions x_n, which are computed from Eq.(3.2) and either Eq.(3.23) or (3.29). Figure 4.21 show a practical block diagram of a suggested adaptive linear array for null steering by element position perturbations, where the element positions are controlled by using servomechanism devices according to the number of nulls needed to be controlled. So, the variable phase shifters are used to steer the main beam only towards the desired signal. From these servomechanism devices is the servomotor which might be thought of as a precision electric motor whose function is to cause motion in the form of rotation or linear motion in proportional to a supplied electrical command signal.

AC servos tend to be more stable, lighter in weight, rugged and require less maintenance. Also, they do have a small torque which suggest that the AC servos can be used as servomechanism controller to control the element positions. Figure 4.22 show a block diagram of the design layout for each element of the array. The set point to the system is 0_n, relative to the element position perturbation Δ_n, as shown in the Figure. The control system will work as described in [53, PP.280], where the amount of rotation 0_n, of the control transmitter's rotor, determine the phase and amplitude of the AC signal going to the amplifier. The phase angle is measured relative to the AC supply voltage. The servomotor's rotor direction and amount of rotation is determined by the

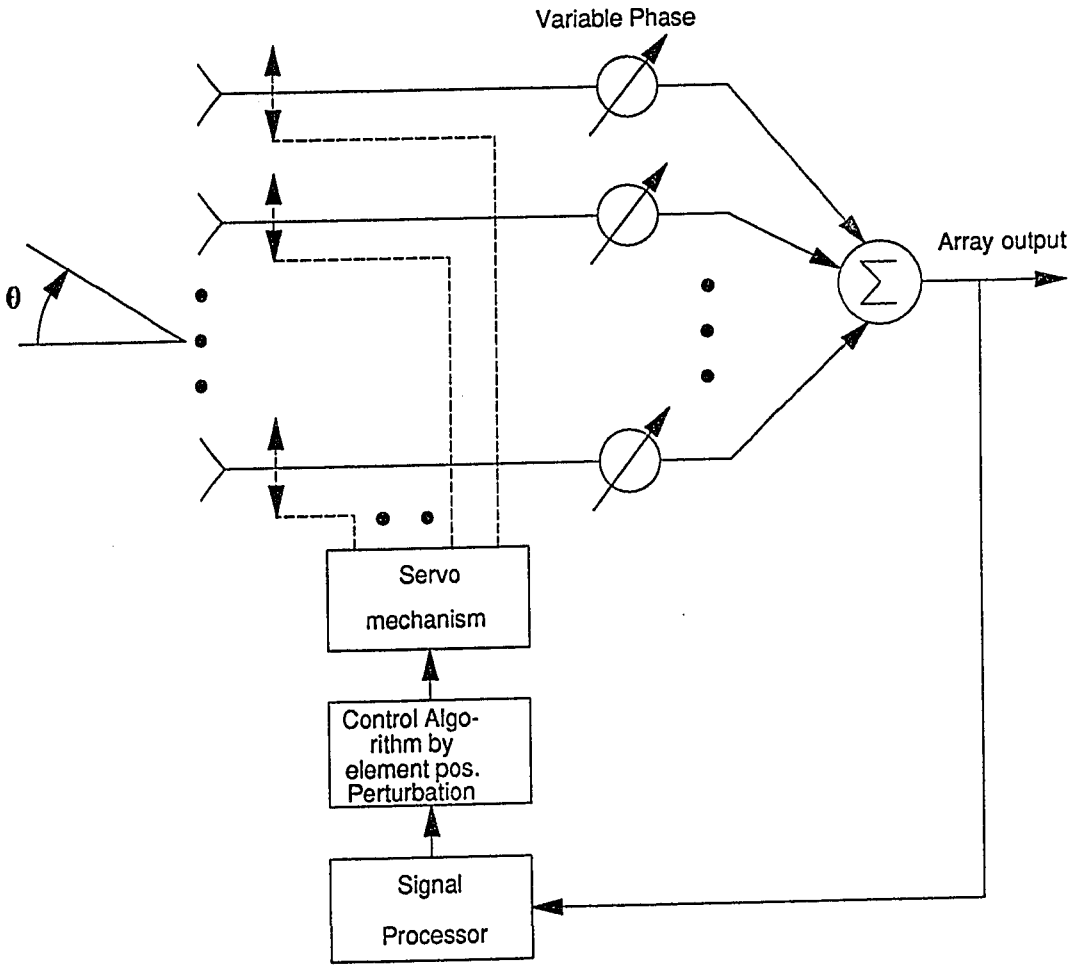

Fig.4.21 : Block diagram of an 8-element adaptive array using element position perturbations.

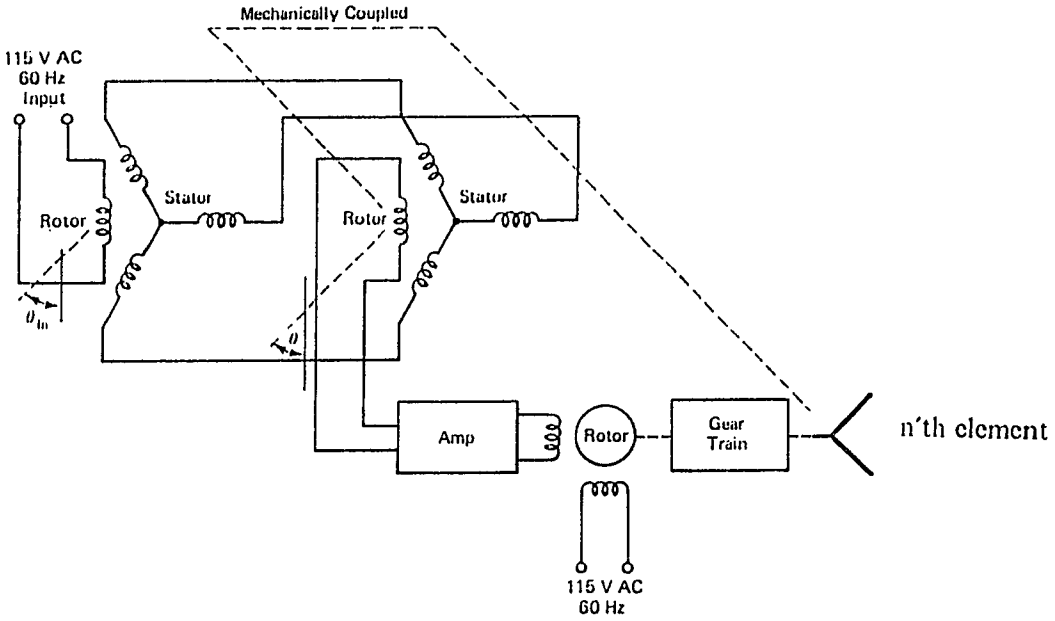

Fig.4.22 : Schematic of remote control antenna element positioner.
From Carstens, [53, *PP*.281].

the amplifiers output voltage phase and amplitude. The gear train's rotational output is mechanically coupled to the antenna element. It is also coupled to the rotor of the control transformer. If the two rotors are at the same angle of rotation, the error signal will be zero. Any difference in the two angles will create an error signal in the form of AC voltage, which will cause the servo to turn in the proper direction to reduce this difference to zero.

On the other hand, the use of digitally controlled positioners means that the element positions can be changed in discrete steps only. Since, the stepper motor responds to digital-like signals, it is a natural servomechanism device that can lend itself to be used in the digital controlling system. The theory of operation of this motor can be found in [53, PP.134-139]. What we discuss here is how to use this motor in an automatic digital control application. A typical stepper motor control system is shown in Fig.4.23 which is entirely digital control system.

Note that since the element position perturbation are odd symmetry, the number of servomotors can be reduced to the half. Each servomotor can control a pair of elements which are located symmetric around the centre of the array.

4.8 Sensitivity analysis

The perturbed patterns shown so far are computed by assuming that the exact position perturbation given by Eq.(3.23) and (3.29) are used. In practice,

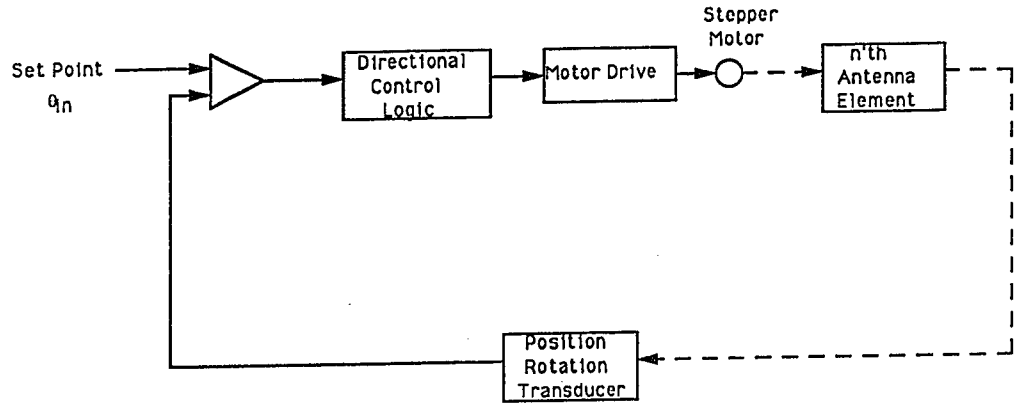

Fig.4.23 : An automatic control system using a stepper motor.

servomechanism devices that are used extensively in automatic control systems can be used to achieve the desired element positions as mentioned in the previous Section. Even though servomotors are designed to operate at relatively high input voltages such that +26 DC or +28 AC, most of their operation lives are spent responding to input voltages that are just a fraction of their rated operating voltage. This is because the input command signals are usually small. However, there is a threshold limit to any servo's ability to respond to weak signals. This is where the dead band comes to appear. Dead band may be defined as a range of input signals that is furnished to a device or system before that system finally responds to this input (see Fig.4.24). Dead band is created by system friction, inertia, magnetic coupling, gear train load, and backlash on the servo or any combination of these quantities. In this case of the servo control characteristics depicted in Fig.4.24, if a rotation of +5.7 of a control device is necessary to produce the +1.5 V for servo rotation, then the dead band is specified as +5.7. Any good servomotor should be able to respond to a voltage as low as about 5% of its rated operating voltage.

In fact, if the magnitude of each element position perturbation, Δ_n, is changed by a small amount, δ_n, i.e. $\hat{\Delta}_n = \Delta_n + \delta_n$, then the new expression F_e, of the perturbed array factor becomes,

$$F_e = \sum_{n=1}^{N} a_n e^{j(d_n \lambda)(u - u_s)} = F + F_1 \qquad (4.10)$$

Where F is the ideal perturbed array pattern and F_1 represents the spurious pattern caused by the truncation error, δ_n,

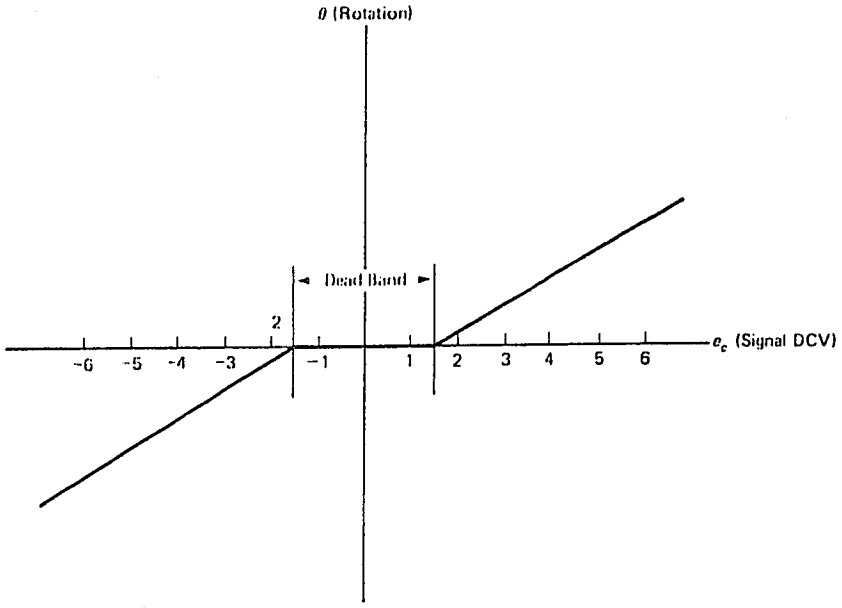

Fig.4.24 : A servomotor's dead band. From Carstens, [53, *PP*.261].

$$F_l = j\,(u - u_s) \sum_{n=1}^{N} \delta_n\, a_n\, e^{j x_n (u - u_s)} \qquad (4.11)$$

The truncation error δ_n, are odd symmetry and real which means that the spurious pattern will be also have its main beam pointed toward the desired signal. In general, its null will not coincide with those of the desired pattern, so that the effect of the quantization error is to fill in the nulls. However, since only the sidelobes of F_l will effect the nulls of the ideal pattern, and if δ_n are very small with respect to Δ_n then the effect of the rounding off the element positions will generally be insignificant.

As an illustration, let us consider the case of Fig.4.11.b with three nulls imposed at 14.5, 20, and 26.1. Ideally, the element position perturbations are given in Table 4-10 (column 2). In particular, if we have a servomechanism which precisely can position the element up to the second digital placed then the new element position perturbation can be truncated as given in Table 4-10 (column 3). Figure 4.25 shows the resulting perturbed pattern of the truncated element position perturbations $\hat{\Delta}_n$, compared with the perturbed pattern of the ideal element position perturbations Δ_n. It is clear that even though the element position perturbations have been truncated to the second decimal digit, the sidelobe structure of the new pattern differs only little from that of the ideal pattern (dotted) shown in Fig.4.25. Note that the main beam characteristics remains the same as the ideal pattern. More importantly, although the nulls at 14.5, 20, and 26.1 have been partially filled, the values of the perturbed pattern

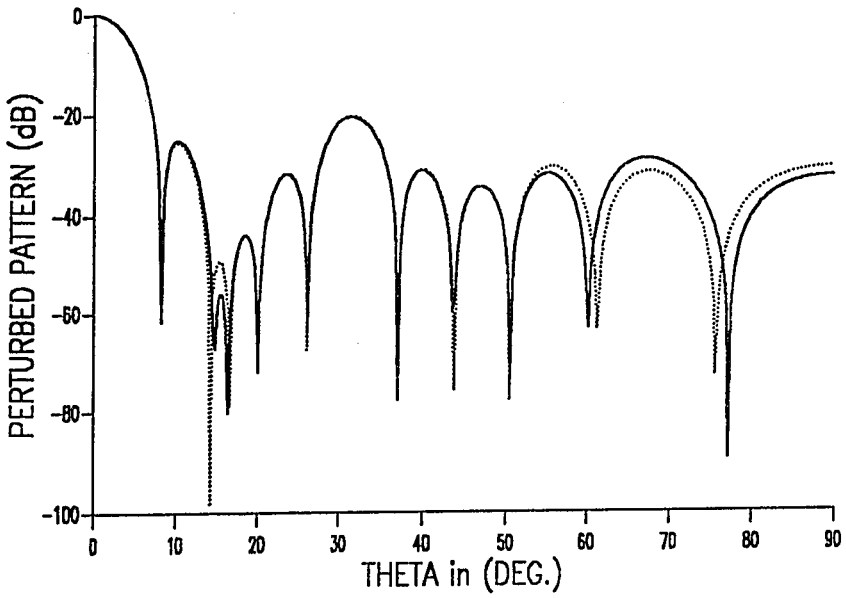

Fig.4.25 : Perturbed pattern with three nulls imposed at 14.5°, 20°, and 26.1°.
Dotted: Ideal element position perturbations for column 2 of table 10.
Solid : Truncated element position perturbations for column 3 of table 10.

Table 4-10

Computed element position perturbations for Figs.(4.25,4.26a-b) in wavelength.

ELEMENT NO.	FIG.4.25		FIG.4.26a	FIG.4.26b
	Δ_n	$\hat{\Delta}_n$	$\hat{\Delta}_n$	$\hat{\Delta}_n$
1	-0.09320	-0.09	-0.008	0.00
2	0.01918	0.01	0.003	0.00
3	0.11121	0.11	0.014	0.01
4	0.09059	0.09	0.012	0.01
5	-0.02066	-0.02	-0.008	0.00
6	-0.07284	-0.07	-0.027	-0.02
7	-0.03481	-0.03	-0.018	-0.01
8	-0.01881	-0.01	0.015	0.01
9	-0.05009	-0.05	0.037	0.03
10	-0.03363	-0.03	0.019	0.01

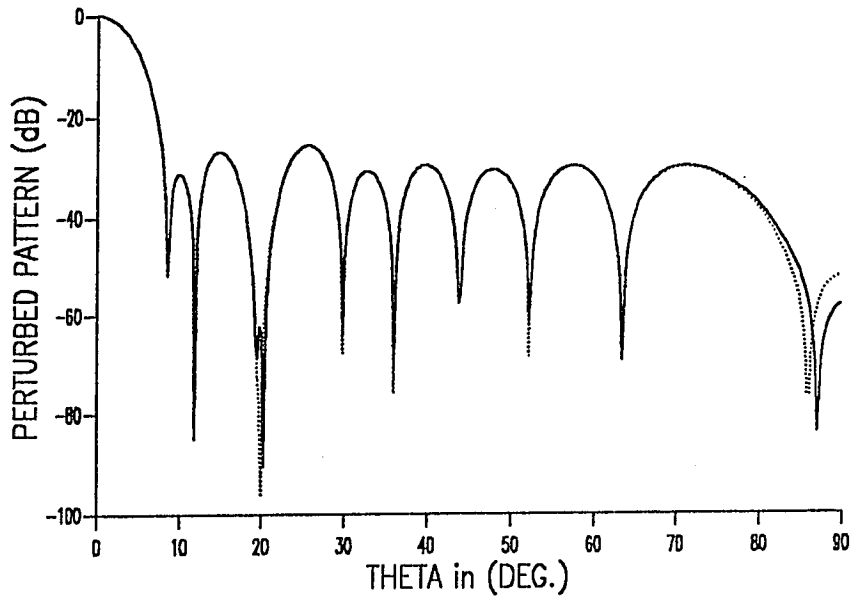

(a)

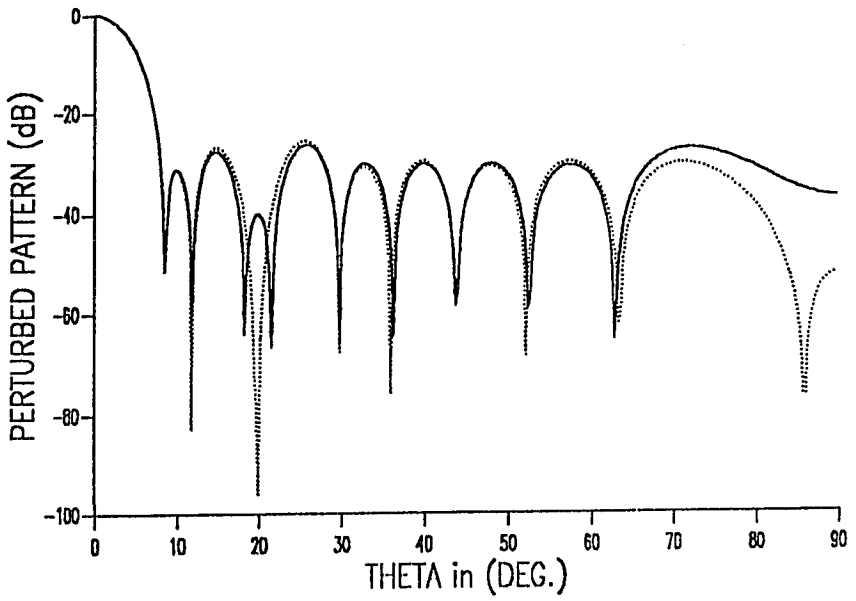

(b)

Fig.4.26 : Perturbed pattern with one null imposed at 20°. Ideal (dotted) and truncated (solid) element position perturbations. $\sum(\Delta_n) = Min.$

a) for column 4 of table 10. b) for column 5 of table 10.

Initial 30-dB Chebyshev pattern, $N = 20$, $d_0 = \frac{\lambda}{2}$.

at these locations still more than 56, 72, and 67 dB below that value at the centre of the main beam, respectively. In other words, even with relatively large round off error, the discrimination against unwanted noise sources is still effective in this case. Figures 4.26a-b show the perturbed pattern with one null imposed at 20, corresponding to the element position perturbations given in Table 4-10 (column 4-5) for truncation up to the third and the second decimal digit, respectively. Note that we need more precise positioner to achieve an accuracy up to the third decimal digit as shown in the Figure. It can be seen that the sensitivity of the perturbed pattern to the element position perturbations are less if the element position perturbations are relatively large, which contradicts with the assumption of small element position perturbations. In general the element position perturbations increases as number of imposed nulls increases for a certain initial pattern type and sidelobe level.

CHAPTER 5

EXPERIMENTAL STUDY OF AN 8-ELEMENT LINEAR ARRAY

An experimental setup of an 8-element linear array has been used to test the validity of null steering by element position perturbations. In this Chapter we present the complete design of an 8-element linear array uniformly excited. In Section 5.2, we describe the experimental setup and the equipment specifications used in this experiment. The last Section show the measurement of the initial pattern of the array to test the experimental setup. Null steering capabilities of the experimental array are given in Chapter 6.

5.1 Description of the experimental antenna array

In this Section, we describe the antenna array which is used in this experimental work. The design procedure require the specification of the type of the elements, number of the array elements, and the feeding network which utilizes the required current distribution. An 8-element monopole array over a ground plane with element spacing of $\frac{\lambda}{2}$ was chosen. The feeding network was

designed in order to provide uniform current distribution.

5.1.1 Antenna array element

The first step in the design procedure is to specify the type of the antenna array elements. In this experimental work a monopole of quarter wavelength ($\frac{\lambda}{4}$) mounted above a perfect conducting plane is used as an antenna array element. In practice, the $\frac{\lambda}{4}$ monopole mounted above the ground plane is widely used. With the aid of image theory, this configuration is equivalent to the $\frac{\lambda}{2}$ dipole as shown in Fig.5.1. Therefore, for analysis purposes, the vertical monopole mounted above an infinite perfect conducting plane will be equivalent to the correspondence analysis of the $\frac{\lambda}{2}$ vertical dipole. Thus, the far zone electric and magnetic fields for the $\frac{\lambda}{4}$ monopole above the ground plane are given as, [56, PP.131]

$$E_\theta = j\,\eta\,\frac{I_0\,e^{-jkr}}{2\pi\,r}\,[EF] \qquad (5.1\text{-a})$$

$$H_\varphi = j\,\frac{I_0\,e^{-jkr}}{2\pi\,r}\,[EF] \qquad (5.1\text{-b})$$

where the element factor

$$EF = \frac{\cos[\frac{\pi}{2}\cos(0)]}{\sin(0)} \qquad (5.1\text{-c})$$

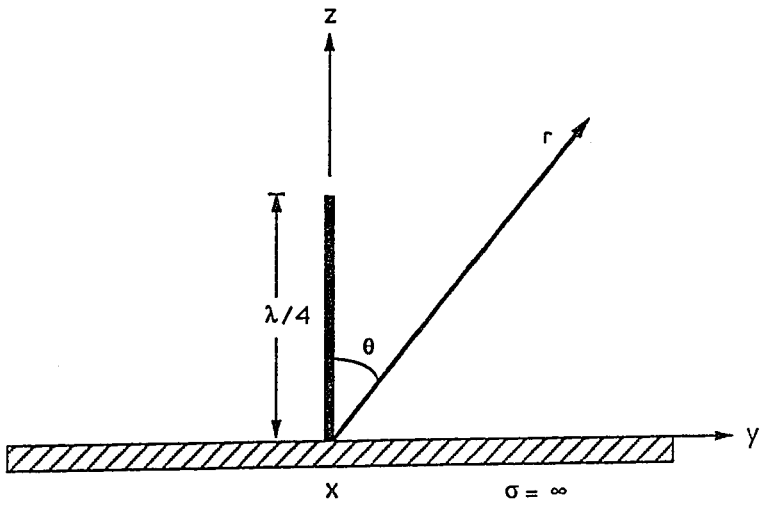

(a) λ /4 monopole on infinite electric conductor.

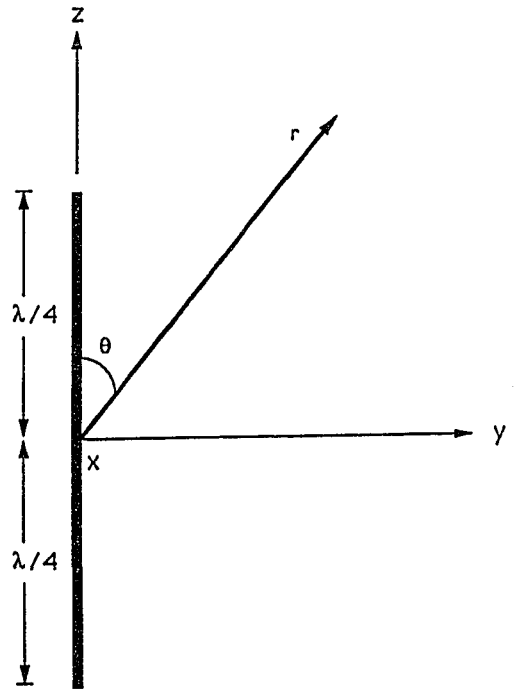

(b) Equivalent of λ /4 monopole on infinite electric conductor.

Fig. 5.1 : Quarter wavelength monopole on an infinite electric conductor.

Also, it follows that the input impedance of a $(\frac{\lambda}{4})$ monopole above the ground is equal to one-half that of an isolated $(\frac{\lambda}{2})$ dipole, or $Z_{in} = 36.5 + j\,21.25$ (ohm).

5.1.2 Design of the feeding network

The feeding network design must satisfy the following requirements for efficient operation:

1) Feeding every radiating element with proper amplitude and phase.

2) Matching every radiating element with its feed line according to its driving point impedance.

3) Minimizing the amount of power wasted through the feeding network and the matching sections. This is a figure of merit of the design to maximize the ratio of the power received to the power reached the radiating elements.

4) The chosen network must be insensitive to small frequency variations.

In our experiment, it important to achieve equally current excitations as this theoretical assumption were used to compute the element position perturbations. Therefore, the requirement of matching the elements is the most important one. In this experiment the required feeding currents are of equal amplitudes and phases. As the objective of this experiment is to verify the null steering using element positions, the requirement of maximizing the received power is not of great importance.

The feeding network of an array depends on both the antenna type and the transmission line used. As mentioned before, the characteristics of a quarter wavelength monopole mounted above perfect conducting plane is equivalent to the characteristics of an isolated half wavelength dipole. The feeding techniques of an antenna array can broadly classified into two methods:

1) Active element feeding network.

2) Passive element feeding network.

The two way power splitter feeding structure is used in our design as it is easy to realize as shown in Fig.5.2. This configuration overcome the mismatching and improper power split problem. This feeding structure is suitable for an element number of the power two. It can provides equiphase and equiamplitude outputs. The coaxial cable is used as a feeding network transmission line with 93 (ohm) characteristic impedance. The length of each cable section has to be multiple of half the propagating wavelength. The wavelength in the cable can be given as,

$$\lambda' = \frac{\lambda}{\varepsilon_r^{\frac{1}{2}}} \tag{5.2}$$

where λ is the free space wavelength and ε_r is the permittivity of the media. For this particular cable the permittivity of the media inside the cable is 2.3, so the propagating wavelength in the cable will be 10 (cm) at 2 GHz. The length of each cable section for the feeding network is given in Fig.5.2.

5.1.3 The matching technique

In a single antenna, the feeding transmission line is matched to the self

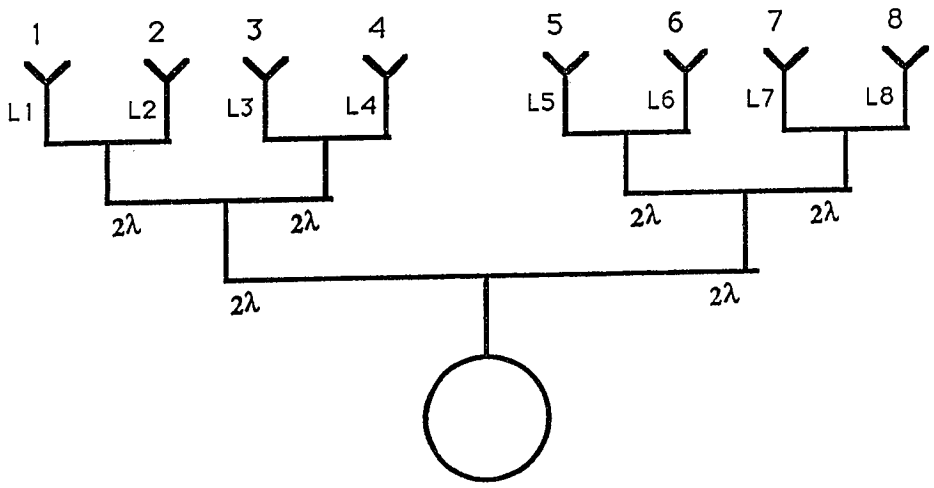

Fig. 5.2 : Tow way power splitter feeding structure.

impedance of the antenna element. However, in antenna array, every element must be matched to the driving point impedance,

$$Zd_i = Z_{i1}\frac{I_1}{I_i} + Z_{i2}\frac{I_2}{I_i} + \ldots\ldots\ldots + Z_{iN}\frac{I_N}{I_i} \qquad (5.3)$$

where $Z_{ij} = Z_{ji}$ is the mutual impedance between the i'th and the j'th element. The mutual impedance depends mainly on the distance between the elements considered and on the type of the element used. For broadside array with symmetrical excitation currents with respect to the center of the array, the driving point impedance are also symmetrical ($Zd_i = Zd_{N-i-.5}$)

The driving point impedance for an 8 monopole elements of length $\frac{\lambda}{4}$ equispaced with $\frac{\lambda}{2}$ are given in Table 5.1 which were computed by the program listed in the Appendix of reference [52]. Using coaxial cable line with 93 (ohm) characteristic impedance, the required transmission line length for element matching, with the help of smith chart, will be as given in Table 5.1 (column 3).

Also, using the feeding structure described in Section 5.1.2 at 2GHz frequency, the corresponding coaxial cable lengths are given in the Table (column 4). Note that the cable length is the minimum length for element matching plus an integer multiple of half wavelength of the wave propagated inside the the coaxial cable. The input impedance of the array at the output of the feeding network is $Z_{in} = 40$ (ohm).

Table 5-1

The driving point impedance Zd, and the coaxial transmission length L, for element matching of an 8 quarter wavelength monopoles linear array with uniformly current excitations.

ELEMENT NO.	Zd (ohm)	L (λ)	*L (cm)* 2 GHz
1	31.612 +j10.379	0.198	22.0
2	25.526 -j 1.873	0.258	22.6
3	27.288 +j 3.843	0.231	22.3
4	26.694 +j 1.463	0.242	22.4
5	26.694 +j 1.463	0.242	22.4
6	27.288 +j 3.843	0.231	22.3
7	25.526 -j 1.873	0.258	22.6
8	31.612 +j10.379	0.198	22.0

5.2 The experimental setup

In the following Section, we describe the set up geometry of the experiment and the equipment specifications used. The experiment setup geometry block diagram is shown in Fig.5.3. The antenna array output is connected to the data acquisition system for pattern measurements. The array is mounted over an elevation over azimuth antenna positioner which is remotely controlled. The array under test will be rotated from $\theta = -90°$ to $90°$ in the azimuth plane ($\varphi = 0$ plane). The data collection system consists of a Programmable Microwave Receiver connected to a microcomputer using the IEEE-488 Standard Digital Interface, where the measurements of the pattern are stored to be processed and plotted. A description of the block diagram of Fig.5.3 is as follows:

Antenna array

The antenna array consists of eight monopoles linear array mounted vertically above a 1×2 (m) aluminium sheet as shown in Picture 5-1. As the element positions are to be changed during this experiment, they had been fixed inside a slot in the centre of the aluminium sheet such that the element positions can be moved along the z-direction only (see Picture 5-2). The array elements are fed through the feeding network designed in the previous Section which can provide a uniform current excitations as shown in Picture 5-2.

Transmitter

The transmitter can be any antenna which has the capability to operate at 2GHz. In our work the transmitter was a dipole with operating frequency up to

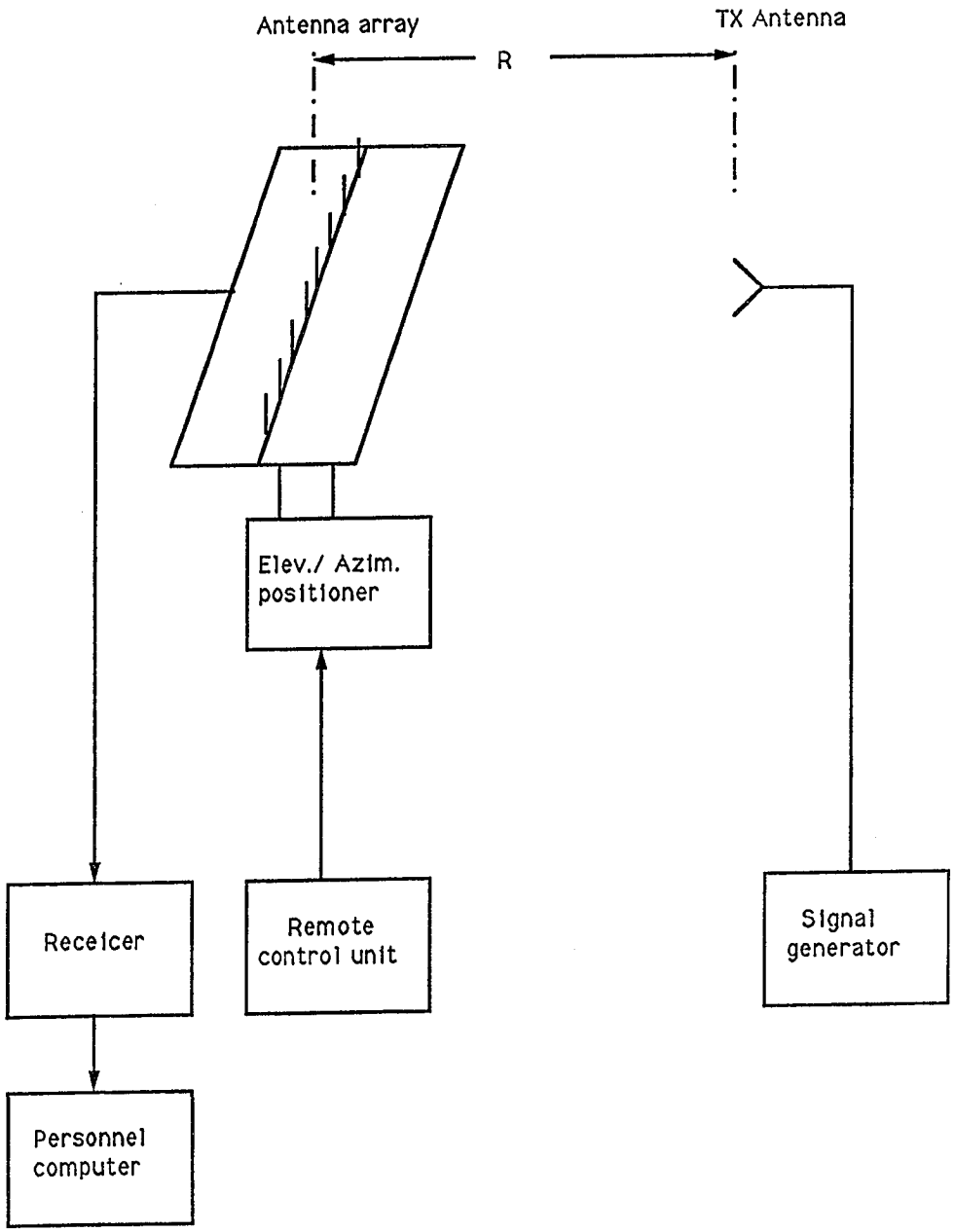

Fig. 5.3 : Block diagram of the experiment setup for measuring the radiaton pattern of antenna array.

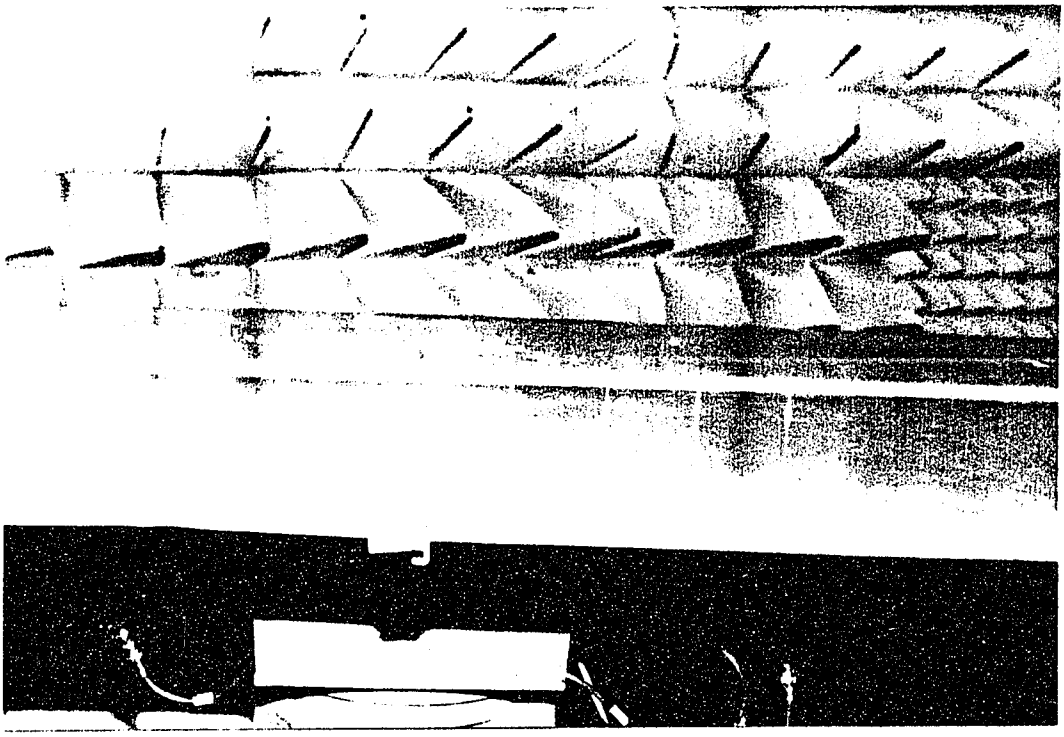

Picture 5-1 : Linear antenna array of eight monopoles mounted vertically above 1X2 (m) aluminium ground plane.

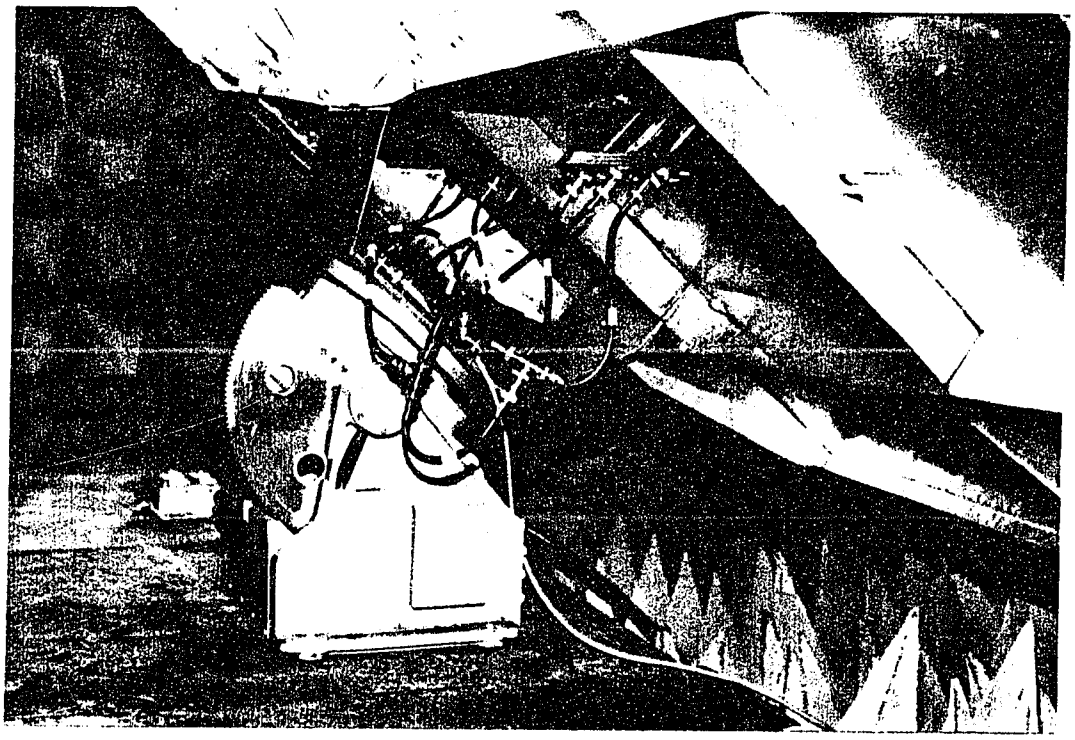

Picture 5-2 : The 8-element monopole array shown inside the anechoic chamber with coaxial feeding network and mounted on the EL/AZ positioner.

700MHz. Thus, mismatching is expected which may cause reflection. The transmitter is fed from a signal generator through a coaxial cable which is capable to provide the sufficient power.

Receiver

The experimental data has been obtained during measurements with the help of Scientific-Atlanta Programmable Microwave receiver Model 1783 which has the following specifications. The Model 1783 three-Channel Programmable receiver is wide band, microprocessor-controlled, precision receiver providing both phase and amplitude measurements capability. The Model 1783 Microwave receiver are designed as high-speed data acquisition receiver for use with computer controlled antenna measurement system. The receiver is used as part of a dedicated automatic antenna pattern measurement system which is connected to microcomputer using the IEEE-488 Standard Digital Interface.

Remote positioner control unit

The array radiation pattern is measured by rotating the array from -90 to 90 in the azimuth plane. This was performed by using the Scientific-Atlanta Model 4116A-10 Remote Control Unit which offers centralized control of three axis positioner. Provisions are made for positioner and axis selection, control of the drive-motor speed direction, and limit indication. Automatic dynamic braking of the drive-motors prevents excessive overtravel when the positioner reach a limit as the control is returned to zero from either directions.

The following paragraphs describe the general test conditions for antenna measurements:

Measurement geometry

Accurate antenna measurements require some restriction on measurement geometry. The antenna separation distance R must be great enough to ensure that the near field effect and antenna-to-antenna mutual coupling effects are negligible. The distance restriction is

$$R > (\frac{2\,D^2}{\lambda}) \tag{5.4}$$

where D is the array dimension and λ is the wavelength of the operating frequency. Antenna heights must be great enough to minimize antenna-to-ground plane mutual impedance and to ensure negligible contribution from the surface wave components of the ground wave. In our work $R > 5(m)$ which satisfies the antenna separation distance and the two antennas are put inside the microwave anechoic chamber where the effect of the ground plane and the electromagnetic radiation are avoided.

Test instrumentation

Signal generators and power amplifiers used in the measurements have 50-ohm output impedance, and all the cables used have a 50-ohm characteristic impedance. An impedance mismatch at the output of the signal source or at the input of the receiver may result in reflection which could cause antenna pattern measurement errors. This could be avoided by the use of padding attenuators of 10 dB, one at the output end of the transmitting cable and one at the receiver

input. The signal source should provide sufficient power to produce a signal at least 10 dB above the ambient noise and equipment receiver noise at the receiver input. Preamplifier may be used at the receiver input to meet this requirement. It is preferable to use preamplifier at the receiver input rather than power amplifier at the source output. This will improve signal-plus-noise-to-noise ratio, while minimizing the potential or interference with susceptible equipment or licensed radiation sources. This test requirement is met simply by using the Scientific-Atlanta Programmable Microwave receiver Model 1783 .

5.3 The measured initial pattern

The objective of this experiment is to test the setup and to measure the radiation pattern of the array with half wavelength element spacing. The test of the experiment setup can be obtained by comparing the measured radiation pattern with the theoretical array pattern of an eight isotropic linear array with half wavelength element spacing and uniform current excitations.

The equidistant element spacing with half wavelength can be obtained by setting the element positions as given in Table 5.2, where the operating frequency is set at 2 GHz. The antenna array was scanned in the $\varphi = 0$ plane from $\theta = -90°$ to $90°$ using the remote control positioner described in Section 5.2. The antenna signal output was measured using the data acquisition system described also in the previous Section. The measured array radiation pattern is depicted in Fig.5.4a. Figure 5.4b shows the measured pattern of the array compared to the theoretical pattern (dotted) achieved through computer

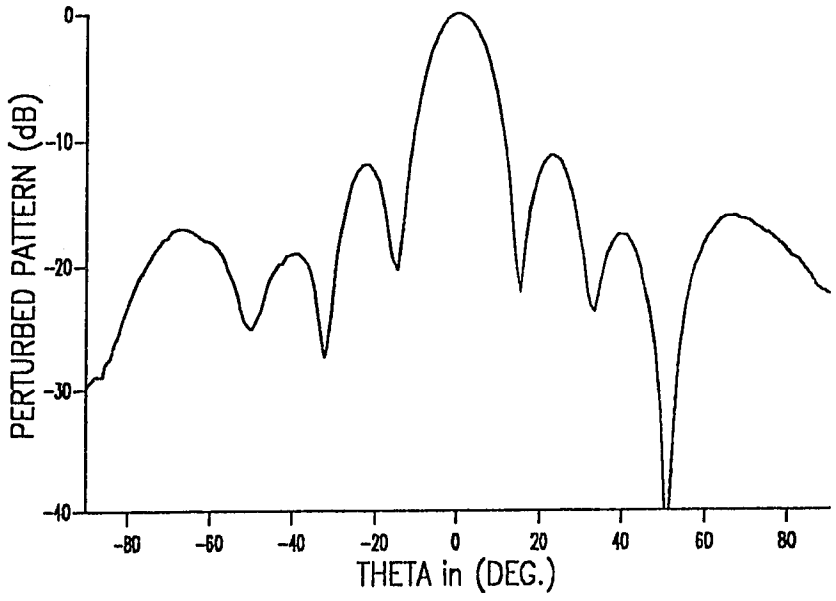

(a)

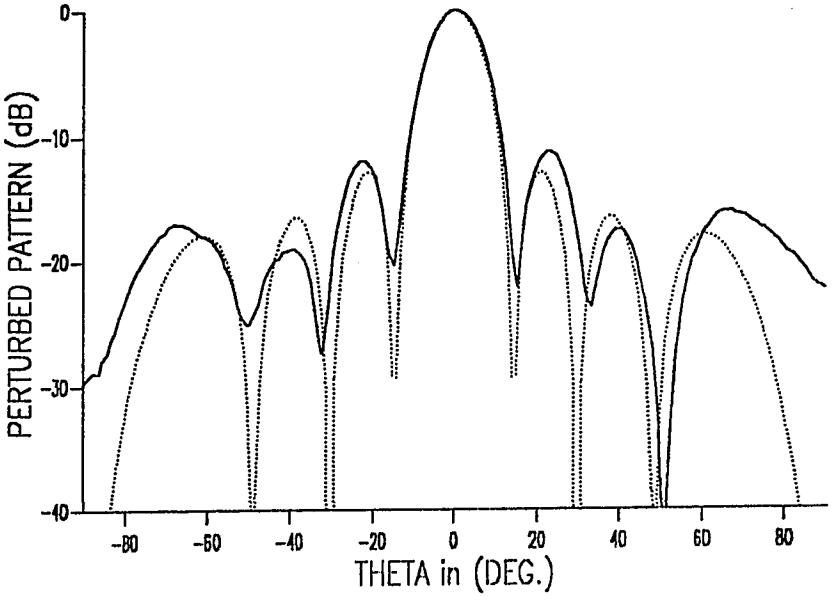

(b)

Fig.5.4 : Radiation pattern of an eight half wavelength equidistant linear array. The array elements are quarter wavelength monopoles uniformly excited. a) Only the experimental pattern. b) The experimental pattern compared to the theoretical pattern (dotted).

Table 5-2

Element positions d_n, of an 8-element linear array for half wavelength element spacing with 2 GHz operating frequency.

n	$d_n(\lambda)$	$d_n(cm)$
1	-1.7500	-26.25
2	-1.2500	-18.75
3	-0.7500	-11.25
4	-0.2500	-3.75
5	0.2500	3.75
6	0.7500	11.25
7	1.2500	18.75
8	1.7500	26.25

Table 5-3

Null directions 0_i $(deg.)$, of the experimental and the theoretical array patterns of Fig.5.4.

i	THEOR. 0_i	EXP. 0_i
1	-90.0	-90.0
2	-48.6	-50.0
3	-30.0	-32.0
4	-14.5	-15.0
5	14.5	15.0
6	30.0	33.5
7	48.6	50.5
8	90.0	90.0

EXPERIMNTAL PATTERN, BW=13.0 , SLL=-11.2 , Dir.=7.82
THEORETICAL PATTERN, BW=12.77, SLL=-12.797, Dir.=8.00

simulation. From this Figure, it can be seen that the main beam of both the measured and the theoretical patterns are almost the same, where they have 13°and12.77° half-power main beam width (BW), respectively. However, the SLL of the measured pattern is -11.2 dB which is little higher than the SLL of the theoretical pattern (-12.8 dB). Also, the directivity of the experimental array pattern is 7.82 compared with the value of 8 for the theoretical pattern, assuming no variation of the field in the elevation plane (φ plane). Note that the nulls of the measured pattern are shifted from the corresponding theoretical null positions. Table 5-3 gives the null positions in (deg.) and the antenna parameters of both the theoretical and the measured array patterns. As conclusion we can say that the experiment setup is satisfactory for our work as can be seen from the Figure and from Table 5-3.

CHAPTER 6

EXPERIMENTAL RESULTS OF NULL STEERING BY ELEMENT POSITION PERTURBATIONS

In this Chapter we present the experimental results of imposing nulls in prescribed directions to test the validity of null steering by element position perturbations. The theoretical results of the eight-element array are first developed in Section 6.1. Section 6.2 contains the experimental results of the array in the form of the measured initial pattern and some perturbed patterns by imposing nulls in different directions. A comparison between the experimental results and the corresponding theoretical results is given in Section 6.3. In the last Section, we discuss the error sources and recommendations to avoid these errors.

6.1 Theoretical results for the eight-element array

The array factor for an equispaced isotropic linear array is given by Eq.(3.1). Since, in practice, the antenna array elements are not isotropic, the array pattern will be modified to include the effect of the antenna elements. The total array pattern can be written as,

$$F(0,\varphi) = AF(0).EF(0,\varphi) \tag{6.1}$$

where, AF is the isotropic array factor given by Eq.(3.1), and EF is the element factor. For a monopole of quarter wavelength dimension mounted vertically above an infinite perfect conducting plane with the geometry as shown in Fig.5.1, the element factor is given by Eq.(5.1-c). In this work, a theoretical study is done on an 8-element array with half wavelength spacing and with geometry as shown in Fig.6.1. The antenna elements are monopoles of quarter wavelengths mounted vertically above an infinite perfect conducting sheet, where they are oriented in the Y-direction as shown in the Figure. The element factor of the standard orientation (z-direction) will be transformed to the following form,

$$EF(0,\varphi) = \frac{\{\cos[\frac{\pi}{2}\sin(0)\sin(\varphi)]\}^2}{1.0 - \sin^2(0)\sin^2(\varphi)} \tag{6.2}$$

Note that the element factor in the above Equation will be reduced to unity when it is evaluated at $\varphi = 0$,

$$EF(0,\varphi)|_{\varphi=0} = 1$$

Thus, the total array pattern F will be equal to the array factor AF in the $\varphi = 0$ plane. In particular, the perturbed pattern of an 8-element linear array uniformly current excited with the main beam directed to broadside, can be written as,

$$F(u) = \sum_{n=1}^{8} c^{j\Delta_n u} c^{j d_n u} \tag{6.3}$$

where, d_n and u are as given by Eq.(3.1). The element position perturbations Δ_n,

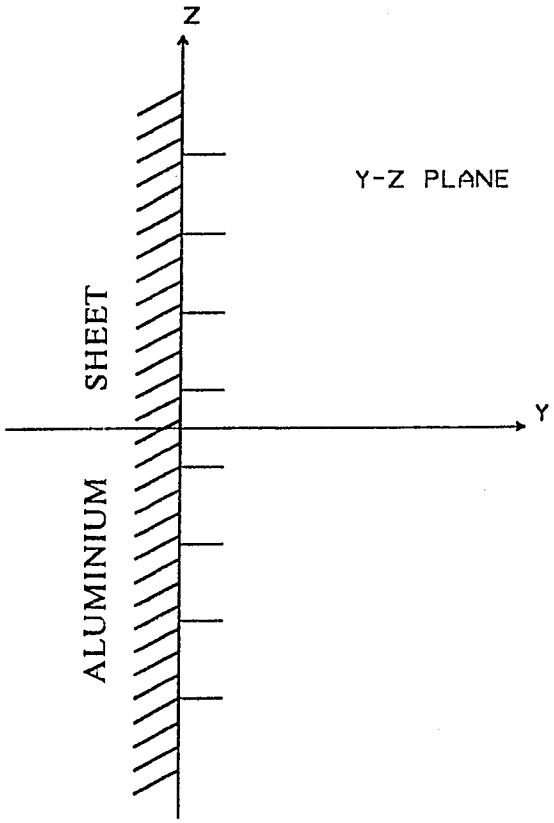

Fig.6.1 : Geometry of linear equispaced antenna array. The array elements are monopoles vertically mounted above a perfect conducting plane in the y-axis direction.

can be computed by Eq.(3.23) where the corresponding computer program is given in Appendix B.

Figures 6.2a-c show the antenna parameters of the perturbed pattern when one null was scanned in the low sidelobe region compared with the initial pattern parameters. In general, the antenna parameters of the perturbed pattern are affected more as the imposed null was closer to the main beam as shown in the Figures. Although the BW and the directivity values of the perturbed pattern are close to the corresponding initial values, the main beam is widened and the directivity value is reduced when the imposed null is in the range $\theta_m = 14.5° - 20°$ (the left side of the first sidelobe). However, the SLL is the important parameter as shown in the Figs.6.2a-c. The SLL value varies in the range (-16)-(-12) dB when the interference location was around 17° as shown in Fig.6.3c. Perturbed patterns for some few examples are shown in Figs.6.3a-d, where one null was imposed at 20°, 40°, 60°, and two nulls at (45°, 75°), respectively. The corresponding antenna parameters and the element position perturbations computed using Appendix C, are given in Table 6-1.

6.2 Experimental results

The objective of this experiment is to test the validity of null steering by element position perturbations. For this objective many experiments were performed to impose nulls in the sidelobe region of the initial pattern by controlling the element positions while keeping the element amplitudes and

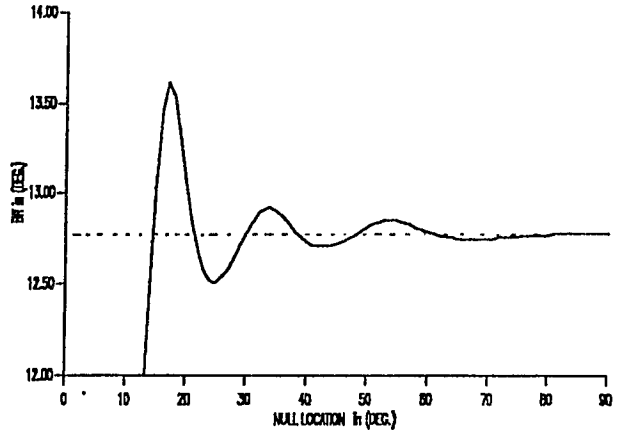

(a)

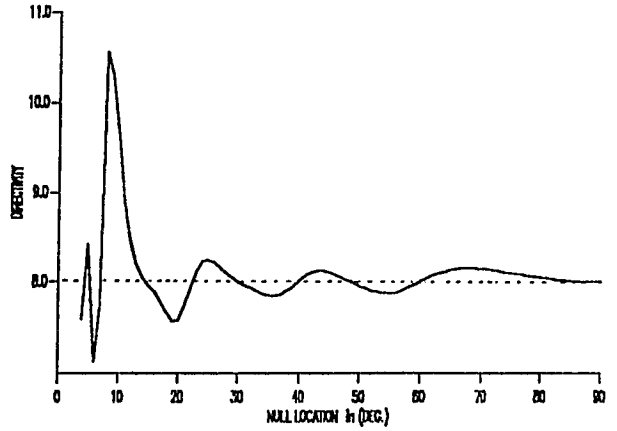

(b)

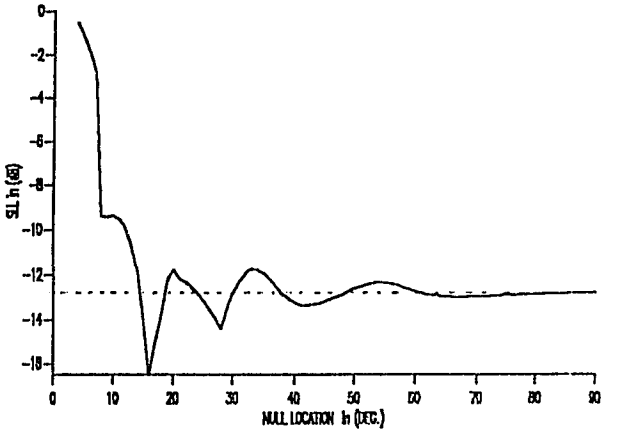

(c)

Fig.6.2 : Perturbed (solid) and initial (dotted) pattern parameters with one imposed null scanned in the sidelobe region.
a) Main beam width (BW). b) Directivity. c) Sidelobe level (SLL.
Initial (dotted) uniform current distribution pattern, $N = 8$, $d_0 = \frac{\lambda}{2}$.

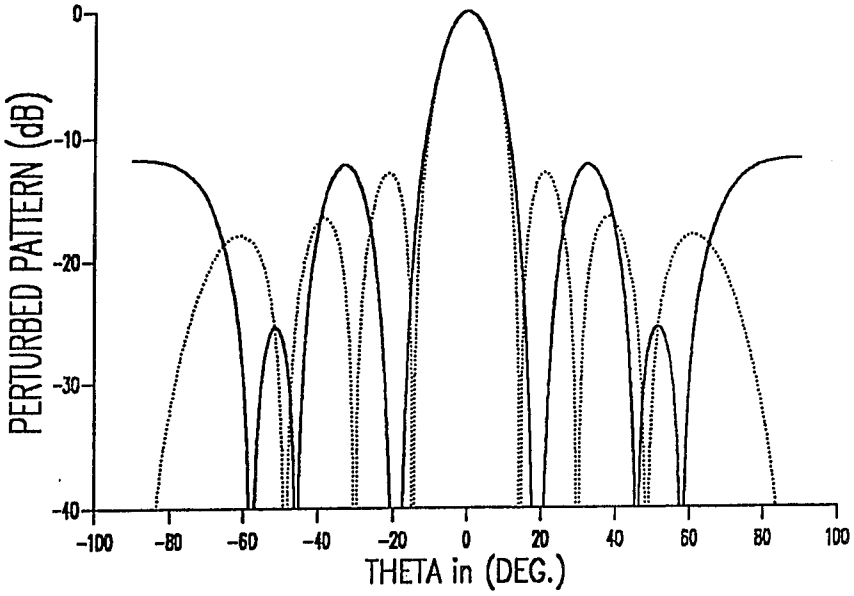

(a)

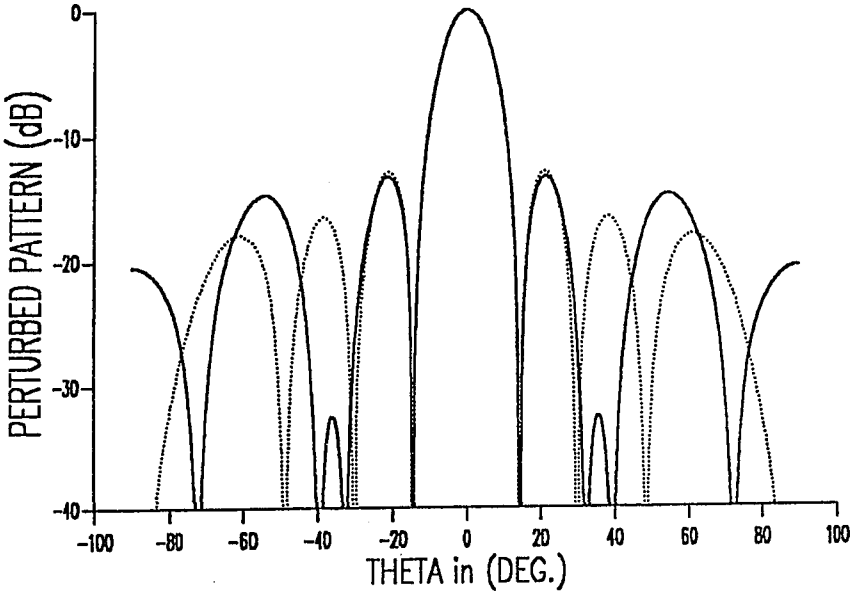

(b)

Fig.6.3 : Theoretical perturbed Patterns (solid) with one null imposed at,
a) 20°, *b*) 40°, *c*) 60°, and d) two nulls at (45°, 75°).
Initial (dotted) uniformly current distribution pattern, $N = 8$, $d_0 = \frac{\lambda}{2}$.

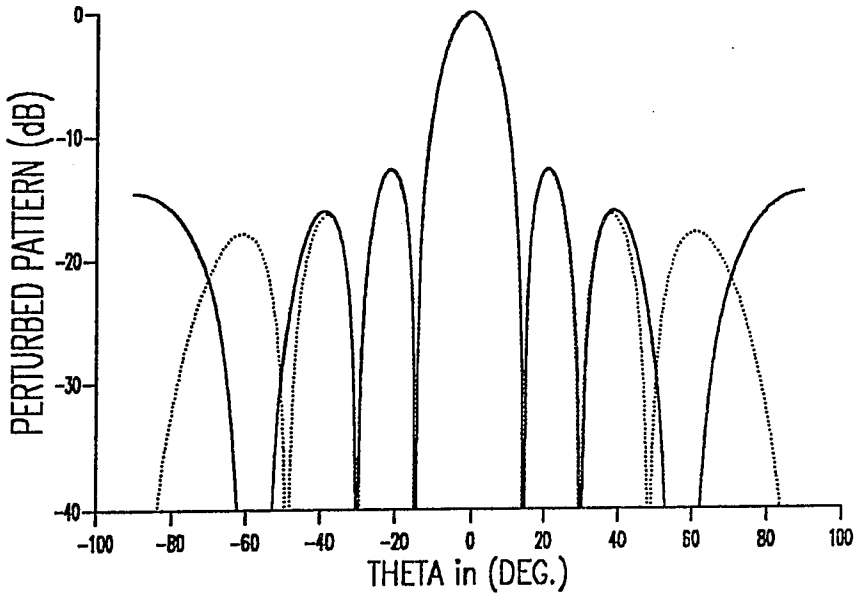

(c)

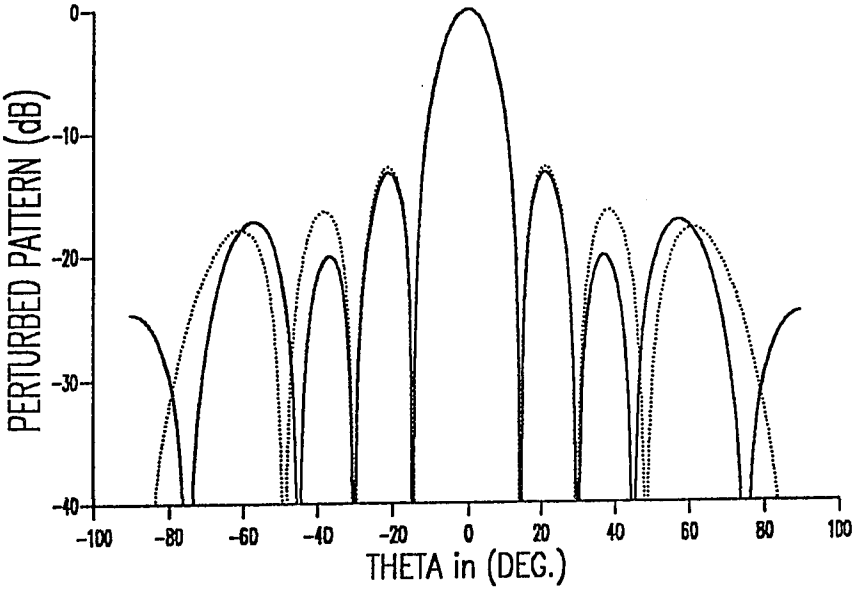

(d)

Fig.6.3 : Continued \ ...

Table 6-1

Computed element position perturbations Δ_n, in wavelength, and the element positions x_n, in wavelength and (cm) when the operating frequency is 2 GHz, for Figs.(6.3a-d).

n	Δ_n	x_n	$x_n(cm)$
			Fig.6.3a : $\theta_1=20°$
1	-0.1349	-1.8849	-28.27
2	0.1022	-1.1478	-17.22
3	0.2322	-0.5178	-7.77
4	0.1190	-0.1310	-1.97
5	-0.1190	0.1310	1.97
6	-0.2322	0.5178	7.77
7	-0.1022	1.1478	17.22
8	0.1349	1.8849	28.27
			Fig.6.3b : $\theta_1=40°$
1	-0.0475	-1.7975	-26.96
2	0.0635	-1.1865	-17.80
3	-0.0076	-0.7576	-11.36
4	-0.0569	-0.3069	-4.60
5	0.0569	0.3069	4.60
6	0.0076	0.7576	11.36
7	-0.0635	1.1865	17.80
8	0.0475	1.7975	26.96

Table 6-1 \ Continued

n	Δ_n	x_n	$x_n(cm)$
			Fig.6.3c : $\theta_1=60°$
1	-0.0049	-1.7549	-26.32
2	0.0248	-1.2252	-18.38
3	-0.0405	-0.7905	-11.86
4	0.0490	-0.2010	-3.01
5	-0.0490	0.2010	3.01
6	0.0405	0.7905	11.86
7	-0.0248	1.2252	18.38
8	0.0049	1.7549	26.32
			Fig.6.3d : $\theta_{1,2}=45°, 75°$
1	-0.0322	-1.7822	-26.73
2	0.0235	-1.2265	-18.40
3	-0.0004	-0.7504	-11.26
4	-0.0187	-0.2687	-4.03
5	0.0187	0.2687	4.03
6	0.0004	0.7504	11.26
7	-0.0235	1.2265	18.40
8	0.0322	1.7822	26.73

phases unchanged. The experiment setup is discussed in Chapter 5, where a linear array of 8 quarter monopole elements mounted vertically above an aluminium sheet was manufactured as can be seen in Pictures 5-1,2. The experiments were done inside the anechoic Chamber where our receiver array and the transmitter antenna were isolated from the the outside environmental electromagnetic radiation. The antenna elements are moved freely inside the track as seen in Picture 5-2. The element currents were uniformly excited through the feeding network designed in Section 5.1 with 2 GHz operating frequency and initial element spacing of half wavelength as given in Table 5-2.

In particular, four experiments corresponding to four cases of imposing nulls in the sidelobe region at 20°, 40°, 60°, and (45°, 75°), were done to verify the validity of null steering by controlling the element positions. The corresponding element positions for the perturbed pattern are given in Table 6-1 for the operating frequency at 2 GHz. The experimental results of the perturbed patterns are shown in Figs.6.4a-d compared with the experimental initial pattern (dotted) which was measured previously and shown in Fig.5.4a. The radiation pattern values were measured by the Scientific-Atlanta receiver and collected by microcomputer using the Standard Digital Interface IEEE-488, as described in Chapter 5.

From the Figures, null depth of 22.2, 55.3, 34.2, and (31.1, 34.4) dB below the maximum value of the perturbed pattern are achieved to impose nulls at 20°, 40°, 60°, and (45°, 75°), respectively.Note that symmetric nulls around the

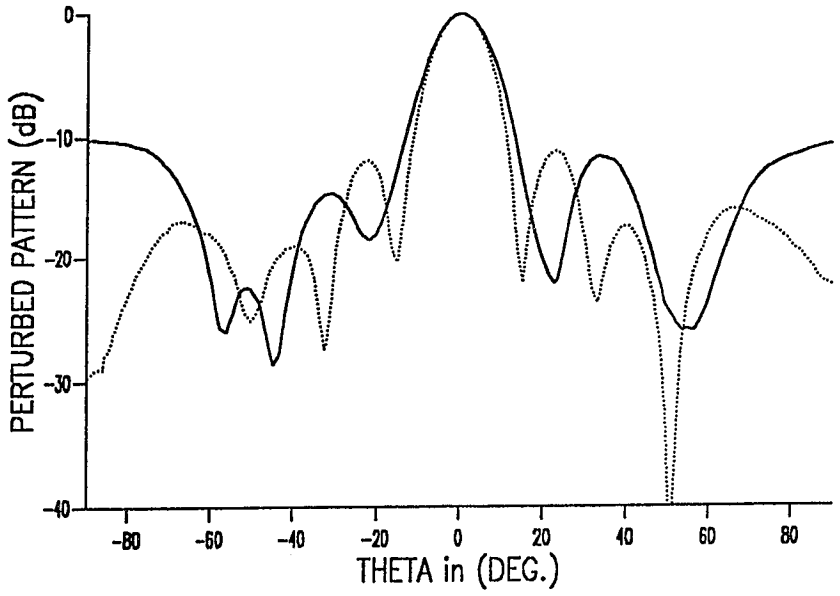

(a)

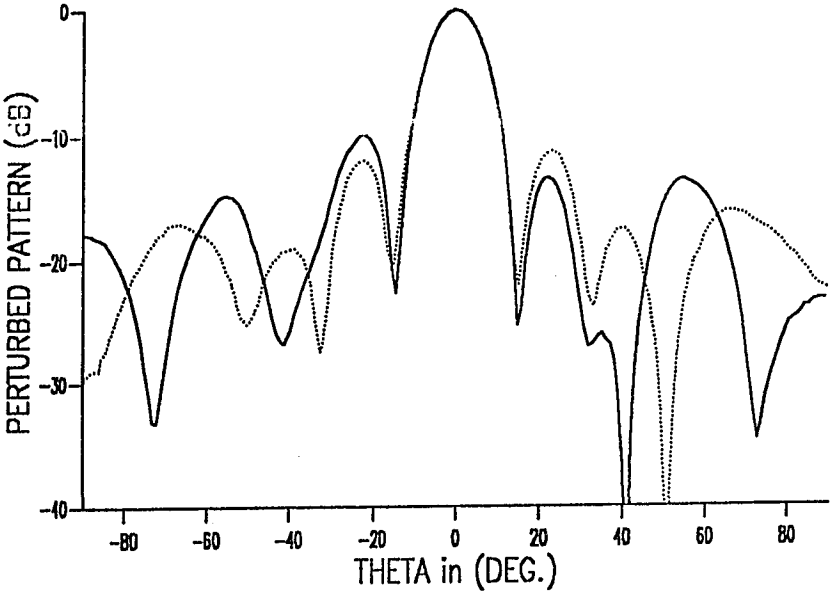

(b)

Fig.6.4 : Experimental perturbed patterns (solid) with one null imposed at,
a) 20°, *b*) 40°, *c*) 60°, and d) two nulls at (45°, 75°).
Initial (dotted) experimental radiation pattern of Fig.5.4a.

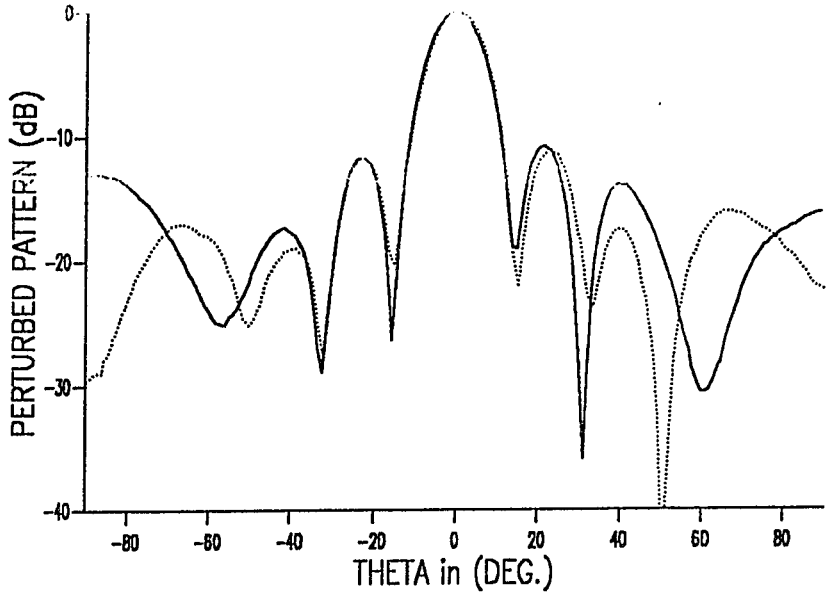

(c)

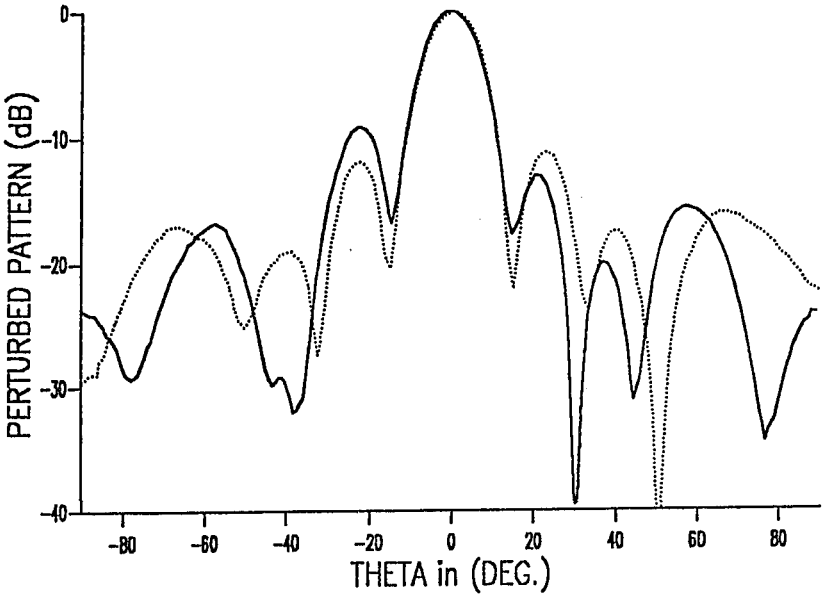

(d)

Fig.6.4 : Continued \ ...

main beam also located due to the symmetric property discussed in Section 3.6. However, the depth is not exactly symmetry due to the lackness of the accuracy of achieving perfectly uniformly current distribution. Also, note that the null locations are shifted from the prescribed null positions as given in Table 6-2. This result is not severe as the nulls are wide enough so that the sidelobe level at the prescribed nulls are lowered with a considerable value as shown in the Figures. The corresponding antenna parameters are given in Table 6-3. It is interesting to compare these results of null steering by element position perturbations with the measured results for the phase-only nulling. Baird and Rassweiler proved the operation of phase-only nulling using 16 element linear array at 4.5-4.6 GHz. The measured pattern with one null imposed at 18° is given in Fig.12 of reference [10]. From that Figure, the SLL of the perturbed pattern is 10 dB compared with 10.1 dB for Fig.6.4a. Note that the number of the elements used in our work is 8 compared with 16 elements of Baird and Rassweiler. As a result of this discussion the null steering by element position perturbations can be successfully achieved.

6.3 Comparison between theoretical and experimental results

As mentioned before, this experiment verify the ability of null steering using element position perturbations. The theoretical and the experimental radiation patterns while imposing nulls in prescribed directions for some cases are shown in Figs.6.3a-c and Figs.6.4a-c. Figures 6.5a-c show the experimental (solid) and the theoretical (dotted) perturbed patterns with nulls imposed at 20°, 40°, 60°,

Table 6-2

Imposed null directions θ_i (*deg.*), and sidelobe cancellation value C, for the experimental perturbed patterns of Figs.(6.4a-d).

FIG.	THEOR. θ_i	EXP. θ_i	C (dB)
6.4a	20.0	22.7	10.1
6.4b	40.0	41.2	37.8
6.4c	60.0	61.6	17.0
6.4d	45.0	44.6	11.0
	75.0	77.5	16.0

Table 6-3

Antenna parameters BW, DIR., and SLL of the perturbed patterns for Figs.6.3a-d and Figs.6.4a-d.

Figures	BW (DEG.)	DIR.	SLL (dB)
6.3a	13.060	7.573	-11.748
6.4a	14.14	6.87	-11.1
6.3b	12.721	8.011	-13.217
6.4b	12.27	7.72	-8.7
6.3c	12.779	7.999	-12.711
6.4c	14.02	7.63	-9.04
6.3d	12.703	8.169	-13.265
6.4d	13.02	7.56	-9.16

and (45°, 75°), respectively. From the Figure, it can be seen that the main beam of both patterns, the experimental and the theoretical, are almost the same except of Fig.6.5a where the main beam of the experimental pattern is little wider. This is due to the imposed null at 20° which is close to the main beam. Also, the experimental pattern follows the corresponding theoretical pattern in most of the sidelobe region. We can see that the experimental pattern did not follow the theoretical pattern in the range of θ=-40° -20° in Fig.6.5b and around -40° in Fig.6.5d. However, the important result is that the imposed nulls of the experimental patterns are very close to the corresponding imposed nulls of the theoretical patterns as shown the Figure.

Table 6-2 give the experimental null depth and positions of the imposed nulls compared with the corresponding theoretical null depth and positions. From the Table, the experimental null positions are shifted from the theoretical null locations. However, the above feature is not critical as the nulls are wide as can be seen from the Figures. Also, the sidelobe cancellation value for the experimental perturbed patterns are given in Table 6-2, compared with the envelop of the experimental initial pattern shown in Fig.5.4a. From the Table, at least 10.1 dB was achieved to impose a null at 20°, while 37.8 dB had been obtained to impose a null at 40°. The antenna parameters of the experimental and the theoretical perturbed patterns are given in Table 6-3. In general, the BW and the directivity are approximately the same for both the experimental and the theoretical perturbed patterns. But the important parameter is the SLL

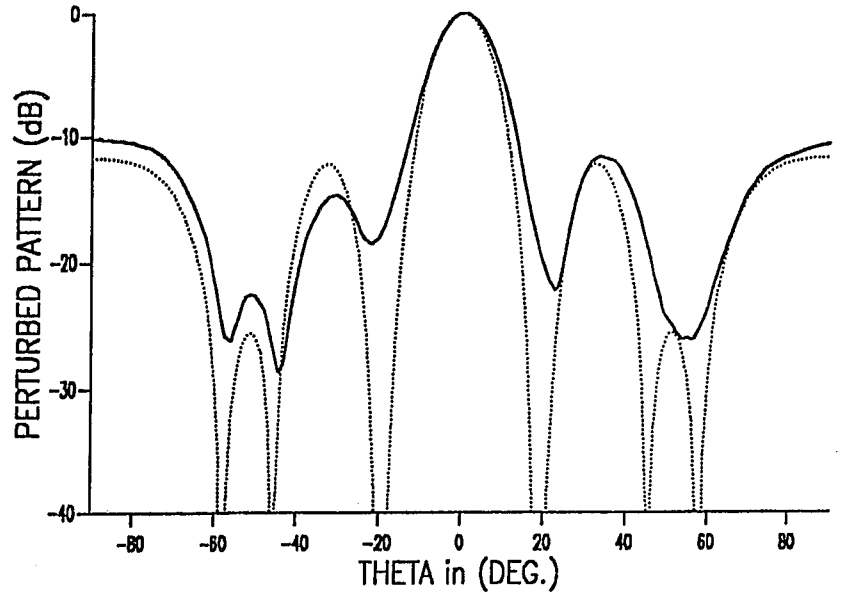

(a)

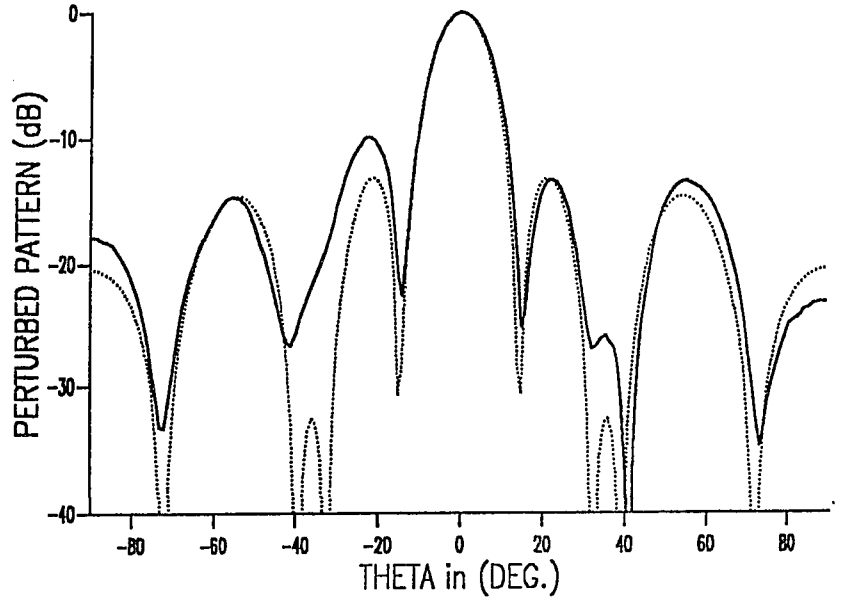

(b)

Fig.6.5 : Experimental (solid) compared to the theoretical (dotted) perturbed patterns with one null imposed at,
a) 20°, *b*) 40°, *c*) 60°, and d) two nulls at (45°, 75°).
Initial uniformly current distribution pattern, $N=8$, $d_0=\frac{\lambda}{2}$.

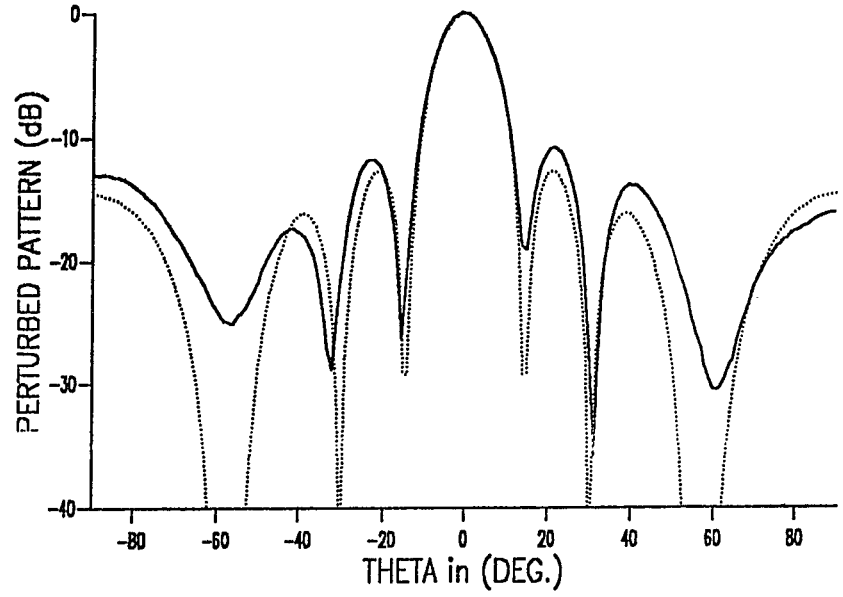

(c)

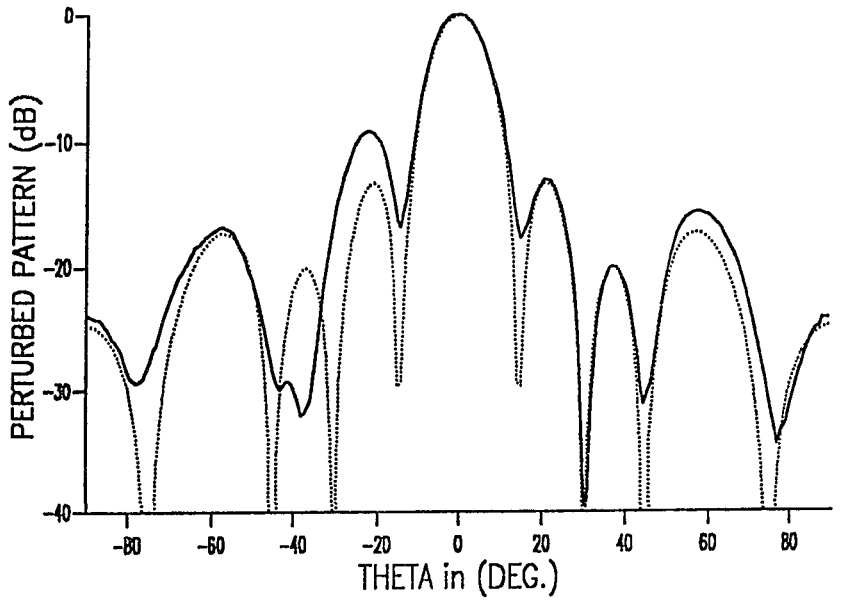

(d)

Fig.6.5 : Continued \ ...

which have larger value for the experimental pattern as given by this Table. As conclusion, the experimental results are satisfactory for imposing nulls in the prescribed directions

6.4 Error sources and discussion

Although the experimental results were sufficient to prove the ability of null steering by controlling the element positions as shown in the previous discussions, they possess some discrepancies compared with the theoretical results. Some of these discrepancies are as follows:

- The experimental patterns are not generally exactly symmetry with respect to the main beam
- The positions of the nulls are slightly shifted from the theoretical positions, even for the initial pattern as shown in Fig.5.4.
- The antenna parameters are slightly deviated from the calculated values especially the SLL value.(see Table 6-3)
- The experimental pattern nulls are not as deep as in the theoretical pattern.

Each of the above discrepancy may be caused by one or more error sources. In the following paragraphs, some of these main error sources and their interactions with the experimental results discrepancies are discussed.

1. Test conditions for antenna measurements:

For accurate antenna measurements it is required that the antenna separation distance must be large enough to ensure that the near field effect and the antenna-to-antenna mutual coupling effect are negligible. The far field

condition is that the antenna separation R must satisfy the antenna distance restriction given by the identity of Eq.(5.4). In our experimental work the antenna separation was approximately 5 (m) where the distance restriction $\frac{2D^2}{\lambda}$, is 3.68 (m). The above value satisfy the identity of Eq.(5.4), however in practice, the near field effect and antenna-to-antenna mutual coupling effect are reduced but not eliminated. This source of error will affect the null depth and the SLL value.

2. Array antenna element mismatch:

The feeding network was designed to match each element of the antenna array to provide uniform current excitations. Thus, we assumed uniformly current distribution for the calculation of the element position perturbations as given in Table 6-1. Any change in the element current values during the experimental measurements will cause errors in the experimental pattern compared to the calculated. The main measurements error is that pattern symmetry with respect to the main beam, null positions, and the SLL value will not be as the theoretical results. In fact, the mismatching problem at any element of the array will change the current distribution and hence will cause a pattern error as mentioned above.

Although the feeding network was designed to match each element of the array, however, the realized coaxial lengths of the feeding network branches do not exactly equal to the calculated lengths given in Table 5-1. Therefore,

mismatch problem between the feeding network and the antenna elements is expected, which will change the current excitations and hence will change the experimental pattern as discussed above.

3. Receiver and transmitter mismatch

Matching the transmitting and the receiving antennas with the output of the signal source and with the input of the receiver is very essential in antenna measurements. As mentioned in the setup section of Chapter 5, an impedance mismatch at the output of the signal source or at the input of the receiver may result in reflection which could cause antenna pattern measurements error. Here, in this work the transmitter was a dipole which was designed to operate below 700 MHz. Therefore, mismatching of the transmitter is expected.

On the other hand the input impedance of the antenna array at the output of the feeding network was approximately 40 (ohm), while the input impedance of the receiver is 50 (ohm). Therefore, mismatching will result which could cause error in the pattern measurements.

4. Edge effect of the ground plane

During our theoretical analysis the $\frac{\lambda}{4}$ monopole mounted above ground plane was treated as $\frac{\lambda}{2}$ dipole as discussed in Section 5.1.1 and shown in Fig.5.1. It should be emphasized that the $\frac{\lambda}{2}$ dipole gives the correct field values

for the actual system of monopole only above the interface ($z \geq 0, 0 \leq \frac{\pi}{2}$), and for infinite conducting plane. However, in this experiment the array elements were monopoles mounted above 1×2 (m) aluminium sheet, which is large enough to reduce the edge effect but not to cancel it. The edges of the aluminium sheet will scatter the wave which will disturb the array pattern and hence cause measurements error .

In addition to the above main sources, there are others but less important. From these sources is the ambient noise which will affect the null depth and the equipment accuracy which could cause all kinds of pattern measurement discrepancies.

A summary of the above error analysis is that the main error source was that the feeding network did not provide us the desired current distribution, since it fails to match exactly each element of the array. So, it is recommended to use other type of transmission lines for the feeding network, as the microstrip transmission line, in place of the coaxial transmission line. The main advantage of using microstrip transmission line for the feeding network is that the exact matching can be easily obtained for both the receiver input and each element of the array at the same time. Also, it is recommended to use another transmitting antenna to reduce reflections from the signal source.

CHAPTER 7

CONCLUSIONS AND FURTHER WORK RECOMMENDATIONS

7.1 Conclusion

In this dissertation a new technique was proposed where the process of null steering is carried out by controlling the element positions. This new technique is attractive since in phased arrays the element phases and amplitudes are used to direct the main beam towards the desired signal and to form the array pattern with the specified antenna parameters; i.e HPBW, SLL, directivity. Thus in order to minimize the complexity and cost, this method can open the research of adaptive null steering by controlling element positions, especially in large communication arrays where rapid scanning is not required.

The problem of finding the element position perturbations is a nonlinear problem which does not have a general solution. The null synthesis method based on small element position perturbations can only be linearized by using two term Taylor expansion of the element position perturbation phase term, which results in an analytic solution. Practically, the case of small element position perturbations are achieved by placing relatively small nulls in the region

of low sidelobes which will constitutes a relatively modest pattern perturbation. The small element position perturbations problem was solved for the generalized minimum weighted norm criterion. By imposing M null constraints on the perturbed pattern, where the new pattern has to be zero at the interference directions, the dimension of the problem of finding N element position perturbations will be reduced to the order of M ($<$ N). Two types of approximation criteria are studied in detail. The first approximation corresponds to the requirement that the solution minimizes the sum of the squares of the total element position perturbations, and the second approximation corresponds to the requirement that the solution minimizes the sum of the squares of the relative element position perturbations.

To validate this new approach, illustrative examples of prescribed nulls have been simulated. The results show the effectiveness of null steering to any arbitrary directions while overcoming some of the limitations associated with the other known techniques. Because the position perturbations possess odd symmetry about the centre of the array, then the computational time is effectively halved. Also the cancellation pattern of this technique possess an even symmetry with respect to the main beam, so that a null located in certain direction will produce an image null about the main beam . In addition the phase shifters are used solely for steering the main beam, thus the coarseness of the phase increment has no effect in the null steering result. The sensitivity of the position perturbations has been investigated by truncating the values Δ_n.

These results show that the formed nulls are insensitive to small variation in the perturbation values when the element position perturbations are relatively large.

The new technique can also be used to realize sidelobe cancellation, which is achieved by imposing equispaced nulls over a prescribed sector. Therefore, this method can be used for wide band jammer nulling. The results show that the extra cost for getting more sector nulling and hence more bandwidth nulling is increasing the number of nulls M.

An experimental eight element linear array of monopoles over a ground plane has been designed to test the theory of null steering by element position perturbations. The experimental results demonstrate the capability of this technique in forming nulls in the required directions. Also, these experimental results show that the null steering using element position perturbations is less complicated compared with the other techniques.

7.2 Suggestions for further research

The developed solution was based on an approximation, where the element position perturbations considered small to obtain an analytic solution of the problem. Even though, the solution gives satisfactory results with most of the practical cases, however some limitations exist as a result of the small perturbations assumption. To overcome these limitations and to get an exact solution, the problem of null steering by element position perturbations can be solved by means of some nonlinear techniques, which are mainly numerical

methods.

The adaptive processor could consists of analog or digital least mean square (LMS) or it could be any analog or digital controller based on some other algorithm which attempt to adjust the element array positions to their desired values computed from Eq.(3.27). In this work, we were not concerned with the specific form of the adaptive processor, but simply assumed that this processor adjusts the weights to their computed values for any given set of desired and interference signals. Therefore, the door is open to study this method of adaptive null steering in phased arrays by using element position perturbations with other iteration algorithms.

If the array size is very large and the number of nulls is relatively small then fewer elements of the array can be used to control the nulls of the array pattern. Therefore, many of the controlling units can be saved and the adaptive speed is increased. The partially adaptive nulling using element position perturbations have to be studied to achieve the optimum nulling performance of the array.

In conclusion further work in this area can be directed along the following directions

1) Investigation of the existing adaptive algorithms to implement a real time adaptive system using element position perturbations.

2) Nonlinear programing techniques can be used to remove the restriction of small element position perturbations.

3) The experimental verification of null steering by element position perturbations has been achieved in this work and further experimental work can be directed towards a complete real time implementations of adaptive array.

4) The partially adaptive nulling using element position perturbations can be used to achieve the optimum nulling performance of the array.

APPENDIX A

MSD OF FULL WEIGHT PERTURBATIONS

In this Appendix the mean square of the pattern perturbations (MSD) is considered when the full element weights are allowed to perturb. During the following analysis, we consider a linear array of N equispaced isotropic elements as shown in Fig.1.5. Letting w_{0n}, be the initial complex weight of the n'th array element, the initial array field pattern can be written as,

$$F_0(u) = \sum_{n=1}^{N} w_{0n}\, e^{j d_n u} \qquad (A.1)$$

where, $d_n = d_0 \left(n - \frac{N}{2} - 0.5\right)$

d_0 : interelement spacing

$u = k \sin(0)$, 0 : angle from broadside

k : wave number $= \frac{2\pi}{\lambda}$

Assuming M nulls in the directions of the interfering signals are located by means of full weight perturbations. In this case, the corresponding perturbed coefficients can be represented as

$$w_n = w_n + \Delta w_n \qquad (A.2)$$

where Δw_n, is the perturbation of the n'th weight. The perturbed array field pattern is then,

$$F(u) = \sum_{n=1}^{N} w_n \, e^{j d_n u} \tag{A.3}$$

The difference between the perturbed and the initial patterns is given as,

$$F(u) - F_0(u) = \sum_{n=1}^{N} (w_n - w_{0n}) \, e^{j d_n u}$$

$$= \sum_{n=1}^{N} (\Delta w_n) \, e^{j d_n u} \tag{A.4}$$

The mean square difference between the patterns is defined as,

$$MSD = \frac{1}{2k} \int_{-k}^{k} |F(u) - F_0(u)|^2 \, du \tag{A.5}$$

The "mean" in this analysis, is taken to be in the visible region $-\frac{\pi}{2} \le 0 \le \frac{\pi}{2}$. So that the variable $u = k\sin(0)$ is to be integrated from -k to k. Substituting Equation (A.4) in (A.5) to get

$$MSD = \frac{1}{2k} \int_{-k}^{k} [\sum_{n=1}^{N} \Delta w_n \, e^{j d_n u}] [\sum_{n=1}^{N} (\Delta w_n)^* \, e^{-j d_n u}] \, du \tag{A.6}$$

After interchanging the summations with the integration and performing the integration to yield

$$MSD = \sum_{n=1}^{N} \sum_{v=1}^{N} (\Delta w_n) (\Delta w_v)^* \, \mathrm{sinc}[(d_n - d_v)] \tag{A.7}$$

For half wavelength element spacing

$$(d_n - d_v)k = d_0 \, k \, (n - v) = (n - v)\pi$$

Using the above result, then the double summation of Equation (A.7) will be reduced to a single summation as

$$MSD = \sum_{n=1}^{N} |\Delta w_n|^2 \tag{A.8}$$

where,

$$\text{sinc}[(n - \nu)\pi] = 1 \qquad n = \nu$$
$$= 0 \qquad n \neq \nu$$

Hence, from Equation (A.8), minimizing the weight perturbations is equivalent to minimizing the pattern perturbations MSD for half wavelength element spacing.

APPENDIX B

COMPUTING THE ARRAY ELEMENT POSITION PERTURBATIONS

The weighted (or relative) element position perturbations to suppress interferences in the given directions are given in Eq.(3.19) which is rewritten as,

$$\Delta_n = \frac{y_n^2}{a_n} \sum_{m=1}^{M} c_m \sin[\, d_n (u_m - u_s)\,] \qquad (B.1)$$

where the beam coefficients c_m are the components of the vector given in Eq.(3.13)

$$C = (AY^{-1}A^{\dagger})^{-1} B \qquad (B.2)$$

Where, $(AY^{-1}A^{T})$ matrix is given as

$$AY^{-1}A^{T} = \begin{bmatrix} \sin(d_1(u_1-u_s)) & \cdots & \sin(d_N(u_1-u_s)) \\ \sin(d_1(u_2-u_s)) & \cdots & \sin(d_N(u_2-u_s)) \\ \cdot & \cdots & \\ \cdot & \cdots & \\ \sin(d_1(u_M-u_s)) & \cdots & \sin(d_N(u_M-u_s)) \end{bmatrix} \cdot \begin{bmatrix} y_1^2 & \cdot & \cdots \\ \cdot & y_2^2 & \cdots \\ \cdot & \cdot & \cdots \\ \cdot & \cdot & \cdots \\ \cdot & \cdot & \cdots\ y_N^2 \end{bmatrix} \cdot \begin{bmatrix} \sin(d_1(u_1-u_s)) & \cdots & \sin(d_1(u_M-u_s)) \\ \sin(d_2(u_1-u_s)) & \cdots & \sin(d_2(u_M-u_s)) \\ \cdot & \cdots & \\ \cdot & \cdots & \\ \sin(d_N(u_1-u_s)) & \cdots & \sin(d_N(u_M-u_s)) \end{bmatrix}$$

$$= \begin{bmatrix} \sin(d_1(u_1-u_s)) & \cdots & \sin(d_N(u_1-u_s)) \\ \sin(d_1(u_2-u_s)) & \cdots & \sin(d_N(u_2-u_s)) \\ \cdot & \cdots & \\ \cdot & \cdots & \\ \sin(d_1(u_M-u_s)) & \cdots & \sin(d_N(u_M-u_s)) \end{bmatrix} \cdot \begin{bmatrix} y_1^2\sin(d_1(u_1-u_s)) & y_1^2\sin(d_1(u_2-u_s)) & \cdots & y_1^2\sin(d_1(u_M-u_s)) \\ y_2^2\sin(d_2(u_1-u_s)) & y_2^2\sin(d_2(u_2-u_s)) & \cdots & y_2^2\sin(d_2(u_M-u_s)) \\ \cdot & \cdot & \cdots & \\ \cdot & \cdot & \cdots & \\ y_N^2\sin(d_N(u_1-u_s)) & y_N^2\sin(d_N(u_2-u_s)) & \cdots & y_N^2\sin(d_N(u_M-u_s)) \end{bmatrix}$$

Performing the above matrix multiplication, then the elements of $(AY^{-1}A^{T})$ matrix are given as

$$[(AY^{-1}A^{T})]_{i,j} = \sum_{1}^{N} y_n^2 \sin[\, d_n (u_i - u_s)\,] \sin[\, d_n (u_j - u_s)\,] \qquad (B.3)$$

In this Appendix, Fortran subroutine listing is given to compute Eq.(B.2) and hence the element position perturbations using Eq.(B.1).

```
      SUBROUTINE POSN(A,D,Y,IN,TH,IM,M,N,D0,THS,DELTA,X,PI)
C
C INPUT:
C     N : Number of the antenna array elements.
C     M : Number of the interference signals . (M < N)
C     A : Vector containing the current amplitudes ( 1xN).
C     D : Vector containing the initial element position (1xN).
C     Y : Weighting vector containing an arbitrary non-zero
C         coefficients. (1xN)
C           Y=A : Minimizing the sum of the square of the total
C             element position perturbations.
C           Y=1 : Minimizing the sum of the square of the relative
C             element position perturbations.
C    IN : Dimension of A, D, Y, X, and DELTA vector as declared
C         in th e main program
C    TH : Vector containing the null locations in degree. (1xM)
C    IM : Dimension of TH vector as declared in the main program
C    THS: Main beam direction in degree.
C
C OUTPUT:
C  DELTA: Vector containing the element position perturbations (1xN
C     X : Vector containing the new element positions (1xN).
C
C DEFINITIONS:
C     AA: MxM matrix which have the components given in Eq.(B.3).
C The values of the components of the vectors DELTA, X and D are
C in wavelengths.
C  LSARG: IMSL subroutine for solving M linear equations of real
C general matrix.
C
C ------------------------------------------------------------------

      REAL DELTA(IN),X(IN),A(IN),Y(IN),D(IN)
      REAL AA(8,8),B(8),C(8),UM(8),TH(IM)
C
      US=2.0*PI*SIN(PI*THS/180.)
```

```
      DO 20 I=1,M
   20 UM(I)=2.0*PI*SIN(PI*TH(I)/180.)
C-------------------------------------
C  Computing AA matrix (MxM)
C-------------------------------------
      DO 60 I=1,M
      DO 60 J=1,M
      AA(I,J)=0.
      DO 50 K=1,N
      VI=D(K)*(UM(I)-US)
      VJ=D(K)*(UM(J)-US)
   50 AA(I,J)=AA(I,J)+Y(K)*Y(K)*SIN(VI)*SIN(VJ)
   60 CONTINUE
C-------------------------------------
C  Computing  B  vector (M X 1)
C-------------------------------------
      DO 80 J=1,M
      B(J)=0.
      DO 70 K=1,N
      VI=D(K)*(UM(J)-US)
   70 B(J)=B(J)+A(K)*COS(VI)
   80 B(J)=B(J)/(UM(J)-US)

C-------------------------------------
C  Finding the solution of  (AA * C =  B)
C-------------------------------------
      LDA=8
      CALL LSARG(M,AA,LDA,B,1,C)

C-------------------------------------
C  Computing the element position perturbations, DELTA
C-------------------------------------
      DO 100 I=1,N
      SUM=0.
      DO 90 J=1,M
      V=D(I)*(UM(J)-US)
   90 SUM=SUM+C(J)*SIN(V)
      DELTA(I)=Y(I)*Y(I)*SUM/A(I)
C
      X(I)=D(I)+DELTA(I)
  100 CONTINUE
C
      RETURN
      END
```

The following main program computes the perturbed array pattern and utilizes the element position perturbations using the POSN subroutine.

```
      PARAMETER (IN=41,IM=8,IDIM=999,NP=360)
      REAL DELTA(IN),X(IN),A(IN),Y(IN),D(IN),F(IDIM),TH(IM)

C..... INITIALIZATION .....
      INTEGER M/2/,N/20/
      REAL D0/.5/,THS/0./
      REAL TL/0./,TU/90.0/
      DATA TH/18.0,22.,55.0,32.7,39.9,48.,2*0./
      WRITE(11,1)N,D0,THS,(TH(I),I=1,M)
    1 FORMAT('N=',I2,2X,'D0=',F4.2,2X,'THS',F6.2,3X,8F6.2)
C
      PI=ATAN(1.0)*4
      US=2.0*PI*SIN(PI*THS/180.)
C
C  Read element current amplitudes (assuming even symmetry)
c
        AMAX=0.0
      DO 10 I=1,N/2
      READ(5,*)A(I)
      A(N-I+1)=A(I)
   10 AMAX=AMAX+A(I)
      AMAX=20.*ALOG10(2.0*AMAX)
C
      DO 20 I=1,N
   20 Y(I)=A(I)
C
      DO 30 I=1,N
   30 D(I) = D0*(I-(N/2.)-0.5)
C
C Computing the element position perturbations using POSN
C
      CALL POSN(A,D,Y,IN,TH,IM,M,N,THS,DELTA,X,PI)
C
      DO 40 I=1,N
   40 WRITE(11,2) I,DELTA(I)
    2 FORMAT(6X,I2,5X,2F10.4)
C
C Computing the perturbed pattern F
C
      DTH=(TU-TL)/NP
      K=1
      DO 110 THETA=TL,TU,DTH
```

```
      U =2.*PI*SIN(THETA*PI/180.)
C
      S =0.0
      DO 100 I =1,N
      V =X(I)*(U-US)
100   S =S +A(I)*COS(V)
      F(K) =20.*ALOG10(ABS(S))-AMAX
      WRITE(11,3) THETA,F(K)
      K =K +1
110   CONTINUE
3     FORMAT(6X,F7.2,3F10.3)
      STOP
      END
```

APPENDIX C

SUBROUTINES FOR COMPUTING THE ANTENNA PARAMETERS

Computing the half power beam width (BW), first null position (FN), sidelobe position (SLP), sidelobe level (SLL)

```
      SUBROUTINE ANPAR(E,IDIM,NP,DTH,BW,FN,SLP,SLL)
C  This subroutine finds BW,FN,SLP & SLL  parameters
C of an antenna where the SLL can be any lobe. the E-
C points must starts from the mid of the main beam.

C INPUT: E: The values of the E-field in dB
C     IDIM: Dimension of the array E
C       NP: Number of points
C      DTH: Increment of the angle of E-points

C OUTPUT:BW: half power Beam Width
C        FN: First Null position
C       SLP: Side Lobe Position
C       SLL: Side Lobe Level
C
        DIMENSION E(IDIM),S(30),SP(30)
        E3=E(1)-3.
        N=NP-1
        J=0
        K=1
        DO 100 I=1,N
        GOTO (10,20,30,40),K
C     IF(K) 10,20,30
   10 IF(E(I).GT.E3) GOTO 100
C
C     COMPUTATION OF BEAMWIDTH.
        BW=-DTH*(E(I)-E3)/(E(I)-E(I-1))
        TH=(I-1)*DTH
        BW=2.*(TH+BW)
        K=2
```

```
          GOTO 100
       20 IF(E(I-1).GT.E(I)) GOTO 100
C
C      DETERMINATION OF FIRST NULL.
          FN=-DTH*(E(I)-3.*E(I-2)+2.*E(I-3))/(E(I+1)-E(I)-E(I-2)+E(I-3))
          TH=(I-1)*DTH
          FN=TH+FN
          K=3
          GOTO 100
       30 IF(E(I).GT.E(I-1)) GOTO 100
C
C      DETERMINATION OF SIDELOBELEVEL AND POSITION.
          SLP=-0.5*DTH*(3.*E(I)-4.*E(I-1)+E(I-2))/(E(I)-2.*E(I-1)+E(I-2))
          TH=(I-1)*DTH
          SLP=TH+SLP
          THH=(I-2)*DTH
          SLL=(E(I-1)*(TH-SLP)**2-E(I)*(THH-SLP)**2)/((TH-
SLP)**2-(THH-SL
         X**2)
C
          J=J+1
          SP(J)=SLP
          S(J)=E(I)+SLL
          K=4
       40 IF(E(I-1).GT.E(I)) GOTO 100
          K=3
      100 CONTINUE
             SLL=E(N)
             SLP=(N-1)*DTH
          DO 102 I=1,J
          IF(S(I).GT.SLL) THEN
          SLP=SP(I)
          SLL=S(I)
          ENDIF
      102 CONTINUE
          RETURN
          END
```

Computing antenna array directivity (DR).

```
      SUBROUTINE DIR(N,A,D,IN,US,DR)
C
C REFERENCE : C. A. BALANIS,"ANTENNA THEORY ANALISIS
C         AND DESIGN", PP.80, 1982.

C  This program computes the radiated power and
C directivity of an antenna provided its radiation
C intensity U = EFR(theta,phi)*AF(theta) is given.
C  The directivity is calculating using the trailing
C edge method in increment of one degree in theta and phi.
C The input data should contain the lower and upper
C bounde on theta and phi ( decliration statement).

C DEFINITIONS: AF: Array Factor
C          EF: Element Factor (= 1)

C INPUT :
C D(vector): positions of the elements.
C A(vector): current amplitudes vector.
C       N : number of the array element.
C      IN : dimensions of the vectors D
C      US : Sin(THETAS), THETAS: main beam steering angle
C         from broadside.

C OUTPUT: DR: antenna directivity
C
      REAL A(IN),D(IN)
C
C DEFINE LOWER AND UPPER BOUNDS ON THETA AND PHI
C
      INTEGER PL/0/,PLL,PU/360/,TL/0/,TLL,TU/180/
      EXTERNAL ARF
      EXTERNAL EFR
C
      PI=4.*ATAN(1.)
C
      PRAD=0.0
      UMAX=0.0
C
C DEFINE THE INCREMENTS
C
      THETA=PI/180.
      PHI=PI/180.
```

```
C
      TLL=TL+1
      DO 2 I=TLL,TU
      XI=FLOAT(I)*PI/180.
      AF=ARF(N,A,D,XI,IN,US,PI)
C
      PLL=PL+1
      DO 2 J=PLL,PU
      XJ=FLOAT(J)*PI/180.
C
C FUNCTION EF (ELEMEN PATTERN) IS CALLED TO OBTAIN
U(XI,XJ)
C
      F=EFR(XI,XJ)*AF
C
C MAXIMUM RADIATION INTENSITY IS FOUND
C
      IF(F.GT.UMAX) UMAX=F
      PRAD=PRAD+THETA*PHI*F*SIN(XI)
    2 CONTINUE
C
C CALCULATE DIRECTIVITY
C
      DR=4.0*PI*UMAX/PRAD
      WRITE(6,*)DR,UMAX
      RETURN
      END
C
C  ARRAY PATTERN CALCULATION
      F=ARF(N,A,D,XI,IN,US,PI)
      FUNCTION ARF(N,A,D,X,IN,US,PI)
C XI: THETA ANGLE AT WHICH THE (AF) WILL BE
C     EVALUATED FROM ENDFIRE.
      REAL ARF,D(IN),A(IN)
      U=(2.*PI*COS(X)-US)
      SUM=0.0
      DO 2 I=1,N
      V=D(I)*U
    2 SUM=SUM+A(I)*COS(V)
      ARF=SUM**2
      RETURN
      END
```

APPENDIX D

The following table lists the current amplitudes for 20-element linear array designed to have a radiation pattern of 30-dB sidelobe level.

30-dB chebyshev current distribution

ELEMENT NO.		CURRENT EXCITATION
1	20	1.00000
2	19	0.87706
3	18	1.20097
4	17	1.54995
5	16	1.90614
6	15	2.24974
7	14	2.56058
8	13	2.81905
9	12	3.00628
10	11	3.10533

30-dB Taylor current distribution

1	20	0.407515
2	19	0.435903
3	18	0.531124
4	17	0.694554
5	16	0.890987
6	15	1.079318
7	14	1.246033
8	13	1.387807
9	12	1.489958
10	11	1.540562

References:

[1] D. D. King, R. F. Packard, R. K. Thomas, "Unequally spaced broadband antenna arrays", IEEE Trans. Antennas propagat., vol. AP-8, PP.380-384, July 1960.

[2] R. T. Wiley, "Space tapering of linear and planar arrays", IEEE Trans. Antennas propagat., vol. AP-10, PP.369-377, July 1962.

[3] S. P. Applebaum , "Adaptive arrays", IEEE Trans. Antennas propagat., vol. AP-24, PP.585-598, Sept. 1976.

[4] B. Widrow, P. E. Mantey, L. J. Griffiths, and B. B. Goode, "Adaptive antenna systems", Proc. IEEE, vol. 55, PP.2143-2159,Dec. 1967.

[5] L. J. Griffiths, "A simple Adaptive algorithm for real-time processing in antenna arrays", Proc. IEEE, vol. 57, PP.1696-1704, Oct. 1969.

[6] O. L. Frost, "An algorithm for linearly constrained adaptive array processing", Proc. IEEE, vol. 60, PP.926-935,Aug. 1972.

[7] S. P. Applebaum and D. J. Chapman, "Adaptive arrays with main beam constraints", IEEE Trans. Antenn & propagat., vol. AP-24, PP.650-661, Sept. 1976.

[8] C. C. Zahm, "Application of adaptive arrays to suppress strong jammers in the presence of weak signals", IEEE Trans. Aerosp. Electron. Syst., vol. AES-9, PP. 260-271, March 1973.

[9] H. Steyskal, R. A. Shore, and R. L. Haupt, "Methods for null control and their effects on radiation pattern", IEEE Trans. Antennas propagat., vol. AP-34, PP.404-409, March 1986.

[10] C. A. Baird and G. G. Rassweiler, "Adaptive sidelobe nulling using digitally controlled phase-shifters", IEEE Trans. Antennas propagat., vol. AP-24, PP.638-649 , Sept. 1976.

[11] Special Issue on "Adaptive Antennas", IEEE Trans. Antennas propagat., vol. AP-24, Sept. 1976.

[12] H. Steyskal, "Simple method for pattern nulling by phase perturbation", IEEE Trans. Antennas Propagat., vol. AP-31, PP.163-166, Jan. 1983.

[13] R. A. Shore, "A proof of the odd -symmetry of the phase for minimum weight perturbation phase-only null synthesis", IEEE Trans. Antennas Propagat., vol. AP-32, PP.528-530, May 1984.

[14] R. A. Shore, "Nulling at symmetric pattern location with phase-only weight control", IEEE Trans. Antennas Propagat., vol. AP-32, PP.530-533, May 1984.

[15] R. L. Haupt, "Null synthesis with phase and amplitude controls at the subarray outputs", IEEE Trans. Antennas Propagat., vol. AP-33, PP.505-509, May 1985.

[16] D. J. Chapman, "Partial adaptive for the large array", IEEE Trans. Antennas Propagat., vol. AP-24, PP.685-696, Sept. 1976.

[17] D. R. Morgan, "Partially adaptive array techniques", IEEE Trans. Antennas Propagat., vol. AP-26, PP.823-833, Nov. 1978.

[18] I. El-Azhary, M. S. Afifi, and P. S. Excell, "A simple algorithm for sidelobe cancellation in a partially adaptive linear array", IEEE Trans. Antennas Propagat., vol. AP-36, PP.1484-1486, Oct. 1988.

[19] T. B. Vu, "Method of null steering without using phase shifters", IEE Proceedings, vol.131, pt. H, PP.242-246, August 1984.

[20] T. B. Vu, "Null steering by controlling current amplitude only", IEEE Trans. Antennas Propagat. Soc. Int. Symp. Dig., PP.811-814, 1984.

[21] T. B. Vu, "Simultaneous nulling in sum and difference pattern by amplitude control", IEEE Trans. Antennas Propagat., vol. AP-34, PP.214-218, Feb. 1986.

[22] B. Widrow, J. M. McCool, "A comparison of Adaptive algorithms based on methods of steepest descent and random search", IEEE Trans. Antennas Propagat., vol. Ap-24, PP.615-637, Sept. 1976.

[23] T. Lo and J. Litva, "Adaptive beam-space nulling of multipath signals", IEEE Trans. Antennas Propagat. , vol. Ap-38, PP.129-133, Jan. 1990.

[24] R. Shore and H. Steyskal, "Nulling in linear array patterns with minimization of weight perturbations", Rep. RADC-TR-82-32, Feb. 1982.

[25] R. Shore, "The use of a beam space representation and nonlinear programming in phase-only nulling", Rep. RADC-TR-83-124-32, (AD 131365), May 1983.

[26] H. Steyskal, "Synthesis of antenna patterns with prescribed nulls", IEEE Trans. Antennas Propagat. , vol. Ap-30, PP.273-279, March 1982.

[27] M. Ueno, K. Kawabata, and T. Morooka, "Systolic array architecture for Applebaum-Howells array", IEEE Trans. Antennas Propagat., vol. Ap-38, PP.1310-1313, Aug. 1990.

[28] M. Ueno, K. Kawabata, and T. Morooka, "Systolic array architecture for Applebaum-Howells array", APS-75-3 , PP.1646-1649, 1989.

[29] I. Gupta and R. Dilsavor, "An experimental SMI adaptive antenna array for weak interfering signals", APS-75-4 , PP.1650-1653, 1989.

[30] T. Ho and J. Litva, "Adaptive beamforming using multimode feed horn antennas", APS-75-5 , PP.1654-1657, 1989.

[31] K. Minamisona, F. Watanabe and N. Baba, "An interference cancellation technique for satellite communication earth stations", APS-75-7 , PP.1662-1665, 1989.

[32] R. L. Haupt, "Adaptive nulling in monopulse antennas", IEEE Trans. Antennas Propagat. , vol. Ap-36, PP.202-208, Feb. 1988.

[33] R. L. Haupt, "Simultaneous nulling in the sum and difference patterns of a monopulse antenna", IEEE Trans. Antennas Propagat. , vol. Ap-32, PP.486-493, May 1984.

[34] H. Steyskal, "Wide-band nulling performance versus number of pattern constraints for an array antenna", IEEE Trans. Antennas Propagat. , vol. Ap-31, PP.159-163, Jan. 1983.

[35] R. A. Monzingo and T. W. Miller, "Introduction to adaptive arrays", John Willy and Sons, 1980.

[36] R. T. Compton, "Adaptive arrays : On power equalization with proportional control", Ohio State Univ. Electoscince Lab., Rep. 3234-1, Contact N00019-71-c-0219, Dec. 1971.

[37] M. K. Leavitt, "A phase adaptation algorithm", IEEE Trans. Antennas Propagat. , vol.

Ap-24, PP.754-756, Sept. 1976.

[38] D. A. Thompson, "Adaptation by direct phase-shift adjustment in narrow-band adaptive antenna systems", IEEE Trans. Antennas Propagat. , vol. Ap-24, PP.756-760, Sept. 1976.

[39] H. C. Lin, "Spatial correlation in adaptive arrays", IEEE Trans. Antennas Propagat. , vol. Ap-30, PP.811-814, March 1982.

[40] C. Drane and J. McLlvenna, "Gain maximization and controlled null placement simultaneously in arial array patterns", Radio Electon. Eng., vol.39, no.1, PP.39-57, Jan. 1970.

[41] M. Dawoud and T. Ismail, "A new method for null steering by element position perturbations", Symp. on Antenna Tech. and Applied Electromag., ANTEM, Winnipeg, Canada, PP.123-128, Aug. 1990.

[42] T. Ismail and M. Dawoud, "Null steering in phased arrays by controlling the element positions", to be published in IEEE Trans. Antennas Propagat. , vol. Ap-39, Sept. 1991.

[43] T. Ismail and M. Dawoud, "Experimental verification of null steering by element position perturbations", submitted to IEEE Trans. Antennas Propagat.

[44] C. Rao and S. Mitra, "Generalized inverse of matrices and its applications", John Wiley and sons, New York,PP.45-46, 1971.

[45] M. H. Er, "Linear antenna array pattern synthesis with prescribed broad nulls", IEEE Trans. Antennas Propagat. , vol. Ap-38, PP.1496-1498, Sept. 1990.

[46] J. Mayhan, "Nulling limitations for a multiple beam antenna", IEEE Trans. Antennas

Propagat. , vol. Ap-24, PP.769-779, Nov. 1976.

[47] K. Takao and K. Komiyama, "An adaptive antenna for rejection of wideband interference", IEEE Trans. Aerosp. Electron. Syst., vol. AES-16, PP.452-459, July 1980.

[48] S. Prasad, "Linear antenna arrays with broad nulls with application to adaptive arrays", IEEE Trans. Antennas Propagat. , vol. Ap-27, PP.185-190, Mar. 1979.

[49] M. H. Er, "Technique for antenna array pattern synthesis with controlled broad nulls", Proc. Inst. Elect. Eng., vol. 135, pt. H, no.6, PP.375-380, Dec. 1988.

[50] D. Liu, R. J. Garbacz, and D. M. Dozar, "Antenna synthesis and optimization using generalized characteristics modes", IEEE Trans. Antennas Propagat., vol. Ap-38, PP.862-869, June 1990.

[51] T. S. Fong, "An interference nulling algorithm for a single receiver phased array", IEEE Trans. Antennas Propagat., vol. Ap-38, PP.951-953, June 1990.

[52] M. A. Hassan, "Design procedure for superdirective endfire antenna arrays", M. S. Thesis, May 1985.

[53] J. R. Carstens, "Automatic control systems and components", New Jersey, Printic Hall, 1990.

[54] R. L. Haupt, "Adaptive nulling in monopulse antennas", IEEE Antenn. Propag. Soc. Int. Symp. Dig., APS-21-6, PP.819-822, 1984.

[55] R. L. Haupt and R. A. Shore, "Experimental partially adaptive nulling in a low sidelobe

phased array", IEEE Antenn. Propag. Soc. Int. Symp. Dig., APS-21-7, PP.823-826, 1984.

[56] T. B. Vu, V. T. Thai and S. K. Lau, "An X-band computer-controlled phased array", IEEE Antenn. Propag. Soc. Int. Symp. Dig., APS-21-8, PP.827-830, 1984.

[57] C. A. Balanis, "Antenna theory analysis and design", Harper and Row Publishers, New York, 1982.

[58] R. S. Elliott, "Antenna theory and design", Prentice-Hall , Inc., Englewood Cliffs, New jersey, 1981.

[59] W. L. Stutzman, and G. A. Thiele, "Antenna theory and design", John Wiley & Sons Inc., 1981.

[60] W. F. Gabriel, "Adaptive arrays-an introduction", Proc. IEEE, vol. 64, PP.239-272, Feb. 1976.

[61] I. El-Azhary, M. S. Afifi, and D. S. Excell, "Fast cancellation of sidelobes in the pattern of uniformly excited array using external elements", IEEE Trans. Antennas Propagat., vol. Ap-38, PP.1962-1964, Dec. 1990.

[62] B. G. Wahlberg, I. M. Y. Marcels, and I. Webster, "Experimental and theoretical comparison of some algorithms for beamforming in single receiver adaptive arrays", IEEE Trans. Antennas Propagat., vol. Ap-39, PP.21-28, Jan. 1991.

[63] C. C. Ko, "A simple, fast adaptive algorithm for broad band null hlberg, I. M. Y. Marcels, and I. Webster, "Experimental steering", IEEE Trans. Antennas Propagat., vol. Ap-39,

PP.122-125, Jan. 1991.

[64] J. D. Kraus, "Antennas", McGraw-Hill, Inc., Singapore, 1988.